ON THE MECHANICAL BEHAVIOR OF STEEL RACK CONNECTIONS AND ITS INFLUENCE ON THE SEISMIC RESPONSE OF INDUSTRIAL STORAGE SYSTEMS

Dissertation

submitted to and approved by the

Faculty of Architecture, Civil Engineering and Environmental Sciences
University of Braunschweig – Institute of Technology

and the

Department of Civil and Environmental Engineering
University of Florence

in candidacy for the degree of a
Doktor-Ingenieur (Dr.-Ing.) /
Dottore di Ricerca in Civil and Environmental Engineering[*)]

by

Federico Gusella
born 16 October 1988
from Bagno a Ripoli (FI), Italy

Submitted on	11 February, 2019
Oral examination on	06 May, 2019
Professorial advisors	Prof. Klaus Thiele Prof. Maurizio Orlando

2019

*) Either the German or the Italian form of the title may be used.

TABLE OF CONTENTS

LIST OF FIGURES

LIST OF TABLES

NOTATION

The following symbols are used through the Thesis, unless notified otherwise:

A_{vc} *gross shear area of the column*

$A_{vc,net}$ *net shear area of the column*

$A_{v,tab}$ *effective shear area of tab*

$b_{eff,b}$ *effective width of the beam*

$b_{eff,t}$ *effective width for column web in tension*

$b'_{eff,c}$ *column effective width for stiffness in compression*

$b'_{eff,t}$ *column effective width for stiffness in tension*

$b'_{eff,co}$ *effective connector web width for stiffness*

$b_{eff,co}$ *effective width of connector web*

$d_{wc,c}$ *clear depth of column web in compression*

$d_{wc,cb}$ *is the clear depth of column web in buckling*

$d_{wc,t}$ *clear depth of column web in tension*

d_m *perimeter of tab in contact with the column*

d_{wco} *clear depth of connector web*

E steel elastic modulus

$f_{u,b}$ *ultimate tensile stress of beam*

$f_{u,cw}$ *ultimate tensile stress of column*

$f_{u,co}$ *ultimate tensile stress of the connector*

$f_{y,b}$ *yielding stress of beam*

$f_{y,cw}$ *yield stress of the column*

$f_{y,co}$ *yield stress of connector*

$f_{y,w}$ *yielding tensile stress of welding*

G steel shear modulus

h_b *height of the beam*

h_{tab} *height of tab*

t_b *thickness of the beam*

t_{cw} *thickness of column*

t_{tab} *thickness of tab*

t_{co} *thickness of the connector web*

J_w *second moment of inertia of weld*

x_w *is the distance of the welding center of area from the beam bottom flange;*

$W_{pl,co}$ *plastic section modulus of connector*

ω_{co} *factor connector web accounting for the interaction with shear*

ω *reduction factor for interaction with shear in the column*

$\alpha = \frac{f_{u,co}}{f_{u,cw}}$ *reduction factor*

k_b *=1.25 [EN 1993-1-8]*

$k_t = 1.5 t_{cw} / d_{M16}$ *[EN 1993-1-8]*

ABSTRACT

Steel storage pallet racks are commonly used worldwide to store goods on pallets and represent complex and challenging structures to design. The main racking system is denoted as “selective steel storage pallet rack”. These racking systems are one pallet deep and are separated by aisles, allowing for each pallet, stored on horizontal beams, to be always accessible. Selective racks behave like bracing system in cross-aisle direction, with uprights connected by diagonal bracings, while in down-aisle direction, bracings are usually not installed to make palletised goods always accessible. Therefore, in down-aisle direction racks behave like moment resisting frames (MRFs) whose stability and seismic resistance depend on the performance of beam-to-column connections. This Thesis is motivated by the need to increase the knowledge about the mechanical behavior of rack joints, investigating how it is affected by structural details and design parameters, and its effect on the global seismic response of rack systems. This is not only a very interesting and challenging problem from a scientific point of view, but it can also have a very large economic impact.

The proposed goal is achieved through: experimental tests, carried out on full-scale boltless rack joints to identify their non-linear moment-rotation curve under monotonic and cyclic loading; the development of a theoretical model to simulate experimental curves of joints; probabilistic analyses to highlight the influence of uncertainties in material strength and geometrical features on the mechanical performance of joints; and finally the development of a numerical model, capable to describe the pinching in hysteresis loops of connections and its effect on the seismic response of industrial storage systems.

To obtain the moment-rotation curve of rack connections and to evaluate how it is affected by structural details, a set of full-scale joints are tested at the Structures and Material Testing Laboratory of the Department of Civil and Environmental Engineering of the University of Florence. In the first part of the Thesis, results of monotonic and cyclic tests are presented. Some joints are also equipped with additional bolts, which could represent an effective solution to improve the seismic response of steel storage pallet racks. Experimental testing is useful to get information about the semi-rigid behavior and ductility of beam-column joints. Nevertheless, despite the success and popularity of experimental testing, tests can be expensive and time-consuming, therefore current state-of-art models for traditional steel joints are based on the Component Method (CM). The CM approach can be applied to any kind of connections because the joint is modeled theoretically as an assembly of components with an elasto-plastic or rigid force-displacement relationship. A mechanical model based on the CM is developed and used to analytically evaluate the non-linear structural response of rack beam-column joints. The accuracy of the proposed approach is checked by the comparison with experimental results.

To explore the impact of the component structural details and the uncertainty in steel mechanical properties and geometrical features, a Monte Carlo simulation of rack connection assemblies is also performed. For the development of simulations, statistical properties of material random variables are assumed on experimental results, the variability in geometric tolerances are assumed in accordance with current standard code requirements and the structural response of rack joints is modeled using the proposed mechanical model based on the CM.

Finally, experimental tests showed a non-negligible pinching in the cyclic moment-rotation curve of rack connections, with a reduction of energy dissipation. This structural behavior is expected to influence the seismic response of rack systems and it is investigated in the last chapter of the Thesis. A simplified Finite Element (FE) numerical model is proposed for the analysis of steel storage pallet racks under cyclic loads, considering the pinching in the joint hysteresis loop. The effectiveness of the proposed model is its fast tuning and easily implementation in commercial software packages, commonly used for non-linear seismic vulnerability analyses. For a deeper understanding of the pinching effect, a case-study is discussed, comparing two models of joints differing in the modeling of the degradation of the rotational stiffness. Results highlight that a non-liner dynamic analysis with the proposed pinching model, which describes the effective non-linear elasto-plastic behavior of rack joints, is suggested to obtain a seismic vulnerability assessment of industrial storage systems on the safe side.

1 INTRODUCTION

1.1 Structural features of rack systems and connections

Cold-formed steel (CFS) is commonly utilized in steel storage selective pallet racks (Figure 1) that are popular in warehouses and other short- and long-term storage facilities [Hancock, 2003]. Rack structures behave like bracing systems in the cross-aisle (transverse) direction, with uprights (columns) connected by diagonal bracing. In down-aisle (longitudinal) direction, bracing systems are rarely installed in order to provide the easy accessibility to stored products; therefore, racks behave like moment resisting frames (MRFs) in which beams sustain pallets and provide down-aisle stability and seismic resistance through the performance of semi-rigid beam-to-column connections at their ends [Tilburgs, 2013].

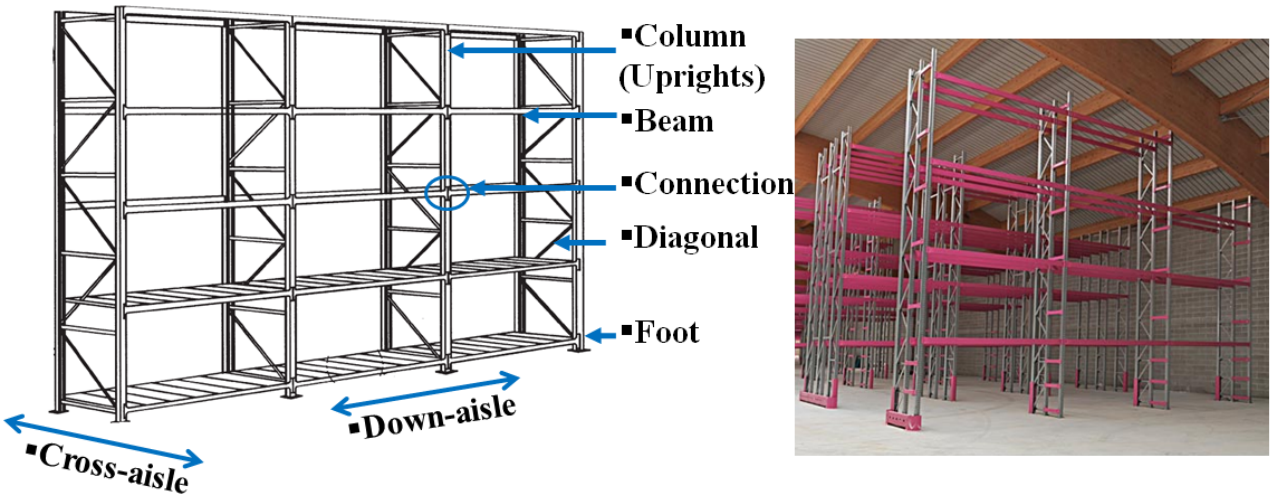

Figure 1. *Typical steel storage selective pallet rack and its members identified.*

Beam-to-column joint behavior plays a fundamental role in seismic response of structures and the necessity to take into account its effective response, in the context of a performance-based seismic design of steel racks, has been highlighted by several researches [Andrè et al., 2006, Peterman et al., 2016, Cardoso and Rasmussen, 2016, Baldassino and Bernuzzi, 2000, Abdel-Jaber et al., 2005, Bernuzzi and Simoncelli, 2016, Rodgers and Mahin, 2011 and Schafer et al., 2016].
Rack connections are boltless beam-to-column joints composed of beams, typically a rectangular tubular cross-section welded to connectors with tabs, and cold-formed thin-walled steel uprights, with arrays of holes along the length (Figure 2). These holes allow for the beam to be connected at various heights without bolts for ease of assembly and adjustment [Markazi et al., 1997]. A sketch of a typical rack connection, with its members identified, is shown in (Figure 2).

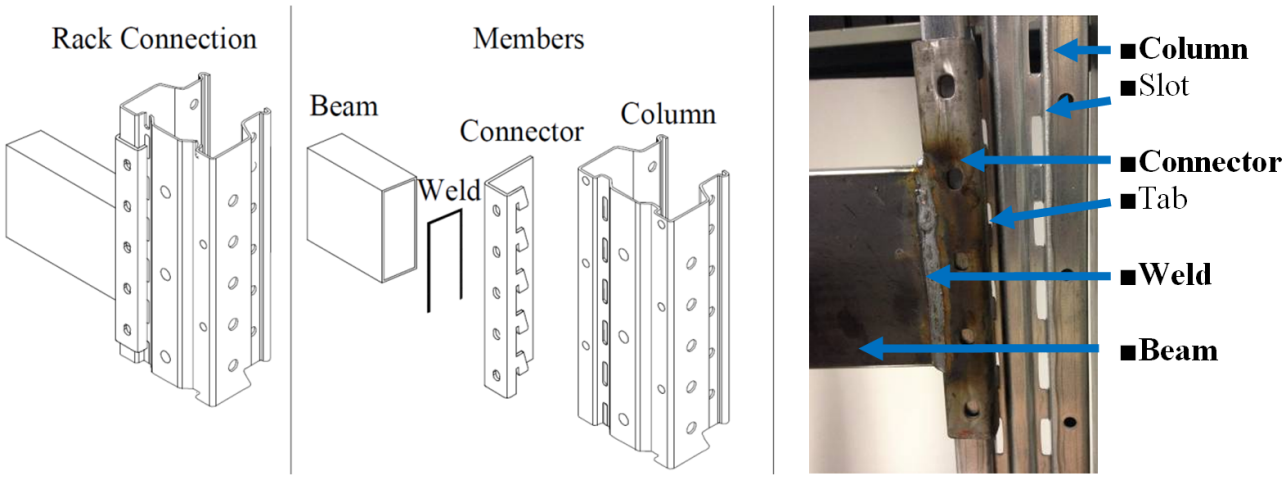

Figure 2. *a) Rack connection 3D view; b) Members of rack connection; c) Front view of rack connection and its members identified.*

1.2 Literature review of beam-to-column joint models

Several methods can be used to evaluate the mechanical behavior of beam-to-column joints: *"experimental testing"*, *"empirical models"*, *"mechanical models"* and *"numerical models"* [Faella et al., 2000].

Because of the great variety of connector types and different profiles used for beams and uprights, the structural response of steel rack connections is not easy to be evaluated theoretically. These construction details result in complex numerical analysis difficult to translate to design recommendations [Dai et al., 2018]. Therefore, according to the design by testing approach [EN 1993-1-1, 2005 and Baldassino and Zandonini, 2011], experimental tests are required by the current design codes [EN 15512, FEM 10.2.02, RMI and AS/NZS 4084] to evaluate the moment-rotation curve of rack connections.

Several *experimental tests* on beam-to-column connections to investigate their structural behavior, in terms of strength, stiffness and dissipative capacity, have been performed by many researchers. The connection flexibility of boltless rack connections was investigate in [Prabha et al., 2010]; the stiffness of joints in bolted connected CFS trusses was evaluated in [Zaharia and Dubina, 2006]. Tests on different types of commercially available connectors, under a monotonic increasing load, were performed in [Markazi et al., 1997], where the effect of the upright's features on the moment-curvature relationship was investigated. Monotonic experimental tests were conducted in [Zhao et al., 2014] to analyze the flexural behavior of connections under hogging loading in a single cantilever testing method. Several groups of beam-to-upright connections with different constructional details, such as the upright's profile, the thickness and the number of tabs in the connector, were investigated. These tests highlighted that the failure mode of connections mainly depends on the relative thickness between the upright and the connector.

Experimental tests aimed to investigate the behavior of beam-to-column joints under cyclic reversal loading were carried out in [Bernuzzi and Castiglioni, 2001], where constant amplitude cyclic tests were performed, highlighting the high ductility of rack connections which can cause large swaying of uprights during earthquakes, thus leading to significant second-order effects. Other experimental findings on beam-column connections under cyclic loads were presented in [Aguirre, 2005]. In these cyclic tests the loading history included series of three cycles of equal maximum displacement and the maximum displacement of the series was increased until the connection failed; obtained results showed a pinching in the moment-rotation hysteresis curve, highlighting the different response of rack connection respect to traditional steel joints with more stable structural behavior [Tsai et al., 1995]. In [Yin et al., 2016] the authors analyzed a specific type of connector, in which tabs work in tension and compression [Zhao et al., 2017]. This connection type was tested in

different configurations, changing its structural details, and the authors observed that the envelope of the cyclic moment-rotation curve was comparable with the monotonic one. The structural response of bolted moment connections, formed by CFS members, was investigated in [Gilbert and Rasmussen, 2010], where the authors observed, after an initial high moment-rotational stiffness of the connection, a significant amount of looseness, which nevertheless does not affect the ultimate limit state design of the whole structure.

Experimental tests provide the most accurate knowledge of the joint load-deformation response, including cyclic strength and stiffness degradation [Moen et al., 2016 and Tao et al., 2016] but this technique is too expensive for everyday design practice [Diaz et al., 2011].

Empirical models are based on empirical formulations obtained using regression analyses of data, which can be derived by means of experimental tests and/or parametric analyses developed by means of numerical models. An empirical formulation, which relates the parameters of the mathematical representation of the moment-rotation curve to the geometrical and mechanical properties of the rack joint, is proposed in [Prabha et al., 2010]. The main disadvantage of this method is that it is applicable to joints whose characteristics match those used to generate the empirical formulations.

On the contrary, *mechanical models* can be applied to any kind of connections because they represent the joint by using a combination of rigid and flexible springs, which are modeled by means of force-displacement relationships obtained from concepts of elastic structural analysis and empirical formulations. Mechanical models, based on the application of this approach "Component Method" [EN 1993-1-8, 2005 and Faella et al., 2000], used to describe steel traditional beam-to-column joints are developed in [Jaspart, 2000, Lima et al., 2004, Silva et al., 2002 and Silva et al., 2004]. Mechanical models for boltless rack connections are developed in [Ślęczka and Kozłowski, 2007 and Zhao et al., 2017]. The drawback of these models is that they cannot be used in the evaluation of the effect of the connections on the structural response of the whole frame structure.

Numerical models can be divided into two categories: explicit macroscopic models and implicit models [Mitra, 2007].

In explicit models the inelastic mechanism governing the joint behavior is modeled by means of a combination of elements, which represent the sources of the strength and deformation. These models, with an adequate calibration, offer the greatest potential for accurately simulating the non-linear response of joints showing the influence of geometrical and mechanical component features on their collapse mode [Markazi et al. 2001]. In [Bajoria and Talikoti, 2006] results of experimental tests on rack connections using both a cantilever and a double cantilever testing method were compared with those obtained through three-dimensional non-linear Finite Element (FE) models, obtained results were found to match well with the full scale frame tests. The effect of the upright behavior on the moment-curvature relation has been analysed in [Markazi et al., 2001], whereas the effect of the number of tabs and beam's depth has been investigated in [Shah et al., 2016 (a)], managing to capture the tearing of column slots due to tabs. In [Zaharia and Dubina, 1997] an experimental research program aiming to evaluate the semi-rigid behavior of some typical bolted connections, used in CFS plane truss joints, was carried out and a numerical analysis of this type of connections was developed to demonstrate the improvement of load capacity in comparison with the classical pinned connection assumption.

Explicit numerical models are the most suitable tool to investigate the response of a joint. They are used to overcome the lack of experimental results, to understand local effects and to generate extensive parametric studies. Their drawbacks are the large data set required for their calibration and difficult implementation in commercial software; moreover, these analyses are computationally expensive.

Implicit models are a tool to account for the actual structural response of joints in estimating the inelastic response of structures. These models are based on the curve fitting so that they are able to represent only the behavior of joints without providing information about the influence of their details. Implicit models introduce springs at the intersection of the beam and column elements to represent the stiffness and strength loss due to the joint damage [Borghini et al., 2016]. The

rotational joint behavior can be approximated through different relationships and levels of precision: from linear [EN 15512, 2009] to non-linear moment-rotation curves [Baldassino and Bernuzzi, 2000 and Abdel-Jaber et al., 2005]. The main advantage of an implicit model is its simplicity and easy implementation in commercial FE non-linear analysis packages currently available in engineering offices; while, the primary disadvantage is its calibration to provide an accurate simulation of the joint response. Referring to CFS joints, which exhibit a pinched cyclic response, the ultimate goal is the calibration of their hysteresis loop, because traditional elastic-plastic or other common hysteresis models are not appropriate. To describe the pinching in the hysteresis loop of CFS members, the Pinching4 model [Mitra, 2012] has been recently developed providing reliable results [Peterman et al., 2014 and Shen et al., 2013]. The drawback of this numerical model is the great number of parameters to be calibrated, that can be obtained only after cyclic experimental tests. This model is based on the curve fitting so that it is able to represent only the cyclic behavior of specimens for which experimental tests are available. It is worth mentioning that the approximate typical Pivot-model [Dowel et al., 1998] has already been used in a numerical study of racks [Haque and Alam, 2015 and Bernuzzi and Simoncelli, 2016]. Nevertheless, it can be unsafe to describe the cyclic response of joints which exhibit high pronounced pinching in their hysteresis loops.

1.3 Objective and Scope

The project is motivated by the high complexity of rack connections, translated in the lack of design guidelines to theoretically evaluate their structural response and to estimate their influence on the performance of rack systems. The objectives of this PhD project are:

(a) to accurately investigate the structural behavior or rack connections;
(b) to analytically evaluate the non-linear moment-rotation curve of typical rack beam-to-column joints and to identify the effects on connection response due to connection members (beam, beam-end weld, connector and column);
(c) to estimate the propagation of the uncertainty in component geometry and mechanical properties to the connection response, and then to ensure reliability of rack joints;
(d) to capture the influence of rack connections on the non-linear dynamic seismic response of industrial steel storage pallet racking systems.

1.4 Methodology and Outline

The objectives of this Thesis are achieved as follows:

(a) in order to gain an understanding of the structural behavior of rack connections, full-scale beam-to-column joints were experimentally tested through the single cantilever testing method, under monotonic and cyclic loads (Chapter: “Experimental Campaign”);
(b) a mechanical model base on the Component Method is developed to theoretically evaluate the initial elastic rotational stiffness and ultimate moment of rack joints. The proposed mechanical model allows to the influence of rack components on the joint response to be estimated. Moreover, an analytical equation is proposed to predict the non-linear moment-rotation curve of rack joints (Chapter: “Theoretical Analysis”);
(c) Monte Carlo simulation of several rack connection assemblies is developed adopting the proposed mechanical model to simulate their structural response, and random values to simulate the effect of the variability in mechanical and geometric features (Chapter: “Theoretical Analysis”);
(d) an implicit FE numerical model, defined by the knowledge of the non-linear monotonic moment-rotation curve obtained thorough the proposed mechanical model is developed. The FE model is capable to describe the cyclic elasto-plastic behavior of rack beam-to-column joints and

can be easily implemented in commercial software. For a deeper understanding of the effects of pinching in the seismic response and to highlight the potentiality of the proposed model a rack system is modeled using two numerical approaches which differ in the deterioration of the rotational stiffness of joints. Non-linear dynamic analyses, with simulated ground acceleration time-histories, have been carried and compared (Chapter: "FE Model").

2 EXPERIMENTAL CAMPAIGN

In order to evaluate the moment-rotation curve of rack connections and to assess the influence of different structural details on its mechanical behavior, a suite of full-scale connections are tested at the Structures and Material Testing Laboratory (SMTL) of the University of Florence. Results of monotonic and cyclic tests on four different types of industrial rack joints are herein presented and compared. Tested connections differ in the number of tabs and the relative thickness between upright and connector. Moreover, they differ from one another for the type of connector, which is obtained by folding the beam-end or is welded to the beam-end section. A peculiar aspect of the experimental campaign is represented by the investigation of the welding layout between the beam-end section and the connector and its influence on the structural response and failure mechanism of joints. In fact, producers of steel pallet racks are interested in minimizing the total length of welding for time efficiency and cost saving. Finally, some joints are equipped with additional bolts to evaluate their influence on the bearing capacity, initial rotational elastic stiffness, ductility and dissipated energy per cycle.

2.1 Tested connections

The behavior of four different types of beam-to- column connections, in the following named *A*, *B*, *C* and *D*, are investigated experimentally. In all tested connections, the beam has a hollow rectangular cross section (height/base/thickness =130/50/2 mm, named 1352), while the upright has a perforated open section (height/base/thickness=100/130/2.5 mm, named 130/250), whose ultimate capacity has been investigate through experimental tests in [Orlando et al., 2017 and Bertocci et al., 2017] under compression and bending with the assessment of its strength domains.
The type *A* connection has a four-tab connector, 4 mm thick (M4f), which is obtained directly from the beam by folding its end. Type *B*, *C* and *D* connections are characterized by the same five-tab connector, 3.5 mm thick, (M5), but they differ from one another for welds used to join the connector to the beam-end section.
In the type *B* joint, the connector is welded to the beam-end through a double-sided welding; in the type *C*, it is welded all-around the beam-end section, and in the type *D* the connector is welded on three sides of the beam-end section (Figure 3). Considering the couple of forces into which the beam-column bending moment can be resolved, it results that, in the load transfer path of tested connections, the tensile force is brought by tabs, which only works in tension, while the compression force is transferred by direct contact between the connector flange and the column web. In all connections, a safety clip is inserted to avoid that the connector unlocks from the upright due to accidental impacts.
To evaluate how the cyclic response of connections changes if additional bolts are installed, some cyclic tests are repeated after replacing the safety clip with a bolt M8 (specimens C-c2b and D-c2b in Figure 4, Table 1) or after inserting two additional bolts M10 in front of the connector plate (specimen D-c3bb in Figure 4).
Following steel grades are used for elements of connections: S350GD (f_{yk}=350 N/mm^2) for columns, S275JR (f_{yk}=275 N/mm^2) for beams, and S235JR (f_{yk}=235 N/mm^2) for connectors. For each member of the connection (column (subscript $_{cw}$), beam (subscript $_b$) and connector (subscript $_{co}$)) three tension coupons were tested [ISO 6892-1]; the mean yielding stress (f_{yi}) and ultimate stress (f_{ui}) are summarized in Table 2. Features and the loading protocol of tested connections are listed in Table 1; Figure 5 shows a view of all connection types.

A connection (front view)

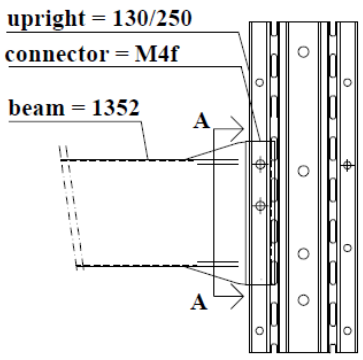

A connection (plan section)

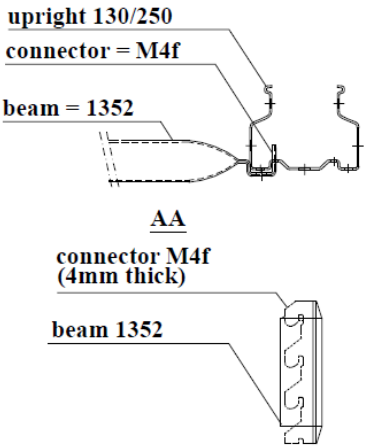

B connection (front view)

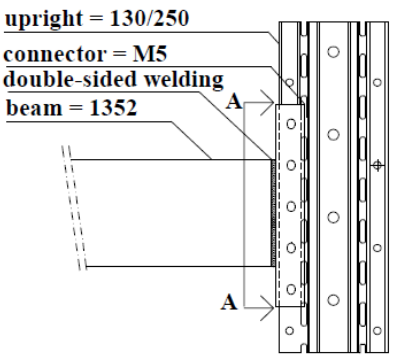

B connection (plan section)

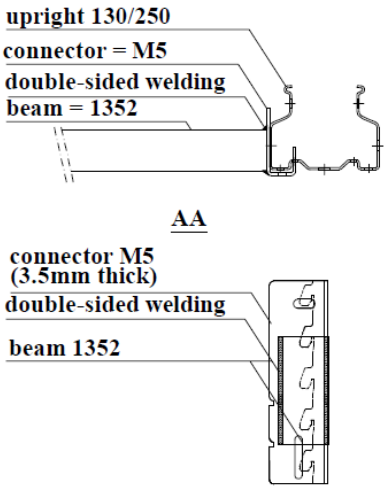

C connection (front view)

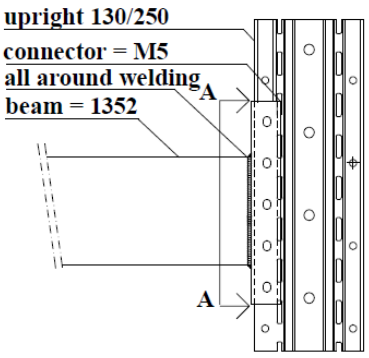

C connection (plan section)

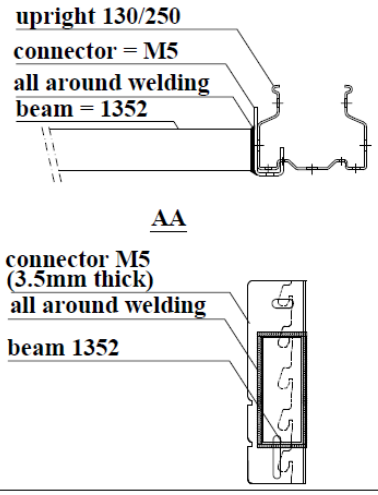

D connection (front view)

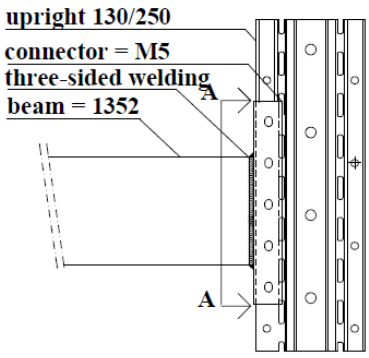

D connection (plan section)

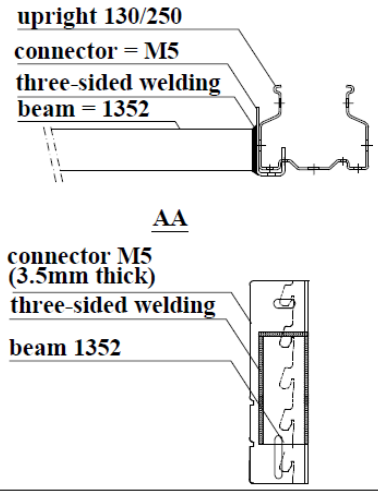

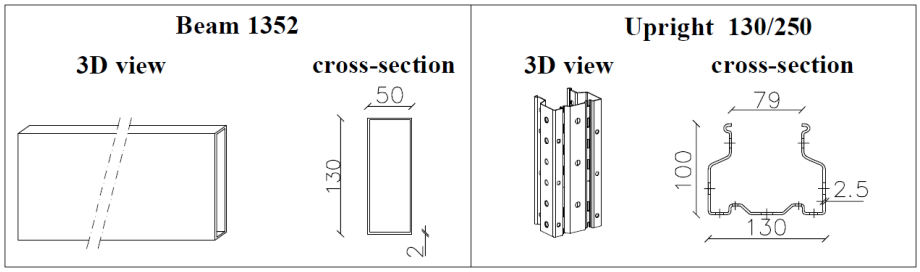

Figure 3. *Geometry and components of tested connections.*

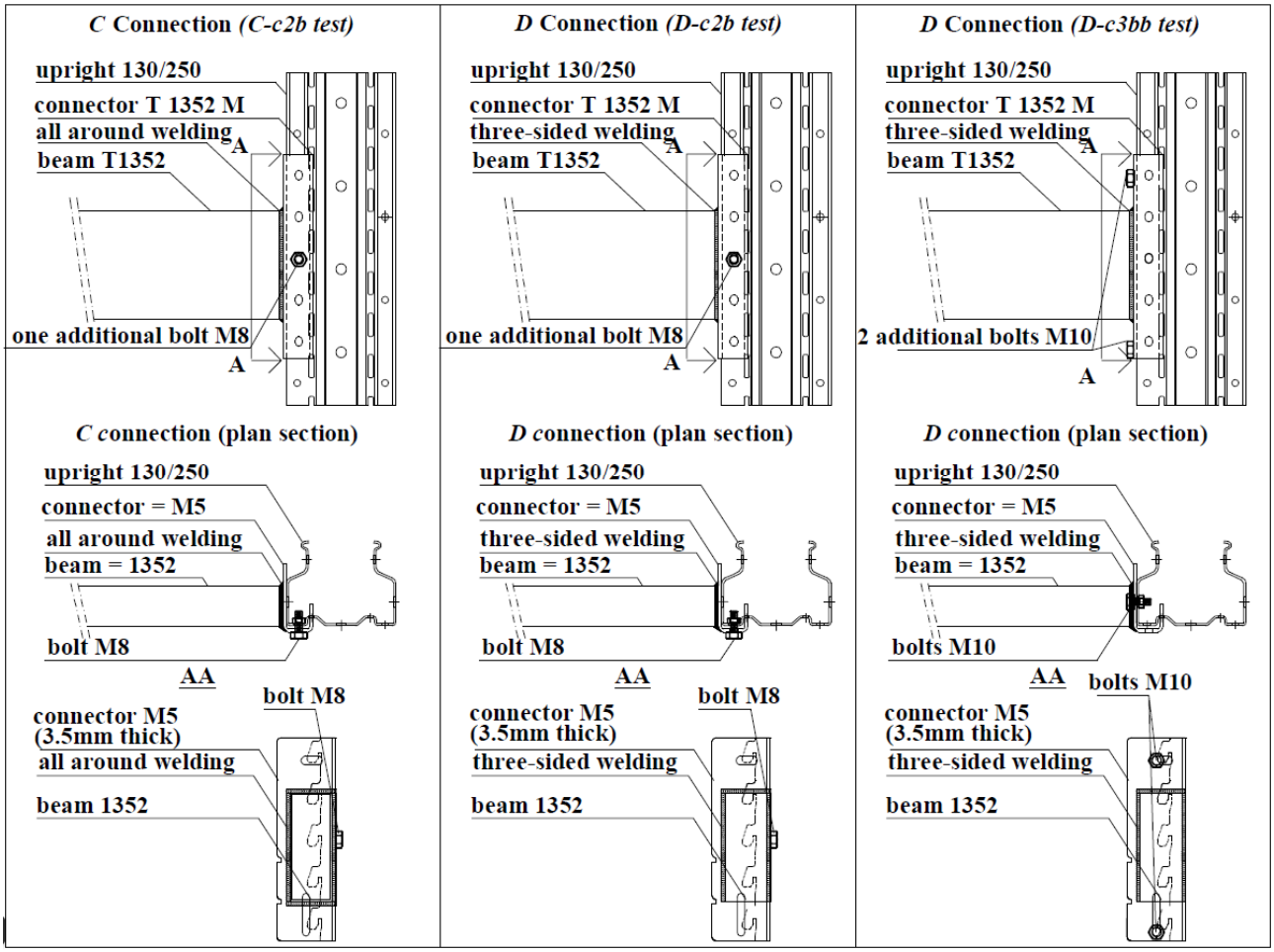

Figure 4. *Tested connections with additional bolts.*

Table 1. *Features of tested connections*

Type	Specimen (T-ln)*	Connector and welding type	Load	Initial displacement (*d*)
A	A-m1	(M4f) folded beam-end	monotonic	0
	A-c1		cyclic	d_o
	A-c2		cyclic	d_o
B	B-m1	(M5) double-sided welding	monotonic	0
	B-c1		cyclic	d_o
	B-c2		cyclic	0
C	C-m1	(M5) all around welding	monotonic	0
	C-c1		cyclic	d_o
	C-c2b**		cyclic	d_o
D	D-c1	(M5) three-sided welding	cyclic	d_o
	D-c2b		cyclic	d_o
	D-c3bb***		cyclic	d_o

Note: * letter T means the type of connection, letter l means the type of load ("m" monotonic - "c" cyclic); n means the test number. ** the letter b means that a bolt has been added to the connector. *** bb means that two bolts have been added to the connector.

Table 2. Material properties from coupon tests

Values	**Members**					
	Beam		**Connector**		**Column**	
Nominal Thickness [mm]	t_b=2		t_{co}=3.5		t_{cw} =2.5	
Mechanical Properties [N/mm^2]	f_{yb}	f_{ub}	f_{yco}	f_{uco}	f_{ycw}	f_{ucw}
	451	474	282	366	416	461

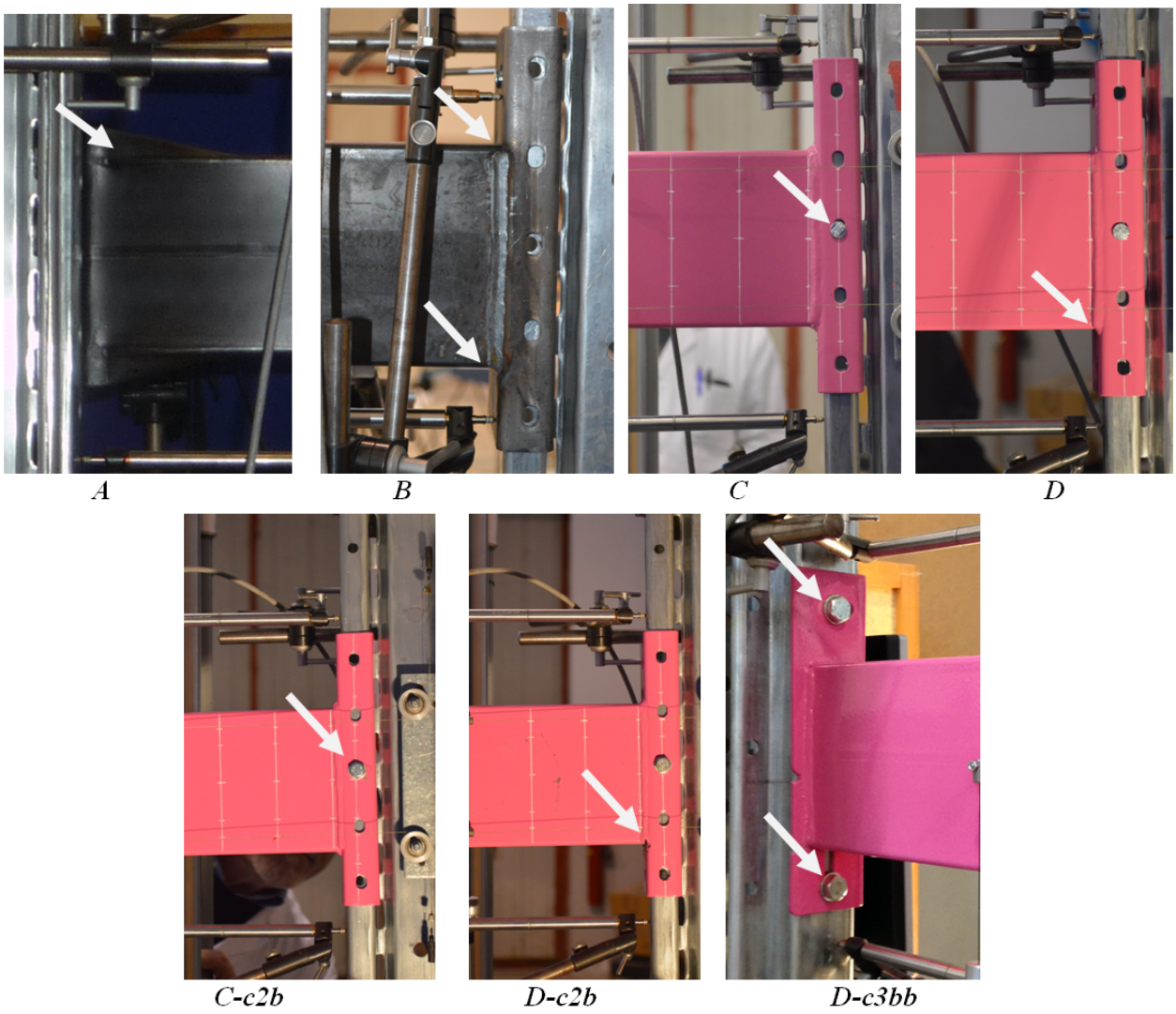

Figure 5. *Beam-column connections: type A (arrow shows the folded beam-end section), type B (arrows show the lack of top and bottom welding), type C (arrow shows the safety clip), type D (arrow shows the lack of bottom welding), test C-c2b (arrow shows the added bolt), test D-c2b (arrow shows the lack of bottom welding) and test D-c3bb (arrows show two additional bolts).*

2.2 Testing apparatus and loading protocol

The testing apparatus (Figure 6) has been built in accordance with [EN 15512]. Each specimen consists of a 600 mm long column and a 600 mm long beam. The concentrated load *P* is applied at

a distance of 400 mm from the column's face. The column of each specimen is clamped at both ends to the stiffer testing frame through bolted connections (Figure 6).

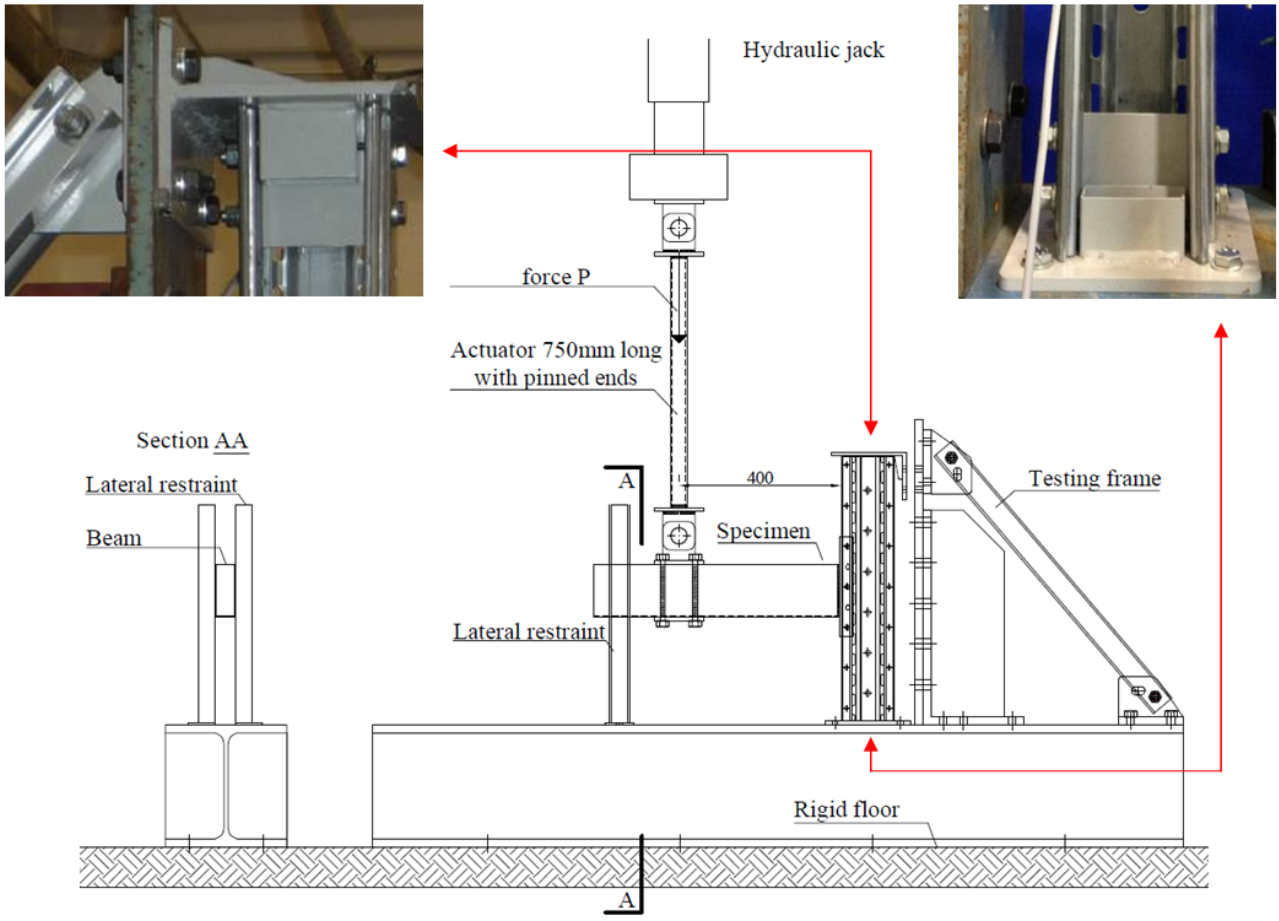

Figure 6. *The testing equipment and frame used in the SMTL of the Department of Civil and Environmental Engineering of Florence. Photos of bolt connections between specimen and testing frame. Measurements in millimeters.*

In monotonic tests, the load P is increased until the connection collapse. In all cyclic tests, with the the displacement history of Figure 7 is applied to the structure starting from an initial imposed displacement d_0 (Table 1), which induces the service bending moment due to three pallets of 1200 kg mass each. Only test *B-c2* started from null displacement just for comparison, obtaining similar results. The displacement history was established according to ATC-24, which well replicates the deformation history in an earthquake [Krawinkler, 2009]. In particular, it includes groups of three cycles of equal amplitudes: $\pm\Delta d$, $\pm 2\Delta d$, $\pm 3\Delta d$, ..., $\pm n\Delta d$ with n increased until the specimen's failure; the amplitude Δd has been chosen according to:

$$\Delta d = \frac{(d_u - d_0)}{4} \approx 9mm \tag{1}$$

where d_u is the displacement corresponding to the maximum bending moment in the *C-m1* monotonic test. Following the approach proposed in [EN 15512], the rotation of the connection is measured and the moment-rotation curve (M-Φ) is plotted.

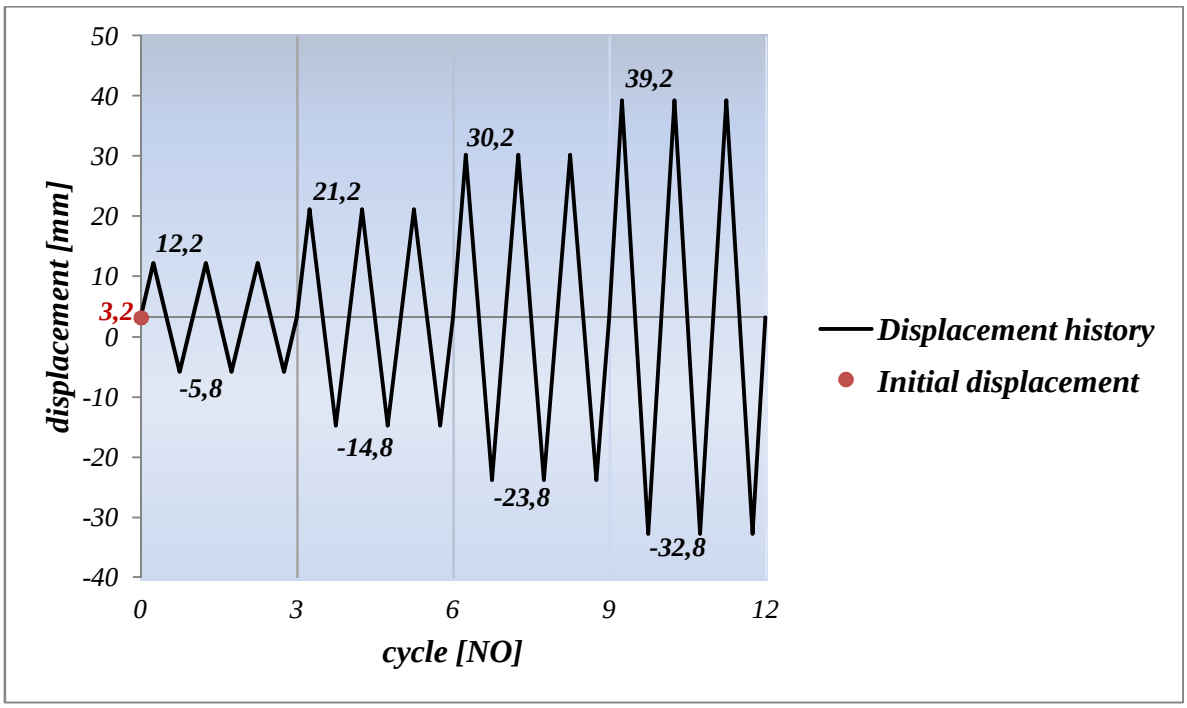

Figure 7. *Loading history* of cyclic tests.

2.3 Instrumentation

The vertical load (P in Figure 8a) and the vertical displacement of the point on the beam where it was applied (s_a in Figure 8a) were monitored by the linear variable differential transducer (LVDT) within the testing machine. LVDTs (m_i in Figure 8a) and wire-actuated encoders (s_i - f_i in Figure 8a) have been connected to a computer assisted data-logging system, together with the load cell.
The rotation Φ_b associated with the deformation of the connector is obtained as (Figure 8b):

$$\Phi_b = \Phi_{cd} - \Phi_c \tag{2}$$

where Φ_{cd} is the total rotation of the connector's end

$$\Phi_{cd} = (s_1 - s_2)/k_{12} \tag{3}$$

Φ_c is the contribution due to the column's deformation

$$\Phi_c = (m_3 - m_4)/k_{34} \tag{4}$$

with s_i and m_i the displacements measured by LVDTs and wire-actuated encoders, respectively, and k_{ij} the distance between instruments (Figure 8a).
The rotation Φ_b can also be obtained as (Figure 8b)

$$\Phi_b = \Phi - \Phi_c - \Phi_t \tag{5}$$

where:

$$\Phi = arctan(f_2 / L_2) \tag{6}$$

is the total rotation of the section at the distance L_2 from the column's face, and

$$\Phi_t = \arctan\left(\frac{\frac{PL_2^3}{3EJ_b} + \frac{\chi PL_2}{GA}}{L_2}\right) \tag{7}$$

is the contribution of the beam's elastic deformation (in correspondence of f_2 LVDT position);
with: f_2 the vertical displacement measured by the LVDT f_2, L_2 the distance between the LVDT f_2 and the upright's face (Figure 8a), P the load applied, E the elastic modulus of steel, J_b the moment of inertia of the beam, χ the shear correction factor, G the steel shear modulus and A the cross-section area of the beam.

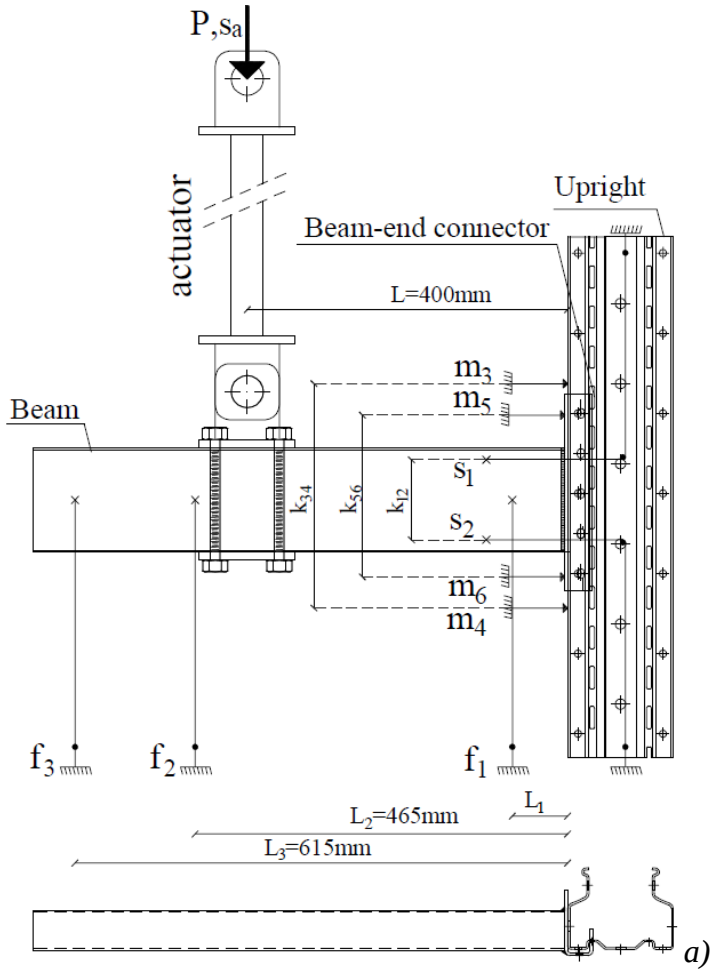

a)

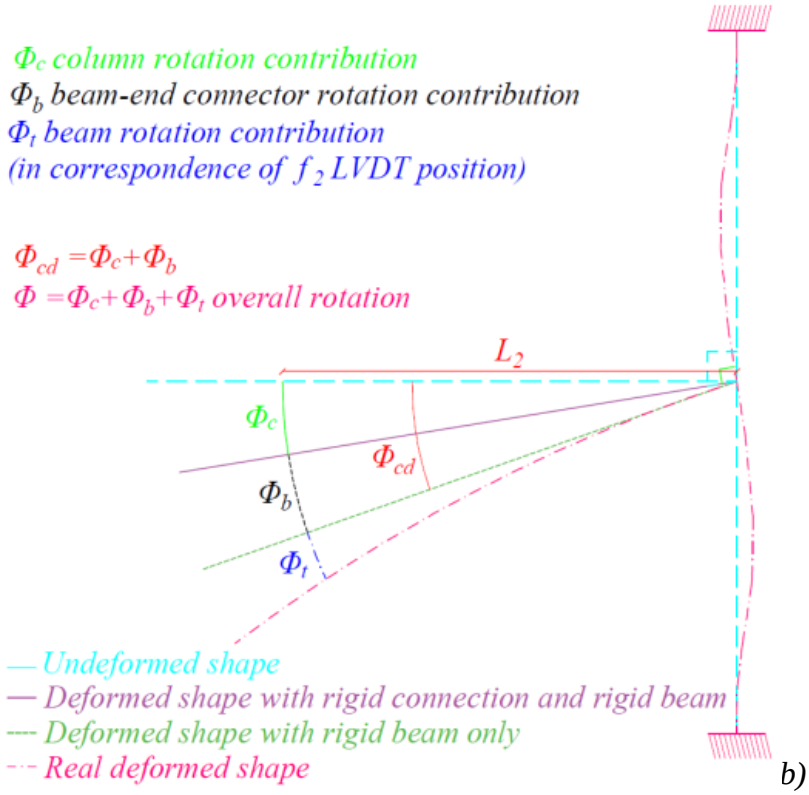

Figure 8. *a) Instrumentation; b) Rotations.*

2.4 Monotonic tests

Monotonic tests enable to identify main behavioral characteristics of all connection types.
The bending moment evaluated considering the undeformed configuration is equal to:

$$M = PL \tag{8}$$

where P is the applied load, $L=400$ *mm* is the initial distance between the point of load application and the geometric centre O of the beam-end section (Figure 9). Nevertheless, during the test, the loading actuator rotates by an angle α, so the bending moment M_1, evaluated with respect to the initial position of O, considering the deformed configuration is:

$$M_1 = PL' \tag{9}$$

where L' is the distance between the inclined axis of action of P and O (Figure 9).

a)

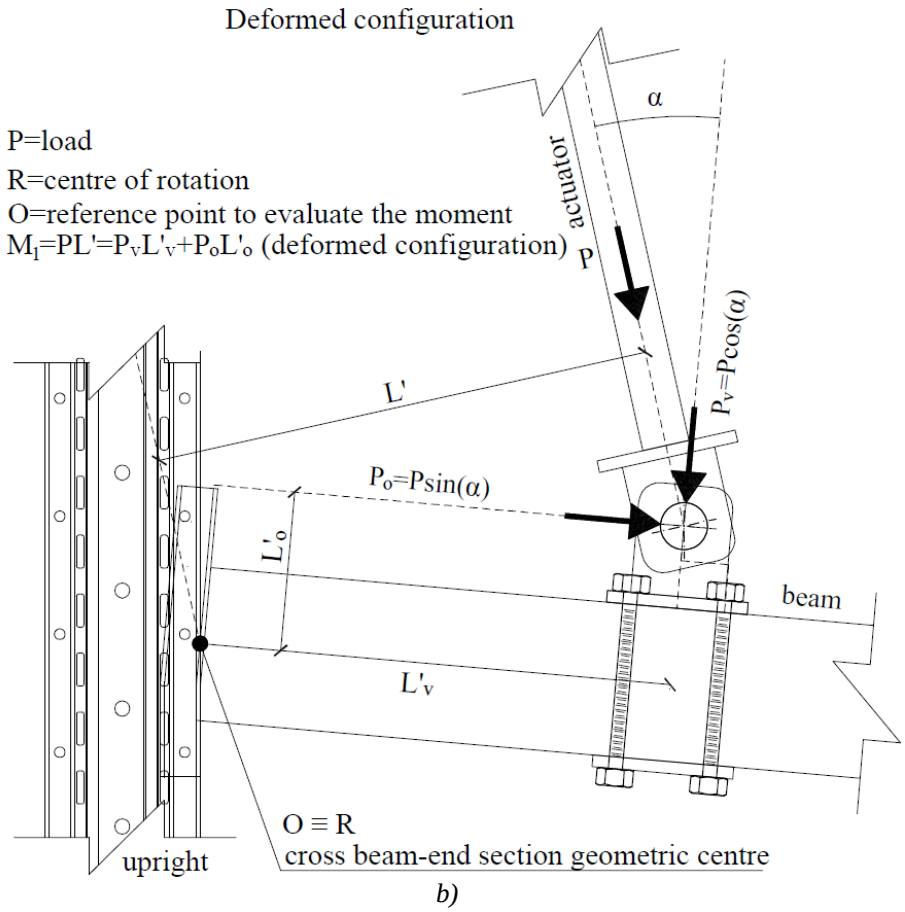

b)

Figure 9. *a) Deformed specimen; b) Scheme of deformed configuration.*

Results are presented in non-dimensional form: bending moments M and M_1 have been adimensionalized with respect to the beam's plastic moment $M_{p,b}$, according to EC3 [EN 1993-1-8, 2005], which has been evaluated using the design yield strength of the steel used for the beam ($f_{yd} = f_{yk}/1.05$):

$$m = \frac{M}{M_{p,b}};\ m_1 = \frac{M_1}{M_{p,b}},$$

(10)

while the non-dimensional rotation of the beam-end connector ϕ_b has been evaluated according to [EN 1993-1-8, 2005] as:

$$\phi_b = \frac{\Phi_b E J_b}{L_b M_{p,b}},$$

(11)

where E is the elastic modulus of steel, J_b is the moment of inertia of the beam, L_b is the length of the beam used in the rack system (2700 mm, as indicated by the manufacturer) and Φ_b is the dimensional rotation of the beam-end connector (5).

Figure 10 shows non-dimensional moment-rotation curves m-ϕ_b and m_1-ϕ_b of tested joints under monotonic loading, with the boundaries for semi-rigid joints in accordance with [EN 1993-1-8, 2005]. In particular, referring to their initial elastic branch, tested joints can be considered semi-rigid joints with reference to the stiffness, and partial-strength joints for the resistance, showing an ultimate bending moment ≈ 0,65 $M_{p,b}$ for connection type A and ≈ 0,9 $M_{p,b}$ for connections type B and C.

In Table 3 maximum differences between m and m_1 are listed; for all connection types the maximum difference is only 5.4%, so differences between m and m_1 may be neglected.

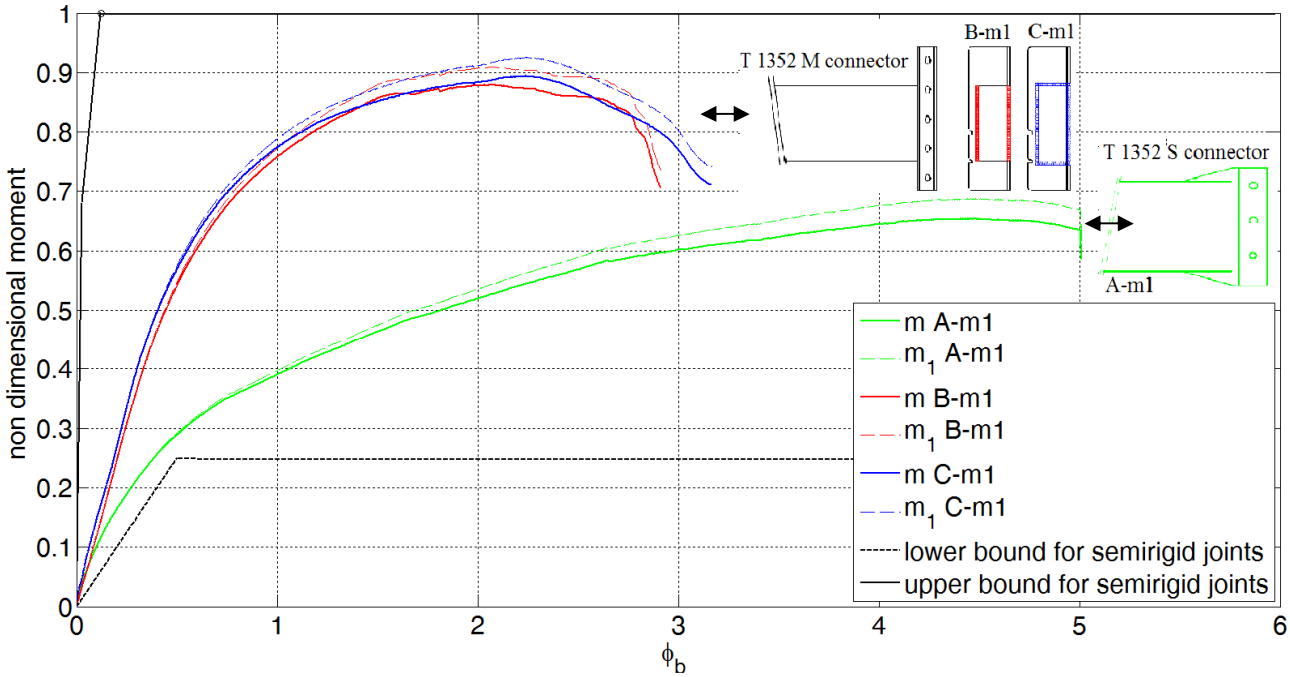

Figure 10. *Non-dimensional moment-rotation curves of monotonic tests. See Table 1 for the type and designation of specimens.*

Table 3. Maximum percentage difference between m and m_1.

Type of connection*	Type *A*	Type *B*	Type *C*
max[(m_1-m)/m]	5.4%	4.2%	4.3%

*Monotonic tests on Type D specimens have not been performed.

The flexural resistance is greater in type *B* and type *C* specimens than in type *A*. The difference is mainly due to the greater number of tabs in type *B* and *C* connectors, which also give a higher lever arm (Figure 3).
Moreover, moment-rotation curves of tested connectors exhibited a different post-elastic branch. For both *B* and *C* types, the collapse was almost brittle: it was associated to the failure of welding in the type *B*, and of tabs in the type *C*, where an adequate welding all around the beam-end section allows maximum bending moment and rotation to be moderately increased. Vice versa, in the type *A* specimen, the rotation ϕ_b of the connector's end achieved higher values, thanks to the high deformation of the folded beam-end which forms the connector (Figure 5); in the type *A* connection, the failure was associated to the punching of the upright steel plate at the slots, due to connector tabs (Figure 11).
The failure mode and the ultimate flexural resistance of connections depend on the weakest component of the joint; moreover, results underline that the collapse of the connector mainly depends on the relative thickness of upright and connector, and on their steel grade.
In the type *B* connection the weakest element is the welding of the beam-end section; in the type *C*, thanks to the welding all around the beam-end section, the weakest component is given by tabs; in the type A (Figure 3), where the thickness of tabs increases from 3.5 to 4 mm, the weakest component is the upright.

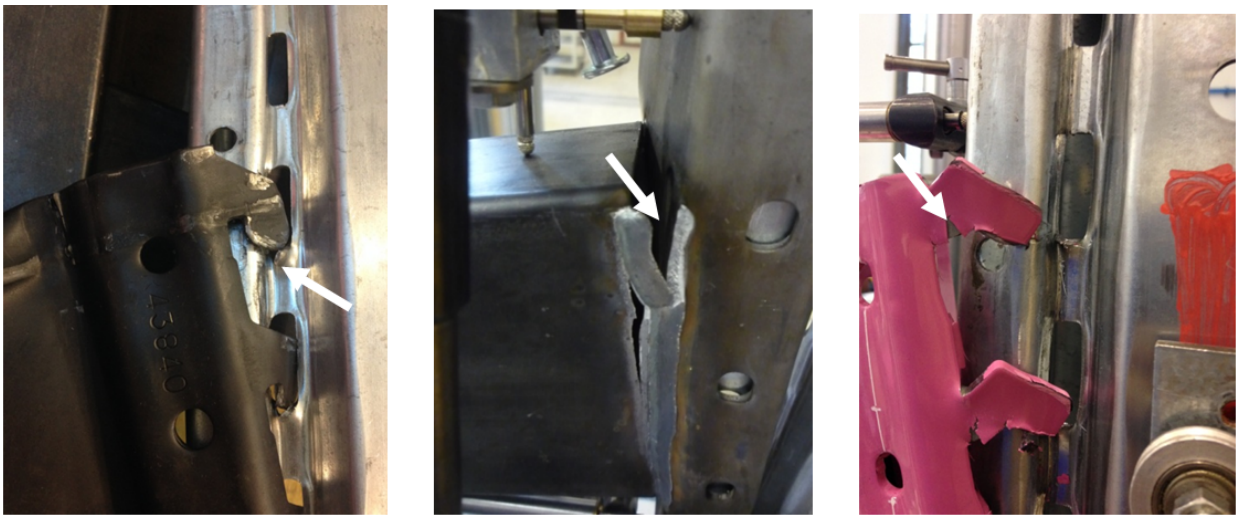

Figure 11. *Different failure modes of connections (A type, punching of the upright plate - B type, fracture of welding - C type, yielding of tabs).*

The total non-dimensional rotation development ϕ of the section at the distance L_2, the development ϕ_b of the connector's rotation, the development ϕ_c of the column's rotation and the development ϕ_t of the beam's rotation versus the non-dimensional bending moment m are shown in Figure 12. An appraisal of the contribution on the global joint rotation can be observed in Figure 13, where the ratios $\frac{\Phi_b}{\Phi}$, $\frac{\Phi_c}{\Phi}$ and $\frac{\Phi_t}{\Phi}$ are presented versus m. Plotted curves confirm that the column contribution is limited, not greater that 25%, and the beam contribution is almost zero, so the overall rotation of the joint is mainly due to the contribution of the connector's deformation.

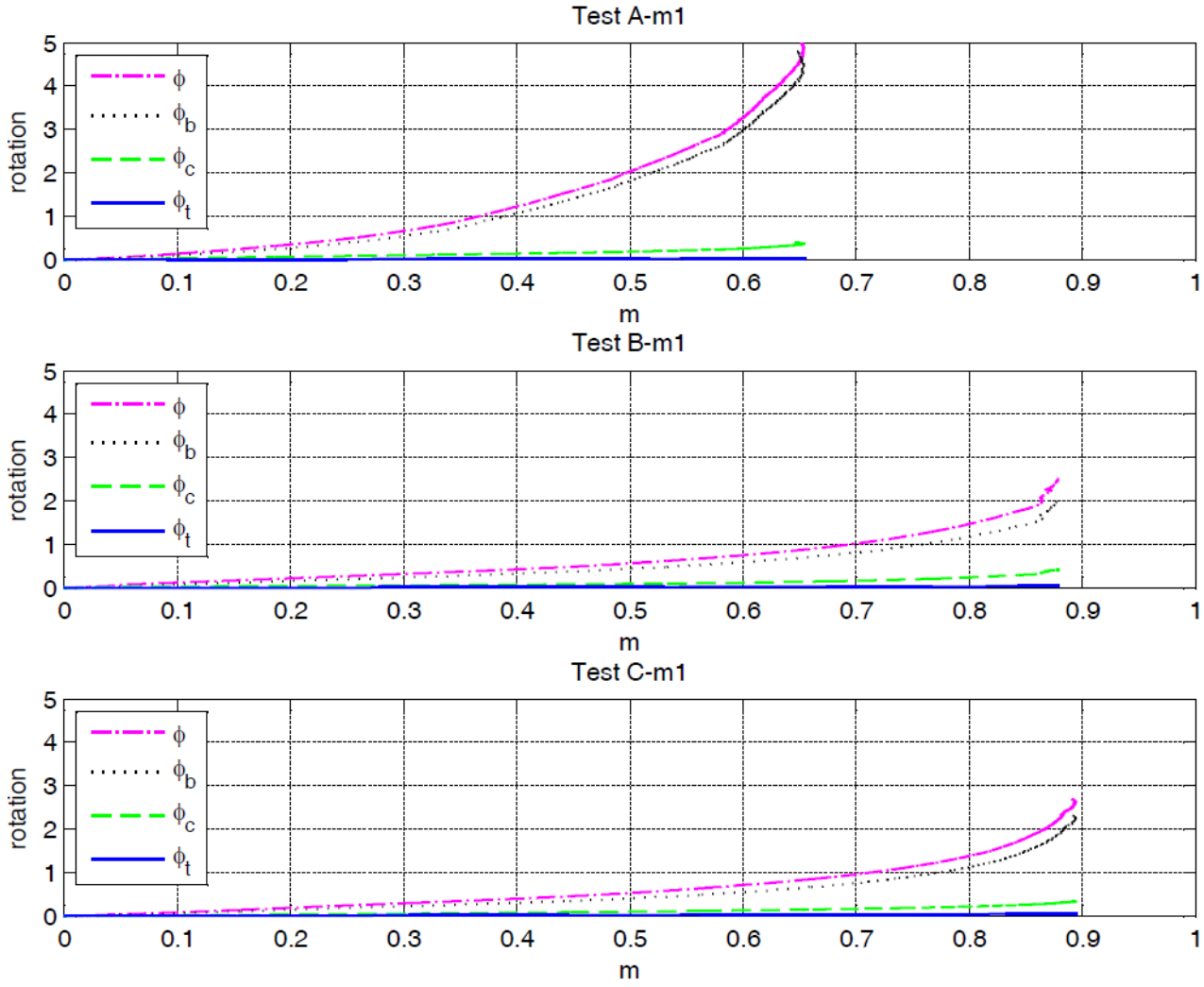

Figure 12. *Development of joint rotation components (the total rotation ϕ is evaluated at the distance L_2). See Table 1 for the type and designation of specimens.*

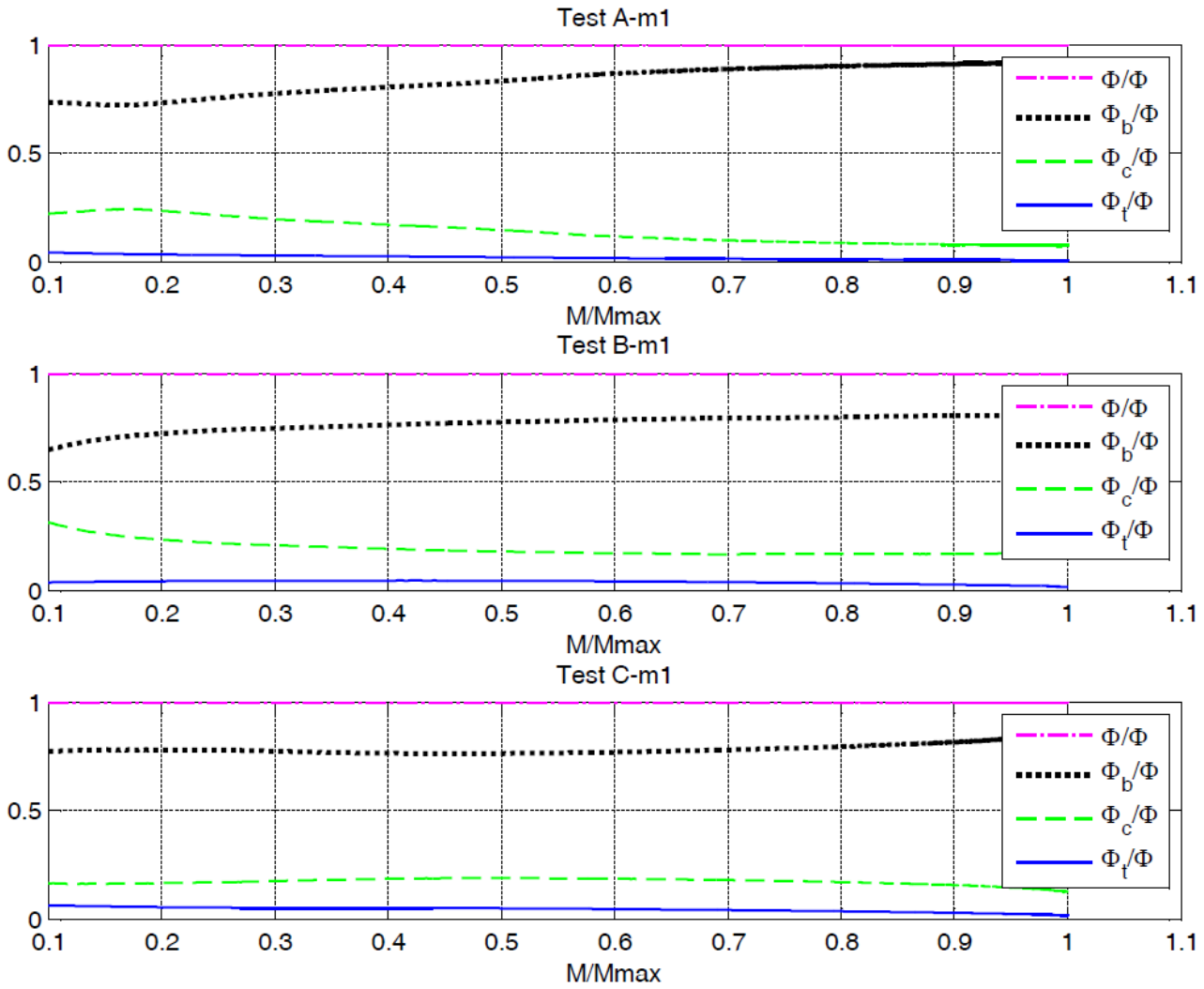

Figure 13. *Contributions to joint rotation.*

See Table 1 *for the type of specimen.*

2.5 Cyclic tests

The non-dimensional moment-rotation curves obtained applying the loading history shown in (Figure 7) are reported in Figure 14. It should be noted that the form of hysteresis loops is influenced by the number of cycles; the maximum bending moment in the first cycle of each group is greater than in subsequent two cycles, because of the degradation undergone by the connector device.

For each connection, the backbone curve, derived from the cyclic load-displacement curve by drawing a line between consecutive peak points of each primary cycle, fits the monotonic moment-rotation curve, larger differences are obtained for the connection of specimen *B-c1*, characterised by a weakest double-sided welding between the beam-end section and the connector.

In all connection types, a degradation of the peak moment can be observed in the second and third cycle of each group of cycles; the same holds for the dissipated energy per cycle, as clearly highlighted by the cumulated dissipated energy; see diagram in Figure 15 and percentage values of dissipated energy in Table 4.

Tabs show the same structural response under hogging and sagging moment as highlighted by the symmetry of the moment-rotation curve; moreover, the unloading branch has the same slope of the initial elastic branch of the first cycle.

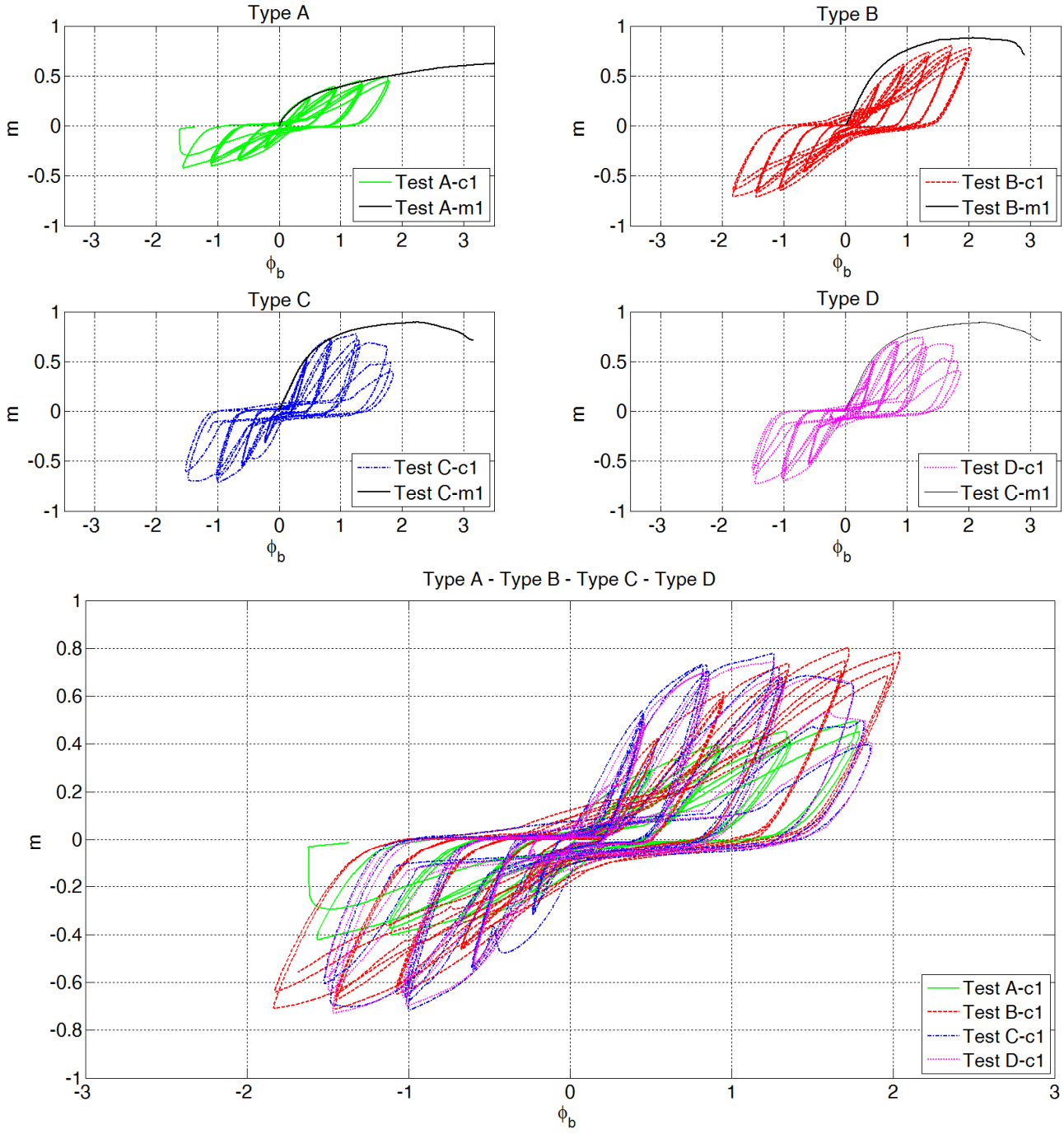

Figure 14. *Non-dimensional moment-rotation curves (with the contribution of the connector's deformation only).*

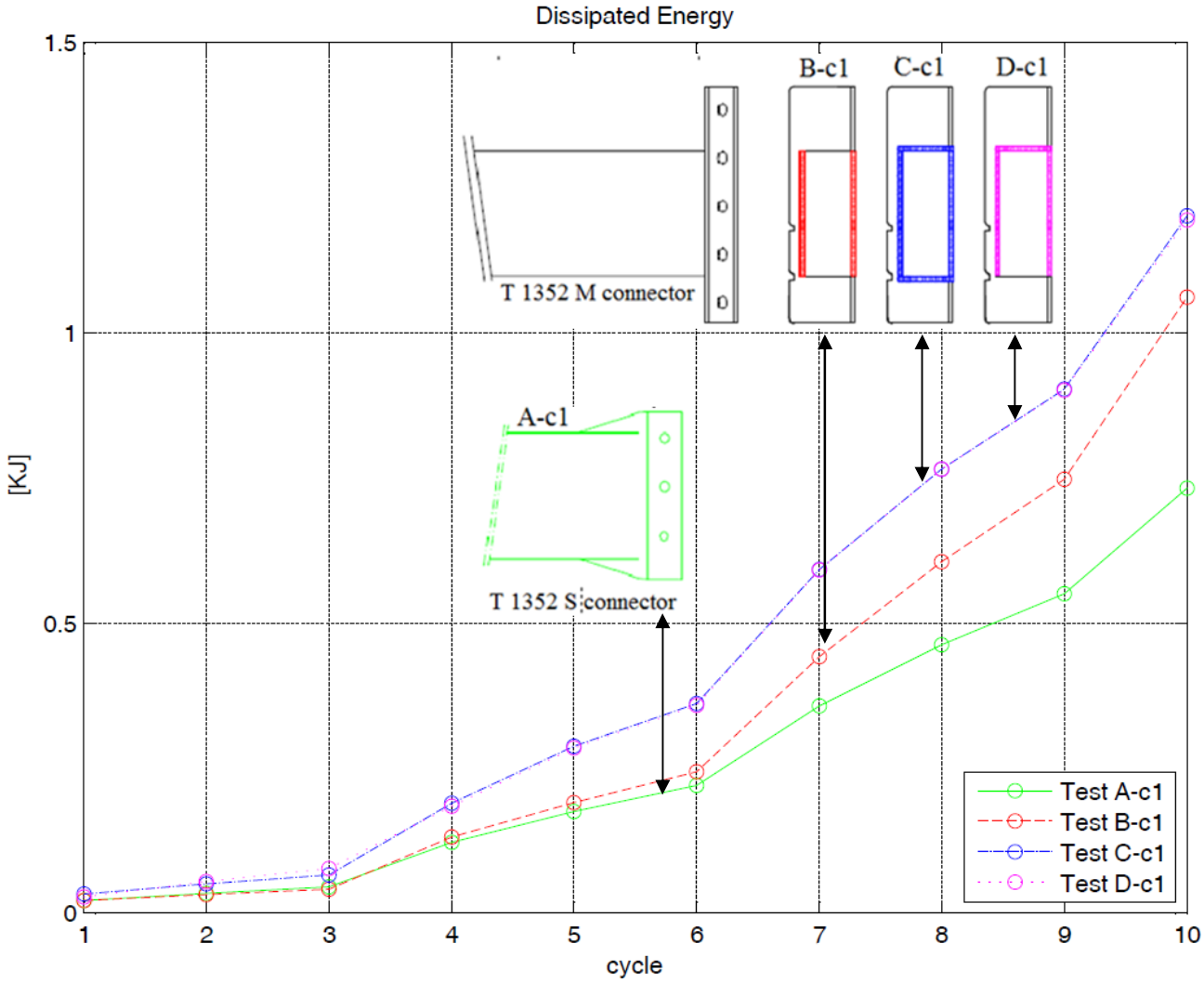

Figure 15. *Cumulated dissipated energy in the first ten cycles.*

Table 4. Degradation of the energy dissipation capabilities in each group of cycles.

Reference cycle	Cycle	$(E_j-E_i)/E_i$			
(i)	*(j)*	Test A-c1	Test B-c1	Test C-c1	Test D-c1
1st	2nd	57.2%	50.2%	53.9%	53.4%
	3rd	53.7%	45.1%	49.4%	48.9%
4th	5th	68.5%	65.9%	79.4%	78.6%
	6th	59.6%	59.3%	59.7%	59.1%
7th	8th	77.4%	82.6%	74.8%	74.1%
	9th	64.4%	72.1%	59.5%	58.9%

In cyclic tests ultimate rotations and bending moments assume lower values than in monotonic tests (Table 5 and Figure 14). The failure mode of type *B* connectors is the same of monotonic tests, as it is governed by the premature failure of welding (Figure 16). In type *A*, *C* and *D* specimens, lower values of ultimate rotations and moments than monotonic tests are due to the premature unlocking of the connector, which is enabled by the combination of residual plastic deformations of tabs and alternate forces in cyclic tests (hogging and sagging moment) (Figure 16).

Table 5. Values and comparisons among non-dimensional moment and connector rotation.

Load	Monotonic (i)	Cyclic (j)		Monotonic (i)	Cyclic (j)		Monotonic (i)	Cyclic (j)	
Test	A-m1	A-c1	A-c2	B-m1	B-c1	B-c2	C-m1	C-c1	D-c1
m_{max}	0,65	0,50	0,48	0,88	0,80	0,75	0,89	0,78	0,74
$\phi_{b\,max}$	5,01	1,79	1,84	2,91	2,04	1,80	3,17	1,86	1,87
$(m_j-m_i)/m_i$	Type A	-24,2%	-26,3%	Type B	-8,8%	-14,2%	Type C-D	-13,1%	-16,8%
$(\phi_{b\,j}-\phi_{b\,i})/\phi_{b\,i}$	Type A	-64,2%	-63,3%	Type B	-29,9%	-38,3%	Type C-D	-41,3%	-41,0%

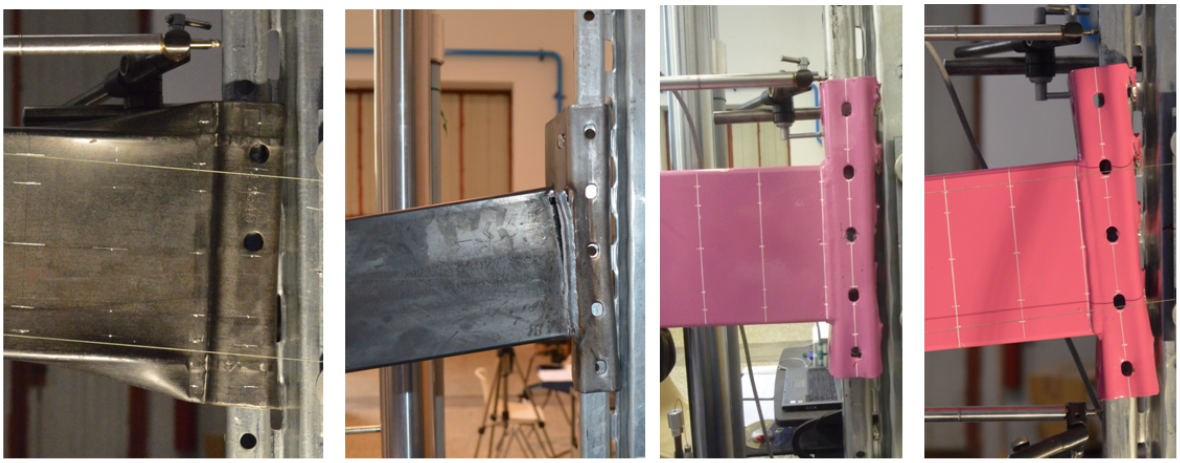

A *B* *C* *D*

Figure 16. *Different failure modes: unlocking of the connector (type A), fracture of the welding (type B), unlocking of the connector (type C) and unlocking of the connector (type D).*

On the base of results of cyclic tests (Table 5), the seismic design of pallet rack structures through non-linear static analyses with increasing horizontal loads (pushover analyses) could be on the unsafe side, as they do not allow for the cyclic degradation of connections and their reduced cyclic deformation capability to be taken into account. On the contrary, a reliable evaluation of the seismic response of these structures requires dynamic non-linear analyses, using a reliable approximation of the actual cyclic moment-rotation curve of rack joints.

2.6 Cyclic tests with additional bolts

Results of those cyclic tests, where the connector unlocked from the upright, suggested to carry out additional cyclic tests after modifying some joints by replacing the safety clip with an additional bolt (*C-c2b* and *D-c2b* specimens) or installing two additional bolts on the front plate of the connector (*D-c3bb* specimen). In Figure 17 non-dimensional bending moment-rotation curves of specimens belonging to the same connection type (*C* and *D*) are compared. It is evident that the additional bolt does not change the structural response of the joint, since neither the moment-rotation curve nor the ultimate moment vary significantly (Table 6). Main consequences of preventing the connector's unlocking through the additional bolt are a higher ultimate rotation (Table 6) and a different failure mode, which is due to the collapse of tabs (Figure 18) like in monotonic tests and not to the connector's unlocking.
The installation of two additional bolts on the front plate of the connector (*D-c3bb* specimen, Figure 5) modifies considerably the moment-rotation curve, as the pinching disappears and is substituted by reloading branches with higher stiffness. Bolts make the connection more resistant and stiffer, so

a higher ultimate moment is achieved at a smaller rotation (Table 6); the weakest element of the connection becomes the welding of the beam-end section (Figure 18).

Table 6. Cyclic non-dimensional moments and connector rotations and comparison with monotonic results.

monotonic test (i)		cyclic test (j)				
C-m1		C-c1	D-c1	C-c2b	D-c2b	D-c3bb
m_{max}	0,89	0,78	0,74	0,71	0,70	0,95
$\phi_{b\ max}$	3,17	1,86	1,87	3,19	3,27	2,24
$(m_j-m_i)/m_i$		-13,1%	-16,8%	-20,2%	-22,0%	6,0%
$(\phi_{b\ j}-\phi_{b\ i})/\phi_{b\ i}$		-41,3%	-41,0%	0,8%	3,3%	-29,4%

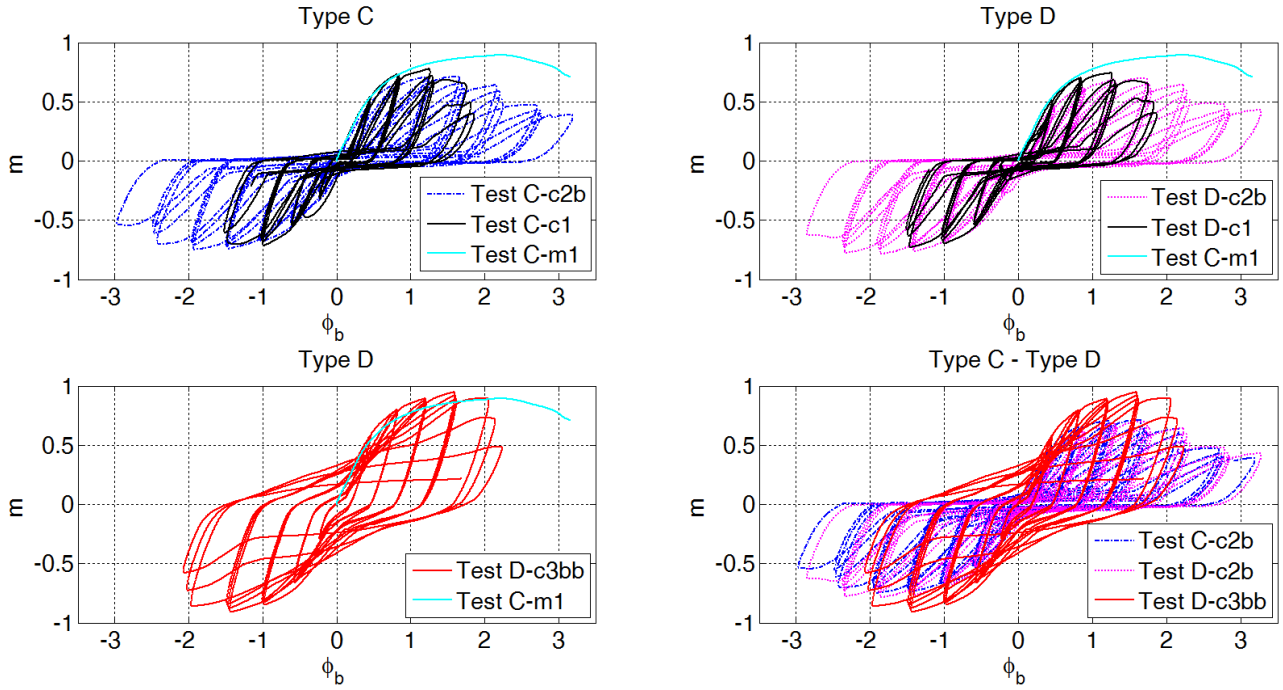

Figure 17. *Non-dimensional moment-rotation curves with the contribution of the connector's deformation only.*

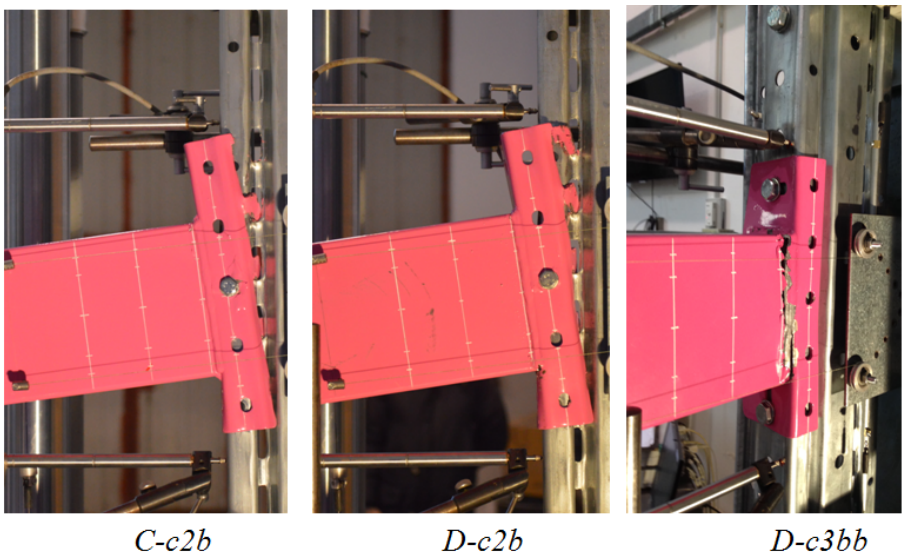

Figure 18. *Different failure modes: Failure of tabs (type C - test C-c2b with one additional bolt), failure of tabs (type D - test D-c2b with one additional bolt) and fracture of the welding (type D - test D-c3bb with two additional bolts).*

Differently from several literature cases [Bernuzzi and Castiglioni, 2001 and Aguirre, 2005] , where reloading branches are characterised by a gap horizontal line (zero moment) which increases as long as loading cycles increase, in tested connections the reloading branch starts when the rotation is reversed. The gap effect is a result of the yielding of tabs and their residual deformations [Aguirre, 2005], which is limited by internal tabs in tested connections (Figure 19). External tabs are distant from the connector's centre of rotation, so they are characterized by high stresses and residual plastic deformations, while internal tabs are close to the centre of rotation, so they remain in the elastic field and provide stiffness during the reloading phase (Figure 20). When all tabs start to perform in tension stress, the bending moment-rotation curve fits the monotonic one. The gap increases when the backbone curve is characterised by a softening branch due to the failure of external tabs and internal tabs plasticize. Internal tabs of connectors increase the stiffness of reloading branches and as a consequence reduce the pinching phenomenon, so that they allow for a greater dissipation of hysteretic energy.

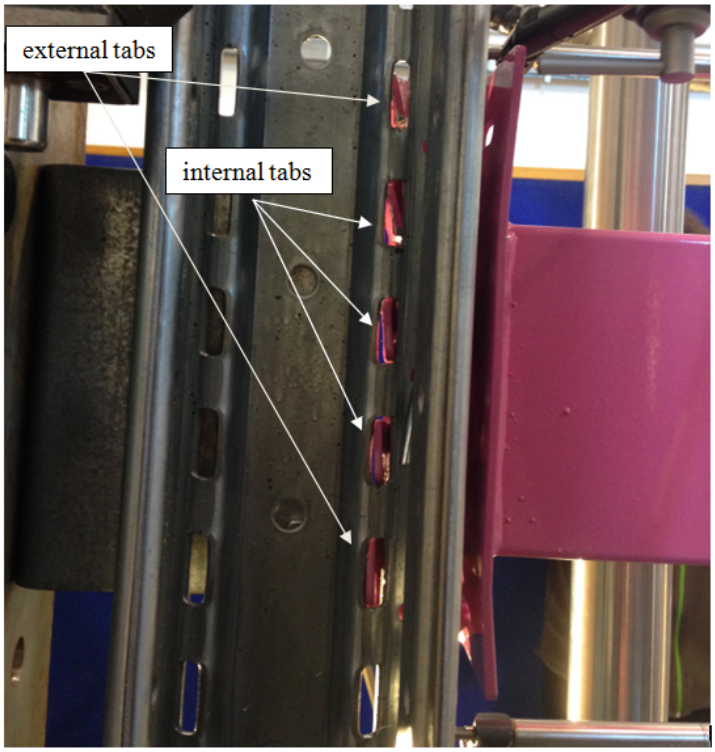

Figure 19. *Deformations of C type connection, in correspondence of the zero load level after several hysteresis cycles. External tabs are characterized by plastic deformations; internal tabs remain in the elastic field.*

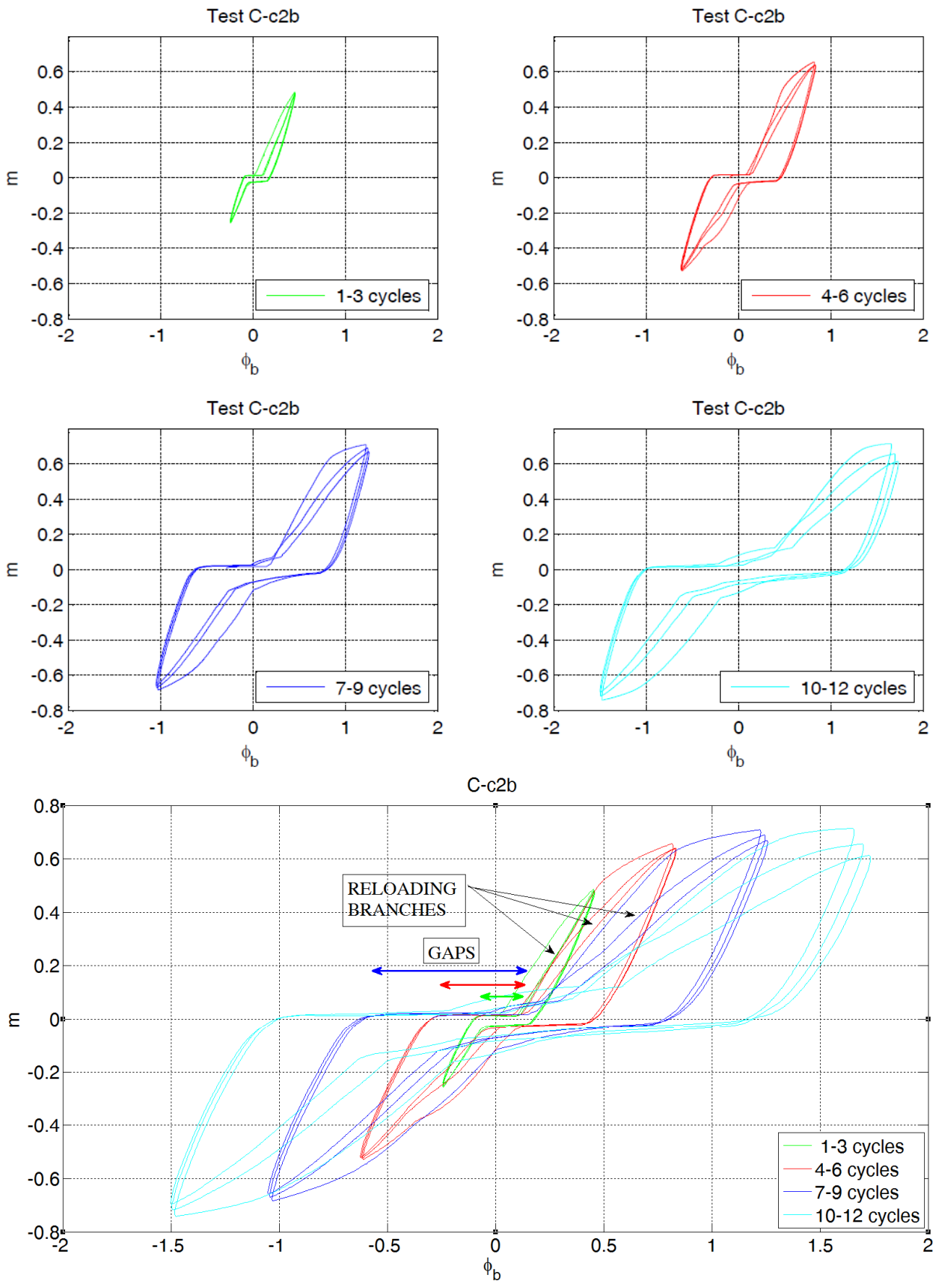

Figure 20. *Comparison of groups of cycles for C-c2b test.*

Regarding the cumulated dissipated energy per cycle (see diagram in Figure 21), it is evident that bolts increase the dissipated energy. Particularly, the installation of two additional bolts in the specimen *D-c3bb* reduces the degradation of the dissipation capability in each group of cycles (Table 7). On the basis of these considerations can be concluded that, by simply bolting the beam-end connectors to the uprights, it is possible to increase the structural response of rack joints. Bolted moment connections may represent a cost-effective alternative to ``tab connectors".

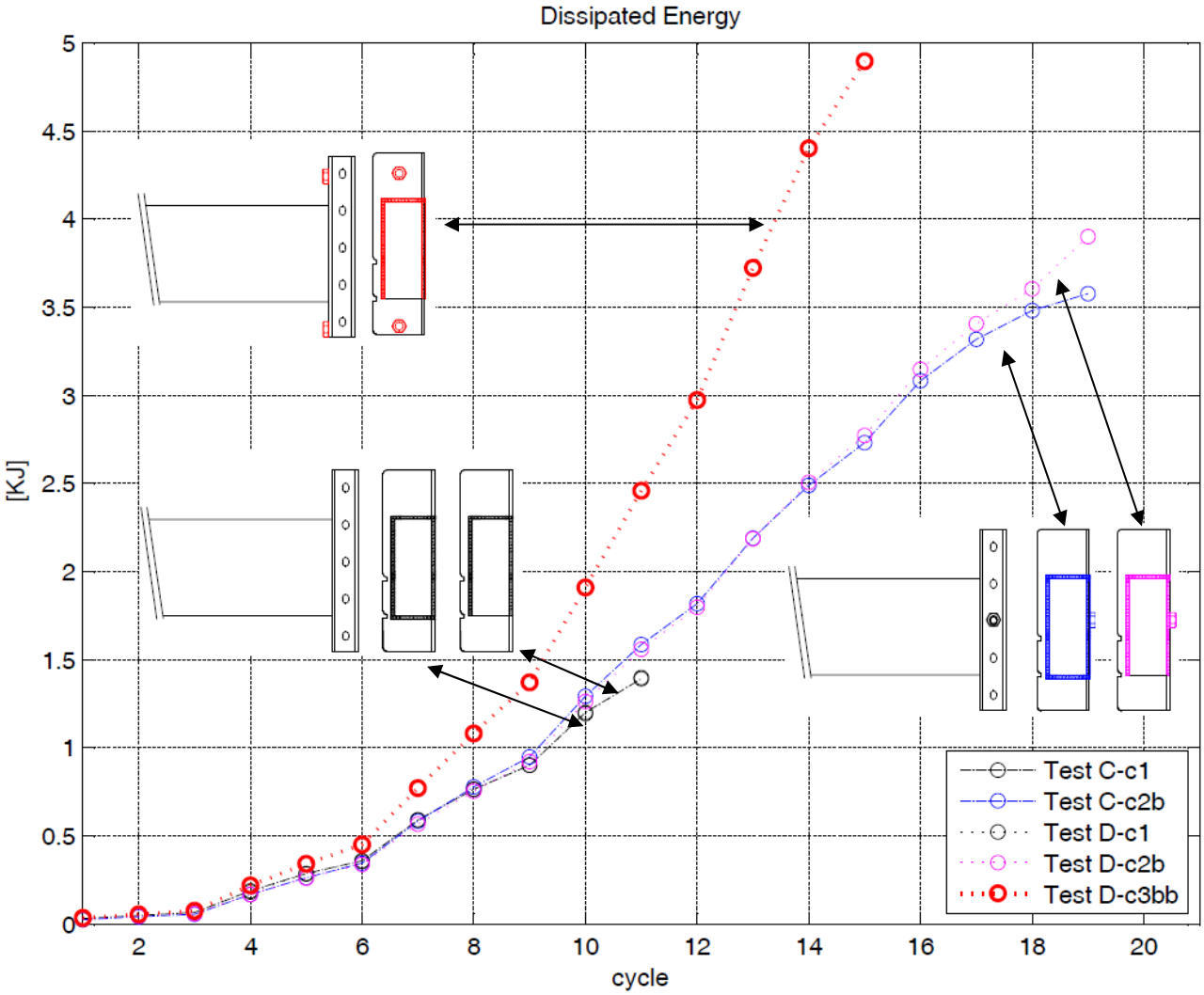

Figure 21. *Cumulated dissipated energy.*

Table 7. Degradation of the energy dissipation capabilities in each group of cycles.

Reference cycle	Cycle	$(E_j-E_i)/E_i$		
(i)	*(j)*	Type C (C-c2b)	Type D (D-c2b)	Type D (D-c3bb)
1st	2nd	63.3%	61.1%	63.1%
	3rd	61.5%	52.9%	59.6%
4th	5th	84.9%	87.4%	86.9%
	6th	73.6%	71.1%	78.5%
7th	8th	81.3%	82.8%	96.7%
	9th	71.4%	73.4%	90.7%
10th	11th	84.8%	85.4%	101.8%
	12th	66.8%	69.4%	95.5%
13th	14th	81.2%	82.1%	90.4%
	15th	64.8%	68.2%	66.1%

With reference to Table 4 and Table 7, because of the slippage phenomenon [Gilbert and Rasmussen, 2010], the degradation of the energy dissipation in the first group of cycles is greater than in subsequent groups of cycles. More precisely, in the first cycle, tabs and bolts start to cut the steel web of the upright (Figure 22), while in the second cycle a slippage occurs due to the sliding of tabs (and nuts in joints with additional bolts) in the upright's holes.

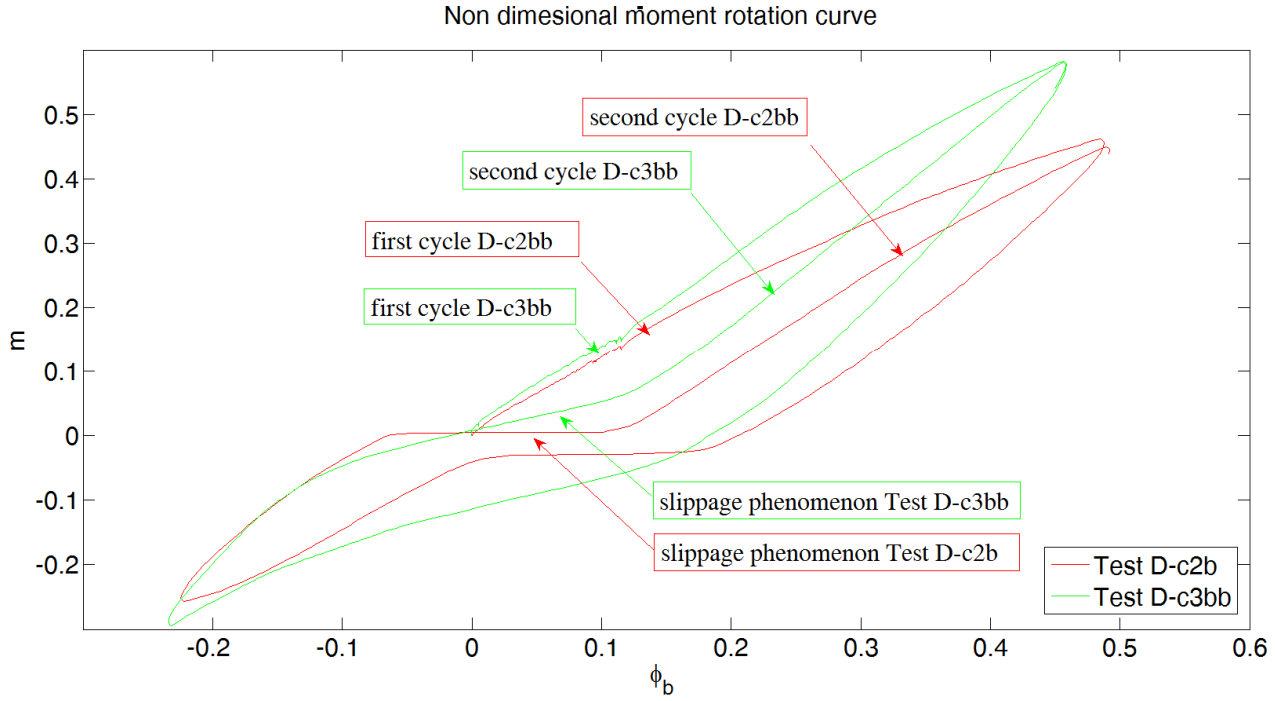

Figure 22. *Slippage phenomenon (first and second loading cycles in tests D-c2bb and D-c3bb).*

2.7 Summary of main results

In order to increase the knowledge about the structural behavior of rack connections, beam-to-column connections of steel storage pallet racks have been tested under monotonic and cyclic loads. Apart from joints where the connector is obtained by folding the beam end, all other joints have the connector welded to the beam and they only differ from one another in the welding layout. The comparison among experimental results, under monotonic and cyclic loading, allowed the relationship between moment-rotation curves and structural details of each type of joints to be identified.

Regarding to monotonic tests, the failure of joints with folded beam-end section is associated to the punching of the upright web, because of the greater thickness of tabs with respect to the upright. This type of joint is more deformable, with a limited ultimate moment due mainly to a lower number of tabs and a lower lever arm.

In the other connection types, where the connector is welded to the beam-end section, the key role of welding has been shown. In particular, in connectors with double-sided welding, the welding is the weakest element of the joint, while in connectors with the welding extended all-around the beam-end section, the connection failure is associated to the collapse of tabs, with higher ultimate moments and rotations.

Results of experimental tests confirmed that the failure mode of connections depends on the weakest component of the joint. In a connection with an adequate beam-connector welding, the failure mode depends on the ratio between the thickness of the upright and the thickness of tabs.

In cyclic tests, for all types of tested connections, hysteresis loops of the bending moment-rotation curve are characterized by pinching, with a reduction of the energy dissipation. Cyclic tests have

highlighted that internal tabs, that is tabs located inside the beam height, behave differently from external tabs, as they undergo a limited plastic deformation also for greater moments, and allow the slope of reloading branches of hysteresis loops to be increased, with higher dissipated hysteretic energy.
During cyclic tests, most specimens collapsed because of the pull out of tabs from upright's slots, with lower ultimate moments and rotations in comparison with monotonic tests.
Finally, some rack connections have been tested with additional bolts which, avoiding the connector's unlocking, allowed the dissipated energy and the ductility of joints to be increased. Last results show that the use of additional bolts can represent an effective solution to improve the seismic response of steel storage pallet racks within the context of a seismic vulnerability analysis.

3 THEORETICAL ANALYSIS

3.1 Component Method applied to rack connections

Experimental testing is particularly useful for determining seismic performance, providing useful information about the semi-rigid behavior and ductility of rack connections. Despite the success and popularity of experimental testing, experimental tests can be expensive and time-consuming. Vice-versa the designer needs a method that starting from features of the connections allows to obtain the main characteristic of the beam-column joint to be used in structural analysis of moment resisting frames (MRFs). Therefore current state-of-art models for steel joints are based on the Component Method (CM) whereby a joint is modeled theoretically as an assembly of components with an elasto-plastic or rigid force-displacement relationship.
Mechanical models based on the CM are able to evaluate the initial elastic rotational (flexural) stiffness $S_{ini,exp}$ and ultimate bending moment $M_{u,exp}$ (Figure 23) of the connection monotonic moment-rotation curve. The initial rotational stiffness $S_{ini,exp}$ is given by the initial linear branch of the experimental moment-rotation curve, while $M_{u,exp}$ is chosen as the maximum value of the moment on the same curve. Both are fundamental parameters in the design and analysis of MRFs, such as racks, under seismic loads [Zhao et al., 2017]. Initial rotational stiffness is also critical for determining deflection limit states under service loads which typically govern rack beam design [Godley, 1997]. Moreover, mechanical models can be adopted to investigate the influence on connection response due to structural details, with the aim to improve beam-column joint structural capacity [Shah et al., 2016 (b)].

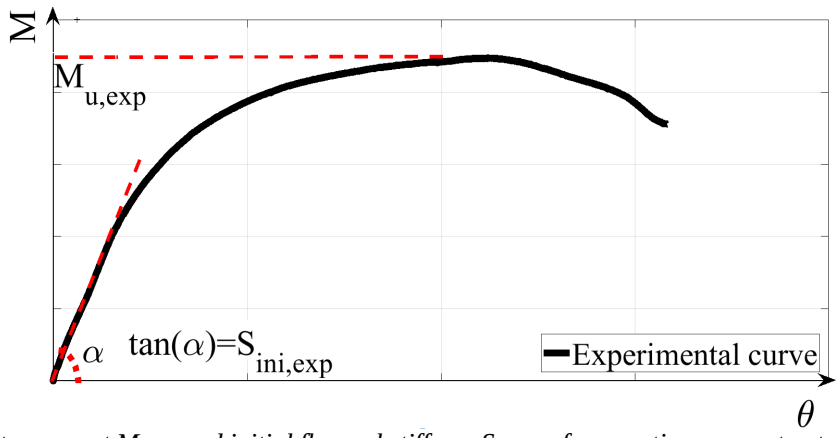

Figure 23. *Ultimate moment $M_{u.exp}$ and initial flexural stiffness $S_{ini,exp}$ of connection moment-rotation experimental curve.*

The CM can be applied to any kind of connection, provided that the basic sources of strength and deformation are properly identified and modeled [Faella et al., 2000]. The CM can be organized in three phases. The first is to identify the components in the connection, contributing to structural response. In the second phase each component is modeled via a force-displacement relationship. Bilinear elasto-plastic models (defined by an initial stiffness and an ultimate strength) are used for components that contribute to the stiffness and strength of the connection, whereas a rigid plastic model is used for components that effect connection strength, but not stiffness. These component models are introduced into the mechanical model of the overall connection with springs joined in series or parallel, each with their own lever arm and axial stiffness [EN 1993-1-8, 2005]. In the last phase, flexural strength (ultimate moment $M_{u,num}$) and initial elastic rotational stiffness ($S_{ini,num}$) of the joint are predicted.
It is worth noting that, in the CM, components are assumed to have infinite ductility, meaning that no predictions about the rotational capacity of the connection are made.

In the following chapter, following the approach proposed in [Ślęczka and Kozłowski, 2007 and Zhao et al., 2017], the CM is applied to the investigated rack connections with the aim to developed a general model for the analysis of rack beam-to-column joints.
The comparison between theoretical and experimental results highlights the accuracy of the proposed model that allows the weakest component of the joint and its failure mode to be evaluated. The CM provides fundamental information about the influence of structural details on the joint behavior, and it could be used in the design of rack connections to improve their structural response.

3.2 Investigated rack connections

To evaluate the accuracy of the proposed mechanical model and to assess the influence of different structural details on the rack connection mechanical behavior, theoretical results have been compared with those obtained through the previous experimental tests and with results of an experimental campaign performed on other full-scale connections, differentiated by varying assemblies of their members, and produced by the same manufacturing company.
In particular, three rectangular tubular cross sections were adopted for the beam (Table 8), two weld configurations between the end of the beam (beam-end section) and connector, two types of connector and five mono-symmetric open cross-section for the column (Table 8). The as-tested experimental configurations are shown in Table 9. Figure 24 depicts the geometric properties of the rack connection members.

Table 8. Parameters varied in experimental testing at the University of Florence

Member	**Type**	**Geometric properties**		
		Height [mm]	Width [mm]	Thickness [mm]
Beam	1042	100	40	2
	1242	120	40	2
	1352	130	50	2
Column	70/150	68	72	1.5
	90/150	78	92	1.5
	110/200	84	112	2
	130/200	102	132	2
	130/250	102	132	2.5
Connector	M4 (4 tabs)	195	82	3.5
	M5 (5 tabs)	245	82	3.5
Weld	A	Three-sided welding		
	B	Double-sided welding		

Table 9. Rack connections tested and members used to assemble them (● Experimental Test).

Beam	**Weld**	**Connector**	**Column**				
			70/150	90/150	110/200	130/200	130/250
1042	A	M4	●	●			
1242	A	M5	●	●	●	●	
1352	A	M5		●	●	●	●
1042	B	M4					
1242	B	M5					
1352	B	M5					●

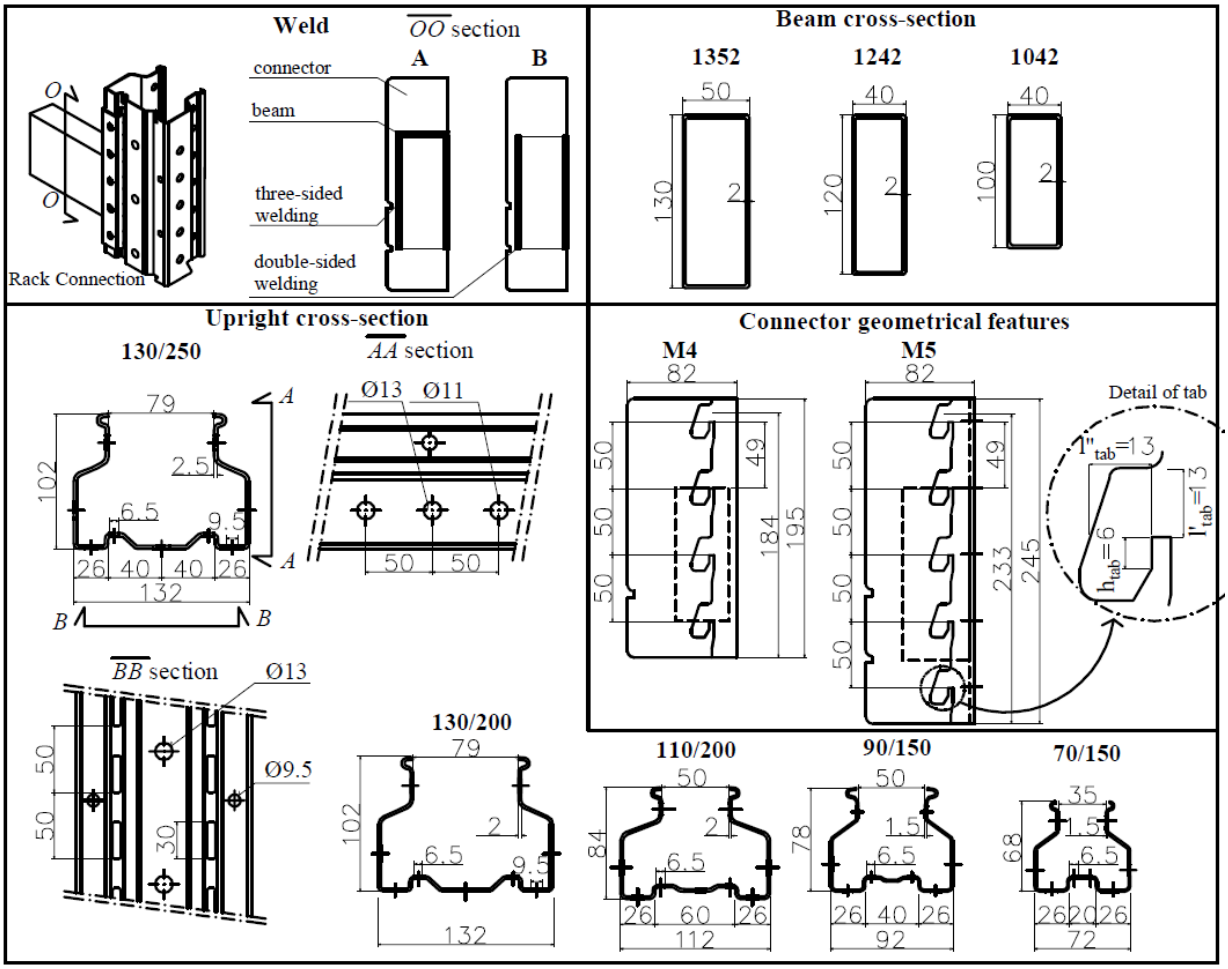

Figure 24. *Geometrical features of rack connection members.*

All connections were tested by the single cantilever testing method (Figure 6). Using the quantities defined in Figure 8a), according to [Yin et al., 2016], it is possible to experimentally determine moment on the connection $M=LP$ and the connection rotation $\theta = \theta_{cd} - \theta_{ce}$; where, $\theta_{cd} = \frac{s_1 - s_2}{k_{12}}$ is the total rotation of the connector and $\theta_{ce} = \frac{Mh_c}{16EJ_c}$ is the elastic rotation of the column at the level of the intersection with the beam; with: h_c the height of the column, E the elastic modulus of steel, J_c the inertia moment of the column, s_1 and s_2 the horizontal displacements measured by wire-actuated encoders placed on top and bottom of the beam-end section, and k_{12} is their relative distance (Figure 8a). Testing procedures, instrumentations and detailed test results of analysed joints can be found in [Giordano et al., 2017 and Bertocci and Comparini, 2015].

3.3 Component models

The mechanical model is established based on a set of realistic assumptions, taking advantage of the Eurocode 3 framework for determining the theoretical load-displacement behavior of basic components [EN 1993-1-8, 2005], as well as the theoretical model of boltless connections presented in [Ślęczka and Kozłowski, 2007 and Zhao et al., 2017]. It is worth noting here that force transfer in rack connections differs in the tension and compression zones. In the tension zone, forces are transferred through tabs while in compression zone, force is transferred through contact between the connector bottom flange and the column. New models are proposed to describe the structural

response of each identified component that, considering the bending moment transfer path from the beam to the column, can be identified in the order:

3.3.1 Weld

The weld is the component that connects the beam-end section with the connector flange (Figure 25); it has to be considered only in the evaluation of the connection resistance and it is modeled by means of a rigid-plastic model with a resistance that can be computed by the equation (12), assuming an elastic distribution of stresses and the welding failure at the reaching of the yield stress in the extreme fibre.

$$F_{wel} = \frac{M_{\max,b}}{h_b} = \frac{J_w f_{y,w}}{h_b y_w} \tag{12}$$

where :
$M_{max,b}$ is the maximum bending moment transferred by the beam;
h_b is the height of the beam;
y_w is the distance between the welding center of area and the welding upper extreme fibre;
$f_{y,w}$ is the welding yielding tensile stress;
J_w is the inertia moment of the welds:

$$J_w = 2J_{wa} \qquad \text{(test with 1352B beam);}$$

$$J_w = 2J_{wa} + 2A_{wa}(x_w - x_{wa})^2 + J_{wb} + A_{wb}(x_w - x_{wb})^2 \qquad \text{(all other tests);}$$

with:

$$J_{wa} = \frac{1}{12} a_{wa} h_b^{*3} \quad \text{and} \quad A_{wa} = a_{wa} h_b^*$$

$$J_{wb} = \frac{1}{12} a_{wb}^3 b_b^* \quad \text{and} \quad A_{wb} = a_{wb} b_b^*$$

where:
a_{wa} is the effective throat thickness of lateral welds;
a_{wb} is the effective throat thickness of the upper weld;
h_b is the height of the beam;
b_b is the width of the beam;
$h^* = h - 2\sqrt{2}a_{wa}$ is the effective height of the weld on the beam;
$b^* = b - 2\sqrt{2}a_{wb}$ is the effective width of the weld on the beam;
x_w is the distance of the welding center of area from the beam bottom flange.
x_{wa} and x_{wb} are the distance of lateral welding center and upper welding center from the beam bottom flange.
The failure mode of welding, observed during the tests is shown in Figure 26.

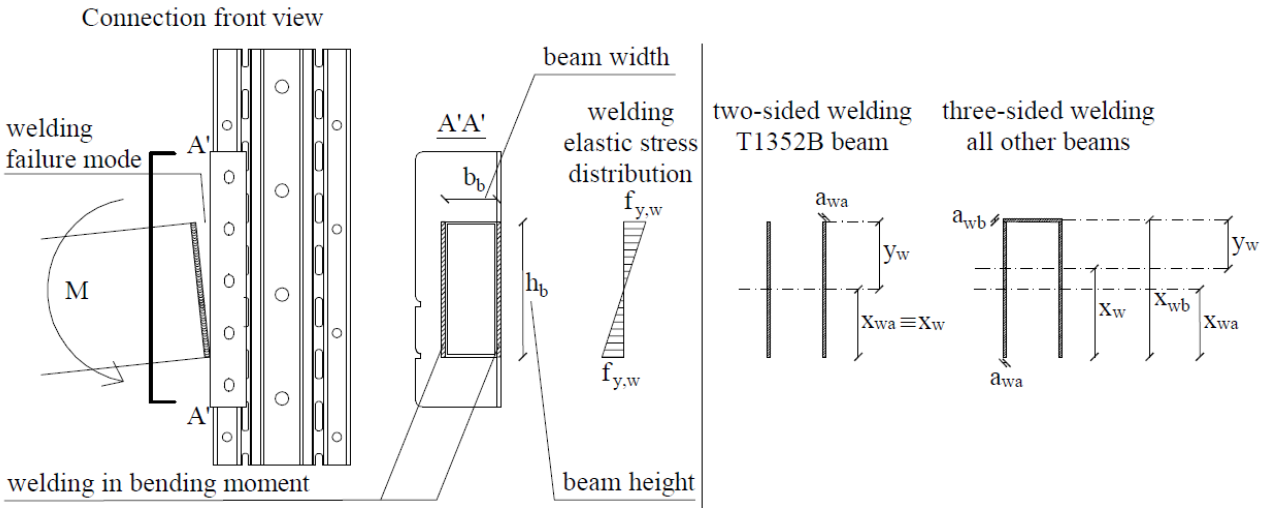

Figure 25. *Failure model of welding in stress (B type of welding).*

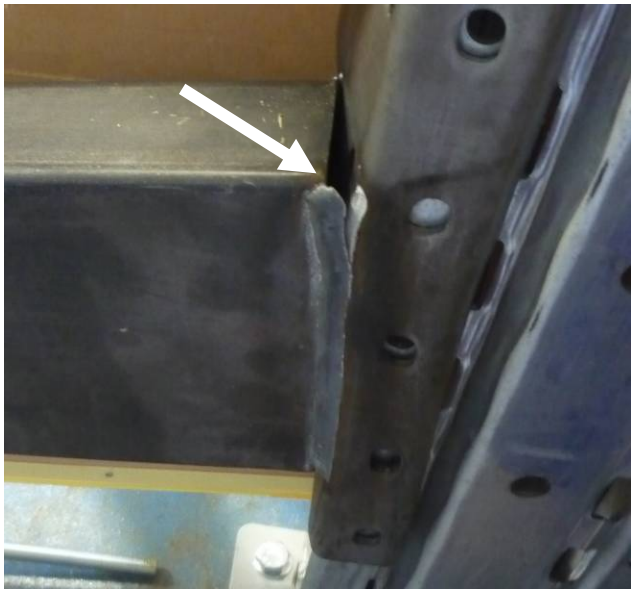

Figure 26. *Failure of welding observed in test 130/250-1352B (two sided – welding).*

It should be noted that the failure of the weld has been assumed considering an elastic distribution of normal stresses and neglecting the shear force effect. For a rectangular cross-section (b=base and h=height) under an elasto-plastic distribution of stress, the following relationship holds: $\frac{\overline{M}}{M_p} = 1 - \frac{3}{4}\left(\frac{\overline{T}}{T_p}\right)^2$, where: $\overline{M}$ and $\overline{T}$ are the effective bending moment and shear force, $M_p = \frac{f_y b h^2}{4}$ and $T_p = \tau b h$ are the plastic moment and the plastic shear, with f_y the yield stress of the material and τ the ultimate shear stress [Pozzati, 1980]. For a cantilever beam, a transversal load $\overline{T} = \frac{M_p}{L} = \frac{f_y b h^2}{4L}$, applied at a distance L from the fixed restraint, produces on the restrained section the plastic moment. Assuming von Mises criterion for the evaluation of the plastic shear and the Jourawsky formula for the evaluation of the shear stress, following expressions hold: $T_p = \frac{f_y}{\sqrt{3}} b h$ and $\frac{\overline{T}}{T_p} = \frac{\sqrt{3} h}{4L}$, which, for L=4$h$ (=400 mm, Figure 6) as in the present case, give

$\frac{\overline{T}}{T_p} = 0.108$ and $\frac{\overline{M}}{M_p} \approx 0.99$, therefore the reduction of the plastic moment due the shear force is negligible.

3.3.2 Beam flange in tension and in compression

In the evaluation of the connection resistance, the beam flange in tension and compression has to be considered. The model assumed to assess the tension and compression beam flange resistance $F_{bf,t}$ and $F_{bf,c}$ respectively (13) is depicted in Figure 27:

$$F_{bf,t} = F_{bf,c} = b_{eff,b} t_b f_{y,b} \tag{13}$$

where:
t_b is the thickness of the beam;
$f_{y,b}$ is the yielding stress of the beam;
$b_{eff,b}$ is the width of the beam considering the tangent of the spread angle 1:x (Figure 27). In literature [Ślęczka and Kozłowski, 2007], or using analogy to column web in compression [EN 1993-1-8, 2005], a value of x=2.5 is proposed. In the present paper, $b_{eff,b}$ has been chosen equal to the beam width. This choice allows for a good evaluation of $F_{bf,c}$ in compression zone, where the force is transferred by the contact between beam bottom flange and column web, and for the evaluation of $F_{bf,t}$ in tension zone for a weld layout type A (three-sided welding). In the case of a welding layout type B (double-sided welding), the beam bottom flange continues to work under compression while the tension force, relative to the beam top flange, is transferred to the connector by the lateral beam web, whose contribution has been neglected in connections type A. If for sake of simplicity the same angle of spread is assumed on the beam web, the $F_{bf,t}$ of connection with a double-sided welding can be evaluated with an adequate accuracy

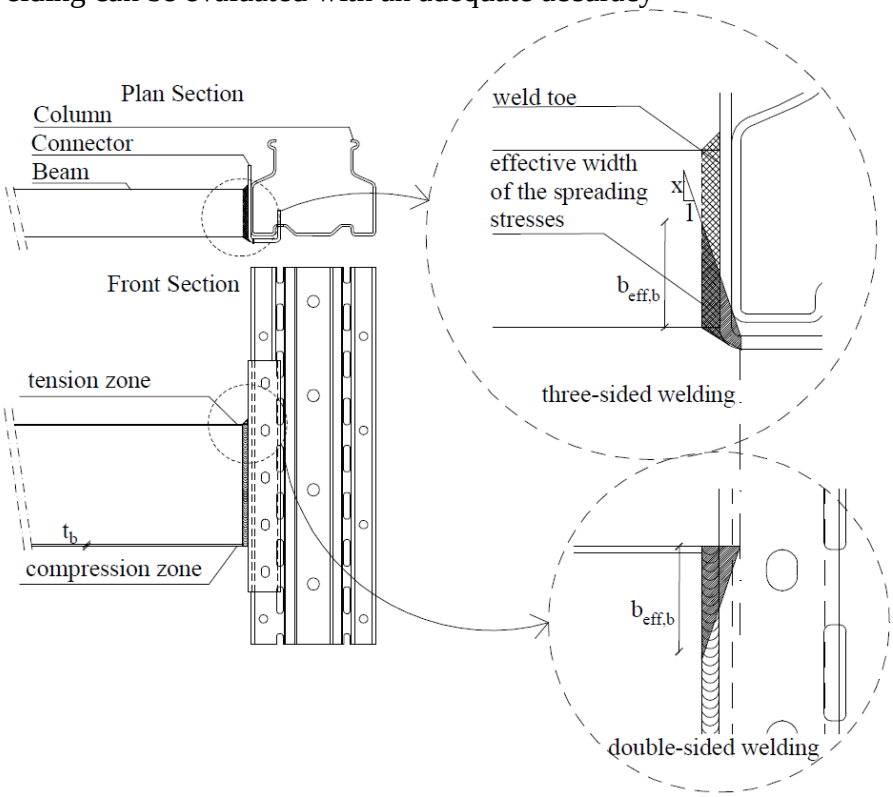

Figure 27. *The spreading of stress distribution in the beam flange (connection with a three-sided welding) and in the beam web (connection with a double-sided welding).*

3.3.3 Connector web in tension and in compression

In according to [EN 1993-1-8, 2005], the connector web resistance in the tension and compression zone, $F_{cow,t}$ and $F_{cow,c}$ respectively, can be estimated by using the equation (14):

$$F_{cow,t} = F_{cow,c} = \omega_{co} b_{eff,co} t_{co} f_{y,co} \tag{14}$$

where:
$f_{y,co}$ is the yield stress of the connector;
ω_{co} is the connector web reduction factor accounting for interaction with shear [EN 1993-1-8, 2005];
t_{co} is the thickness of the connector web;
$b_{eff,co}$ is the effective width of the connector web accounts for the spreading of the stresses transmitted by the beam flange, assuming the tangent of the spreading angle 1:2.5.
The axial stiffness assumed to describe the joint component behavior modeling the connector web in tension and compression, $K_{cow,t}$ and $K_{cow,c}$ respectively, is obtained by the relationship (15), assuming an angle of 45° for the load spreading (Figure 28).

$$k_{cow,t} = k_{cow,c} = \frac{E b'_{eff,co} t_{co}}{d_{wco}} \tag{15}$$

where:
d_{wco} is the clear depth of the connector web;
t_{co} is the thickness of the connector web;
E is the steel elastic modulus;
$b'_{eff,co}$ is the effective connector web width for stiffness (assuming the tangent of the spreading angle 1:1).

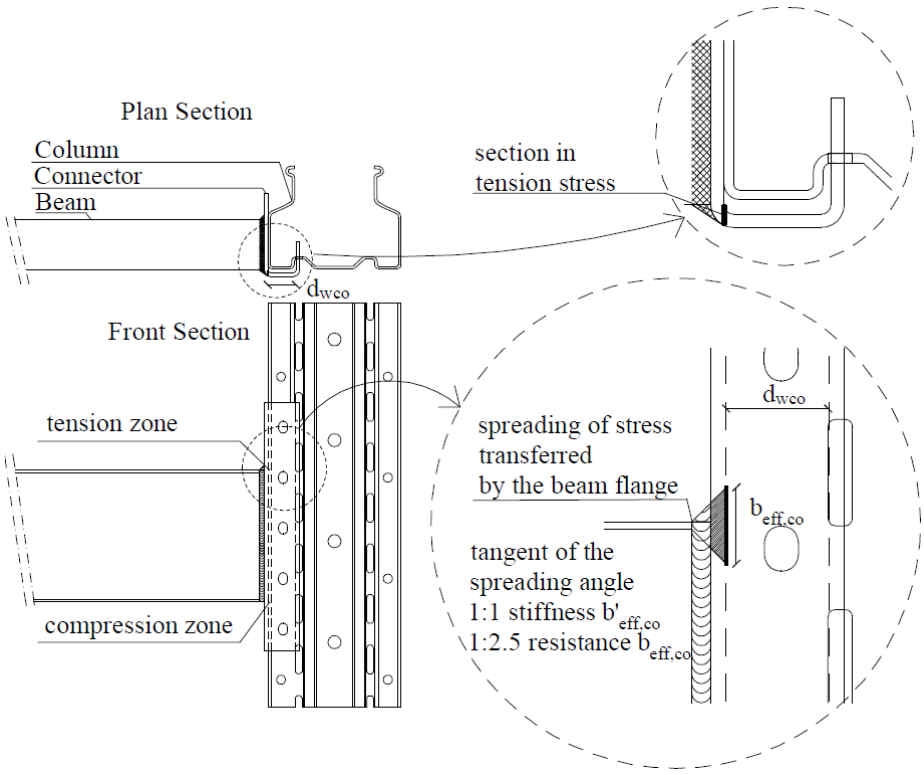

Figure 28. *Model of connector web in tension and compression.*

3.3.4 Connector in bending

The connector bending resistance, $M_{co,b}$, can be assumed equal to the plastic resistance (16) of a cantilever beam protruding over the flange surface of the beam (Figure 29).

$$M_{co,b} = W_{pl,co} f_{y,co} \tag{16}$$

where:
$W_{pl,co}$ is the plastic section modulus of the connector;
$f_{y,co}$ is the yield stress of the connector.
The initial elastic stiffness of this component can be evaluated by means of the relationship (17):

$$k_{co,i} = \frac{F}{\delta} \tag{17}$$

where:
F is the applied force;
δ is the deflection under the force F taking into account the effects of bending and shear.
In each connection, different values of stiffness have been calculated for external slot (force is acting in tab more distant to the beam flange) and internal slot (force is acting in tab closer to the beam flange). The connector, in correspondence of the tabs at the level of the beam, is considered rigid. Regarding to the compression zone, a uniform load is considered acting on the connector bottom flange for a length of $2z_c$, where z_c is the distance between the centre of compression and the beam bottom flange (Figure 29). The connector in bending, observed during the tests is shown in Figure 30.
It should be noted that, in the evaluation of the connector bending resistance, a plastic distribution of stresses has been assumed after checking that outstand elements forming the connector do not buckle under compression. Taking into account the connector protruding over the upper beam flange, because of forces transferred by tabs, the A outstand element (Figure 29), which belongs to 4th class according to [EN 1993-1-1, 2005], is in tension and the B outstand element (2nd class and restrained by tabs) is under compression. On the contrary, taking into account the connector flange protruding over the bottom beam flange, because of the force transferred by the contact with column web, the B element is in tension and the A plate is in compression and could undergo local buckling. Following the current standard code recommendation [EN 1993-1-5, 2006], the plate slenderness holds: $\bar{\lambda}_p = \frac{b_p / t_{co}}{28.4\varepsilon\sqrt{k_\sigma}} = 0.722 < 0.748$ and the reduction factor is ρ=1, with: b_p=75 mm the appropriate width of A element, t_{co}=3.5 mm the thickness of the connector, ε=0.924 and k_σ=1.277 the buckling factor evaluate according to [Ballio and Mazzolani, 1983] for fixed restrained outstand element; this result shows that the A element does not buckle under compression.

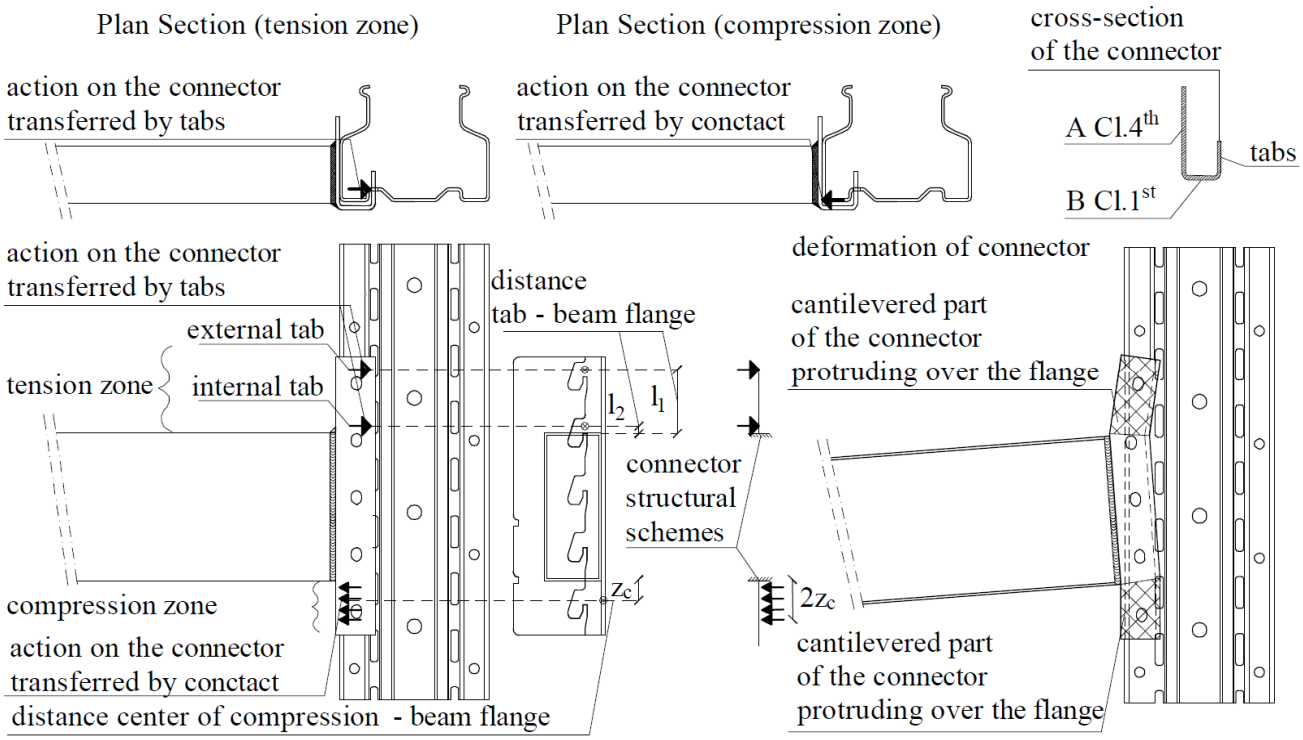

Figure 29. *Model of connector in bending.*

Figure 30. *Deformation of the connector in bending observed in the experimental test 130/250-1352A).*

3.3.5 Tabs in bending and in shear

The rotational behavior of the connection is affected by tab structural response. Tabs are in bending moment (Phase 1, Figure 31) and the structural scheme of a cantilever beam is used to evaluate their initial stiffness $k_{t,s}$ (18):

$$k_{t,s} = \frac{F}{\delta} \tag{18}$$

where:

$\delta = \left(\frac{l_F^3}{3EI} + \frac{1.2 l_F}{G A_v} \right) F$ is the deflection of the cantilever beam at the point where the concentrated load *F*, exerted by the column wall, is acting;
where:
G is the steel shear modulus;
E is the steel elastic modulus;
l_F is the lever arm of the force *F*;
$I = \frac{t_{tab}^3 l_{tab}^{'}}{12}$ is the inertia moment of the cantilever beam cross section area ;
$A_v = l_{tab}^{'} t_{tab}$ is the effective area of tab under bending moment (in Phase 1).
with:
t_{ab} the thickness of the tab;
$l_{tab}^{'}$ the length of the tab shear cross section (see Figure 31).
After the bending deformation, the tab is subjected to shear stress (Phase 2, Figure 31), and the column is in punching. This condition influences only the connection flexural resistance by means of the ultimate shear resistance of the tab $F_{t,s}$ (19):

$$F_{t,s} = \frac{f_{u,co} A_{v,tab}}{\sqrt{3}} \tag{19}$$

where:
$f_{u,co}$ is the ultimate stress of the connector;
$A_{v,tab} = t_{tab} l^{''}_{tab}$ is the effective shear area of the tab;
where:
t_{ab} the thickness of the tab;
$l^{''}_{tab}$ is the length of the tab shear cross section (Figure 31).
Deformations of tabs, due to bending in Phase 1 and its failure mode due to the shear in Phase 2, observed during the tests are depicted in Figure 32 *a)* and *b)* respectively. This component is active in the tension zone of the connection.

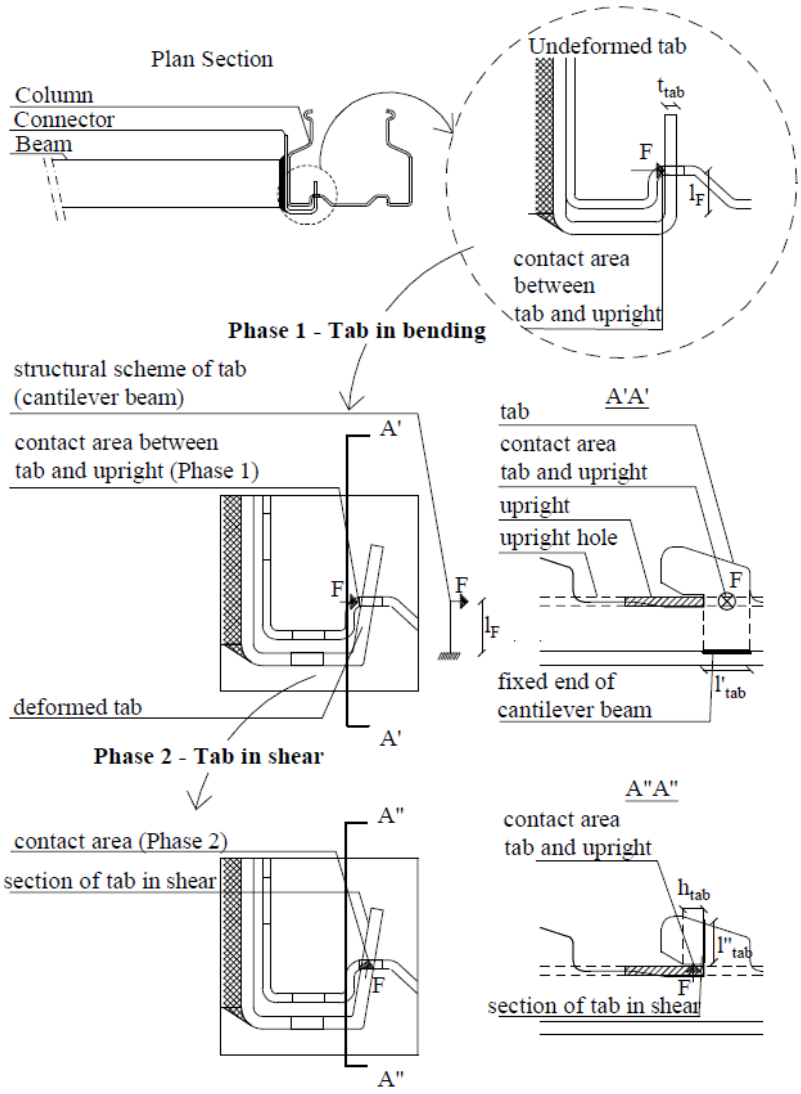

Figure 31. *Model used for tab component.*

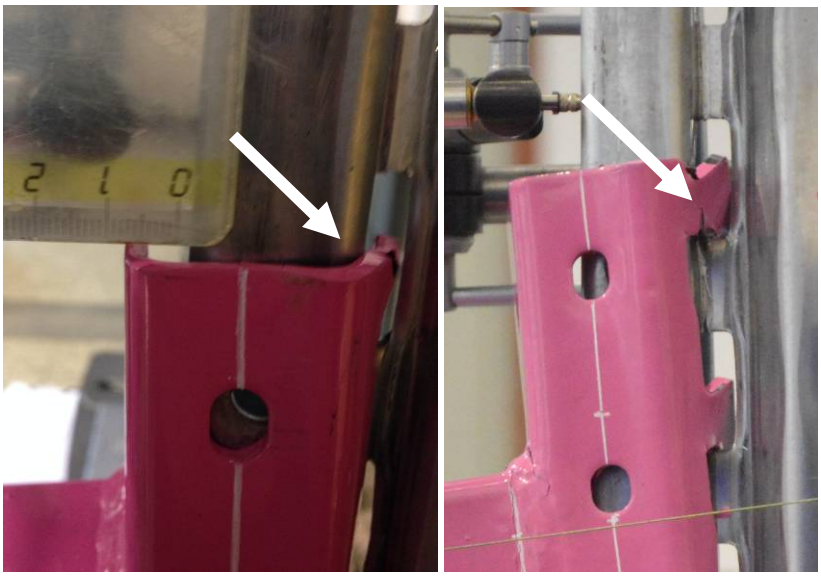

a) b)

Figure 32. *a) Initial bending deformation of the tab. b) Failure of the tab. Behavior shows in test 130/250-1352).*

3.3.6 Column web in punching

Among the column components, a part of the column web in correspondence of the slots is in punching, because of the load transferred via tabs (Figure 33). A fixed-ended beam of a span equal to the distance between two folds of column web, loaded by the contact force *F* transferred by tab, can be used to model the behavior of this component (Figure 33).

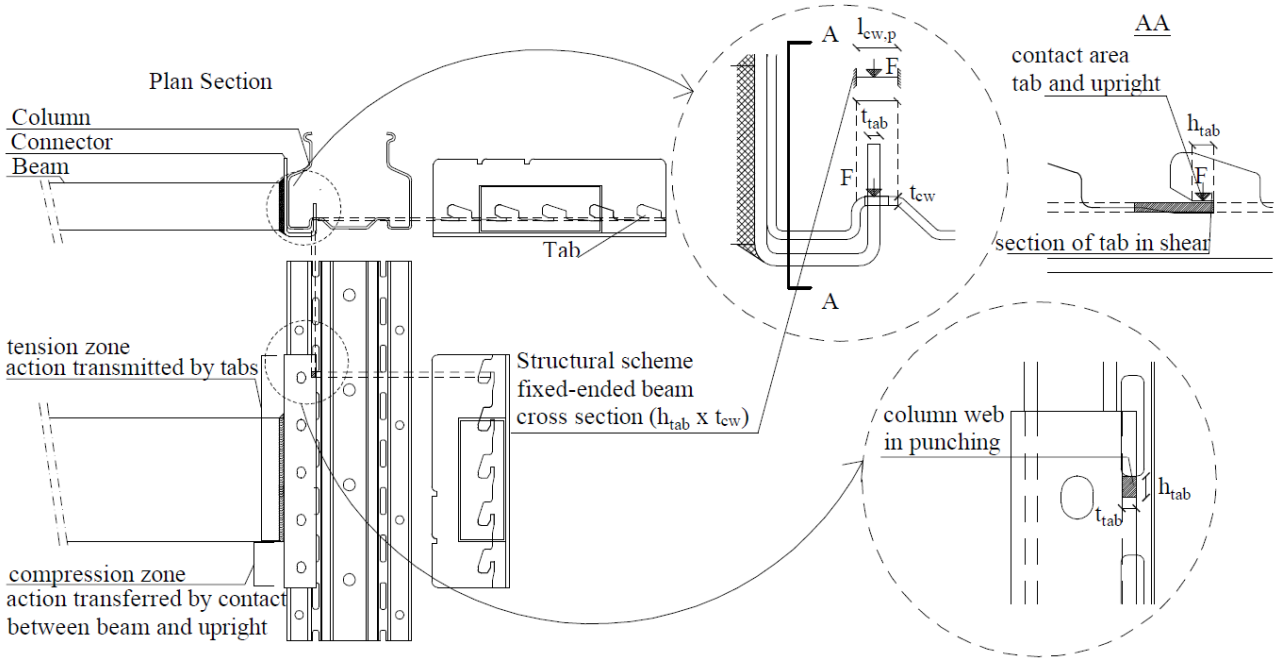

Figure 33. *Modeling of the column web in punching to evaluate its resistance and stiffness.*

This component is active only in the tension zone of the connection, because the *F* force is transferred by tabs which work only in tension. The component resistance depends mainly on punching shear stress resistance of the column web $F_{cw,p}$ which can be obtained, considering the analogy to bolted connections, by using the relationship (20), in according to [EN 1993-1-8, 2005].

$$F_{cw,p} = 0.6 d_m t_{cw} f_{u,cw} \tag{20}$$

where:

t_{cw} is the thickness of the column;

$f_{u,cw}$ is the ultimate tensile stress of the column;

d_m is the perimeter of tab in contact with the column: $d_m = t_{tab} + 2h_{tab}$ (Figure 33);

where:

t_{tab} is the thickness of the tab;

h_{tab} is height of the tab.

The spring element modeling column web in punching has an initial elastic stiffness $k_{cw,p}$, given by general rule (21):

$$k_{cw,p} = \frac{F}{\delta} \tag{21}$$

where:

F is the force applied to the fixed-ended beam modeling this component;

$\delta = \left(\frac{\chi l_{cw,p}}{4GA_{cw,p}} + \frac{l_{cw,p}^3}{192EJ_{cw,p}} \right) F$ is the deflection caused by bending and shear deformation under load F

with:

G the steel shear modulus;

χ the shear correction factor;

$l_{cw,p}$ fixed-ended beam length;

E the steel elastic modulus;

$A_{cw,p} = t_{cw} h_{tab}$ the cross-section of the fixed-ended beam;

$J_{cw,p} = \frac{1}{12} h_{tab} t_{cw}^3$ the inertia moment of the fixed-ended beam, where h_{tab} is height of the tab assumed equal to the width of the fixed-ended beam cross-section and t_{cw} is the thickness of column.

The effect of punching of the column web observed during the tests is shown in Figure 34.

Figure 34. *Punching of the column. Behavior shows in test 90/150-1352A.*

3.3.7 Column web in bearing

The action transferred by tabs cause the column web bearing, the resistance $F_{cw,b}$ of this component, which is active in the tension zone of the joint (Figure 35), is evaluated, using the analogy to bolted connections, by the equation (22) in according to [EN 1993-1-8, 2005].

$$F_{cw,b} = 2.5 \alpha f_{u,cw} h_{tab} t_{cw} \tag{22}$$

where:

t_{cw} is the thickness of the column;

$f_{u,cw}$ is the ultimate tensile stress of the column;

h_{tab} is the height of the tab;

$\alpha = \frac{f_{u,co}}{f_{u,cw}}$ is the reduction factor.

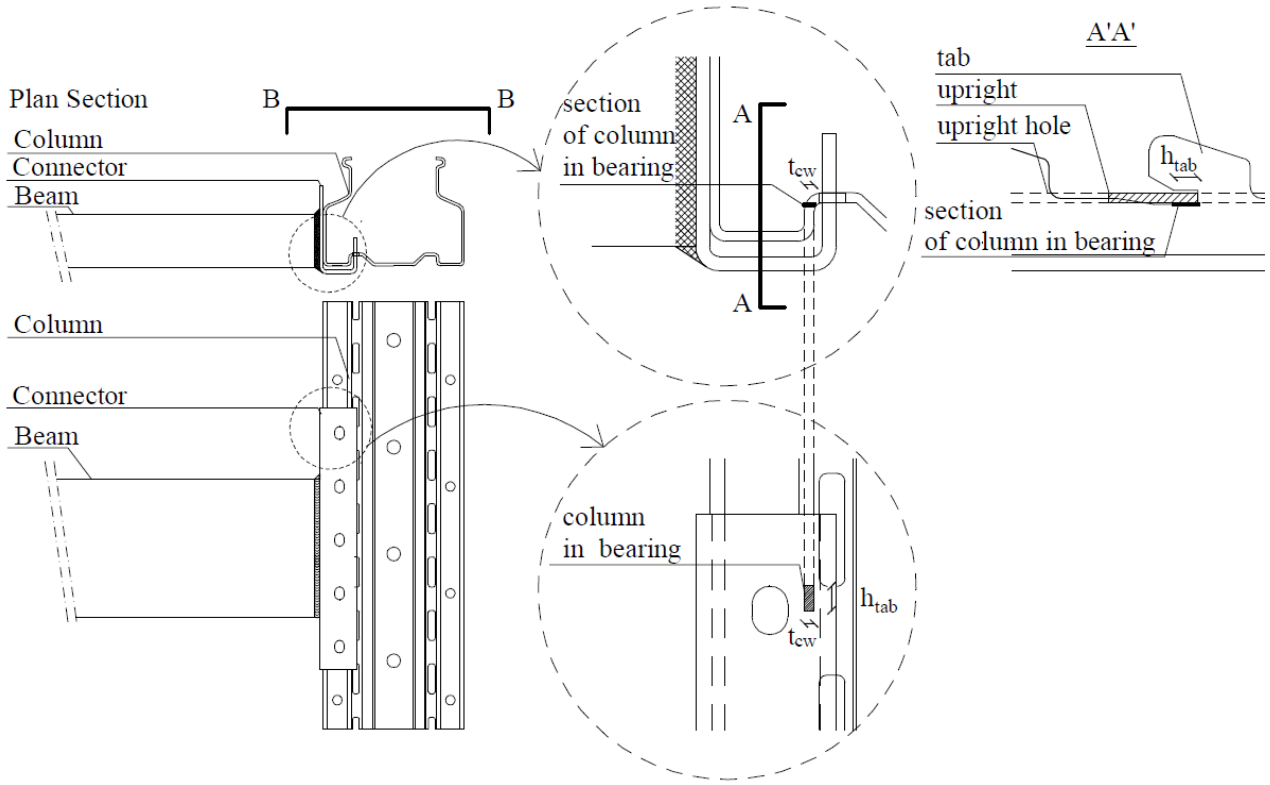

Figure 35. *Model to determine the resistance and stiffness of column web in bearing.*

The stiffness of this component $k_{cw,b}$ can be estimated by means of the equation (23), as suggested by [EN 1993-1-8, 2005].

$$k_{cw,b} = 12 k_b k_t h_{tab} f_{u,cw} \tag{23}$$

where:
$f_{u,cw}$ is the ultimate tensile stress of the column;
$k_b = 1.25$ [EN 1993-1-8, 2005];
$k_t = 1.5 t_{cw} / d_{M16}$ [EN 1993-1-8, 2005];
h_{tab} is height of the tab.
The effect of bearing of the column web observed during the tests is shown in Figure 36.

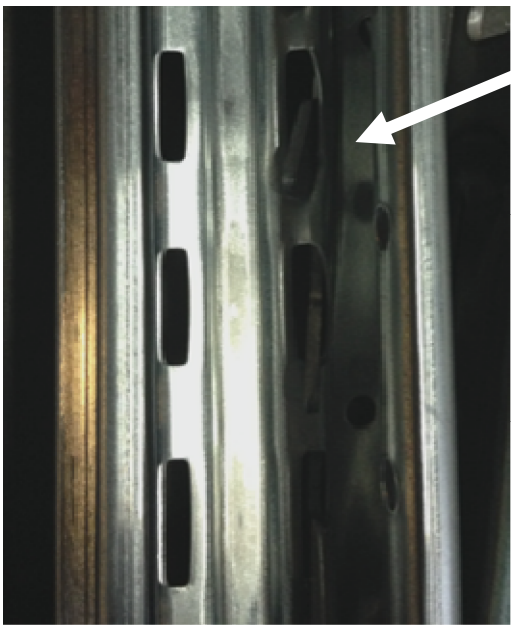

Figure 36. *Bearing of the column web (view BB Figure 35). Deformation due to the pressure acting on the column by means of tabs. Behavior shows in test 90/150- 1242A.*

3.3.8 Column web in tension and in compression

The resistance of compression part of the column web $F_{cw,r}$ can be determined according to [EN 1993-1-8, 2005].

$$F_{cw,cr} = \omega b_{eff,c} t_{cw} f_{y,cw}$$

where:

E is the steel elastic modulus;
t_{cw} is the thickness of the column;
$d_{wc,cb}$ is the clear depth of column web in buckling.
Several equations can be found in literature [Chen and Newlin, 1973 and Aribert et al., 1990] and in current design provisions [AISC, 2010], to check the stability of the column web in compression. In the present paper the buckling resistance of the column web $F_{cw,b}$ in compression is computed in according to the Winter formula [Winter, 1947].

$$F_{cw,b} = F_{cw,cr}\left[\frac{1}{\lambda}\left(1-\frac{0.22}{\lambda}\right)\right]$$

where:

$$\lambda = \left(\frac{b_{eff,c} t_{cw} f_{y,cw}}{F_{cr}}\right)^{1/2}$$

$$F_{cr} = \frac{\pi E t_{cw}^{3}}{3(1-\nu^{2})d_{wc,cb}}$$

E is the steel elastic modulus;
t_{cw} is the thickness of the column;
$b_{eff,c}$ is the effective width for column web in compression assumed equal to the connector flange.
$d_{wc,cb}$ is the clear depth of column web in buckling;
$f_{y,cw}$ is the yield stress of the column;
ν Poisson's ratio;
The resistance of the column web in compression $F_{cw,c}$ used in the proposed model is obtained by equation (24):

$$F_{cw,c} = \min(F_{cw,cb}; F_{cw,cr})$$

(24)

The resistance of the tensioned part of the column web (25) can be determined according to [EN 1993-1-8, 2005].

$$F_{cw,t} = \omega b_{eff,t} t_{cw} f_{y,cw}$$

(25)

where:

$f_{y,cw}$ is the yield stress of the column;

t_{cw} is the thickness of the column;

ω is reduction factor for interaction with shear in the column;

$b_{eff,t}$ is the effective width for column web in tension (assuming the tangent of the spreading angle 1:2.5).

The model of the column web subjected to tension or compression actions is depicted in Figure 37.

The axial elastic stiffness of the column web in compression pre-buckling and tension can be evaluated by the relationships (26) and (27) respectively, in according to [EN 1993-1-8, 2005].

$$k_{cw,c} = \frac{E b'_{eff,c} t_{cw}}{d_{wc,c}}$$

(26)

where:

E is the steel elastic modulus;

t_{cw} is the thickness of the column;

$d_{wc,c}$ is the clear depth of the column web in compression assumed;

$b'_{eff,c}$ is the effective column width for stiffness in compression (2/5 $b_{eff,c}$).

$$k_{cw,t} = \frac{E b'_{eff,t} t_{cw}}{d_{wc,t}}$$

(27)

where:

E is the steel elastic modulus;

t_{cw} is the thickness of the column;

$d_{wc,t}$ is the clear depth of the column web in tension;

$b'_{eff,t}$ is the effective column width for stiffness in tension (assuming the tangent of the spreading angle 1:1).

The load spreading angle in tension zone for stiffness calculation was assumed equal to the length of the zone where load from punching is acting and considering the tangent of the spreading angle 1:1, until the greater stiffness of column provided by its folds (Figure 37).

The local buckling of column web, in compression, observed during the tests is shown in Figure 38.

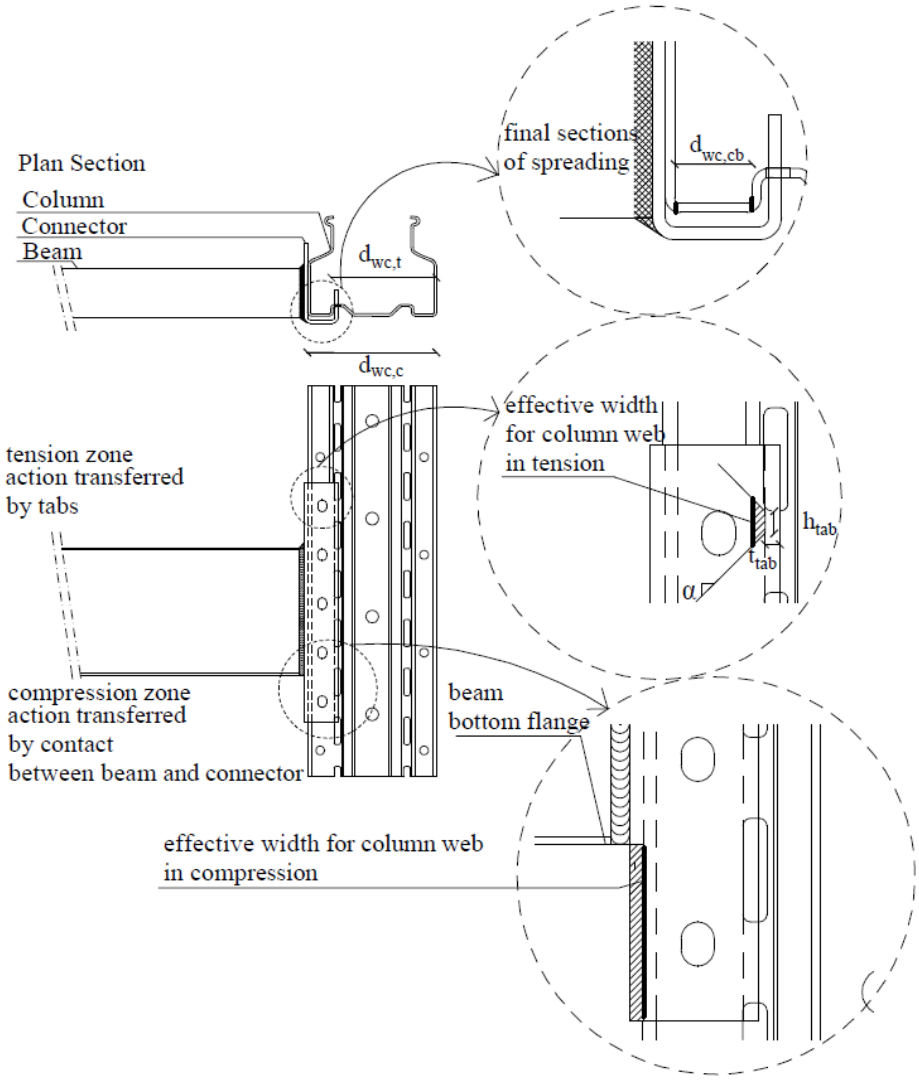

Figure 37. *Model to determine the resistance and stiffness of column web in tension and in compression.*

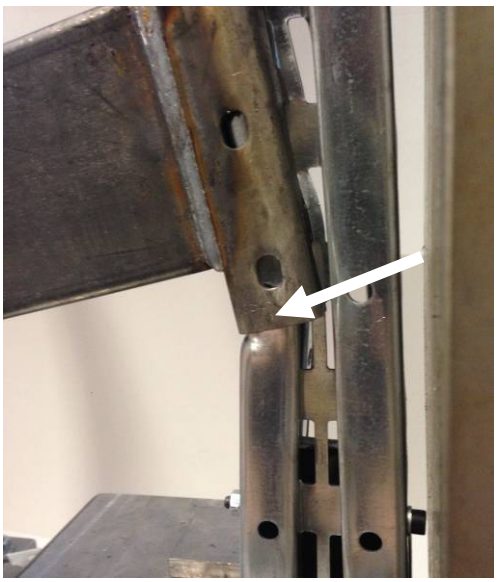

Figure 38. *Buckling of column web in experimental test 70/150-1042A.*

3.3.9 Column web in shear

For external connection, characterised by one-sided bending moment acting from the beam, like the specimens of the case study, the contribution on the connection stiffness and flexural resistance of the shear deformation of panel zone has to be taken into account. The resistance of panel zone in shear is given by (28):

$$F_{cw,s} = \frac{f_{y,cw} A_{vc,net}}{\sqrt{3}} \tag{28}$$

where:
$f_{y,cw}$ is the yield stress of the column;
$A_{vc,net}$ is the net shear area of the column: equal to the gross shear area excluding the width of slots;
The stiffness of panel zone in shear can be assumed by means of equation (29):

$$k_{cw,s} = \frac{0{,}38E}{\left(\frac{\sum h_1}{A_{vc}} + \frac{\sum h_2}{A_{vc,net}}\right)} \tag{29}$$

where:
E is the steel elastic modulus;
$A_{vc} = l_{wc,s}\, t_{cw}$ is the gross shear area of the column, with $l_{wc,s}$ is the length of the column web and t_{cw} is the thickness of the column;
$A_{vc,net}$ is the net shear area of the column: equal to the gross shear area excluding the width of slots;
$\sum h_1$ and $\sum h_2$ are the total height of the gross shear area A_{vc} and of the net shear area $A_{vc,net}$ respectively.
The model adopted for the column web in shear is shown in Figure 39. The column web in shear, observed during the tests is shown in Figure 40.

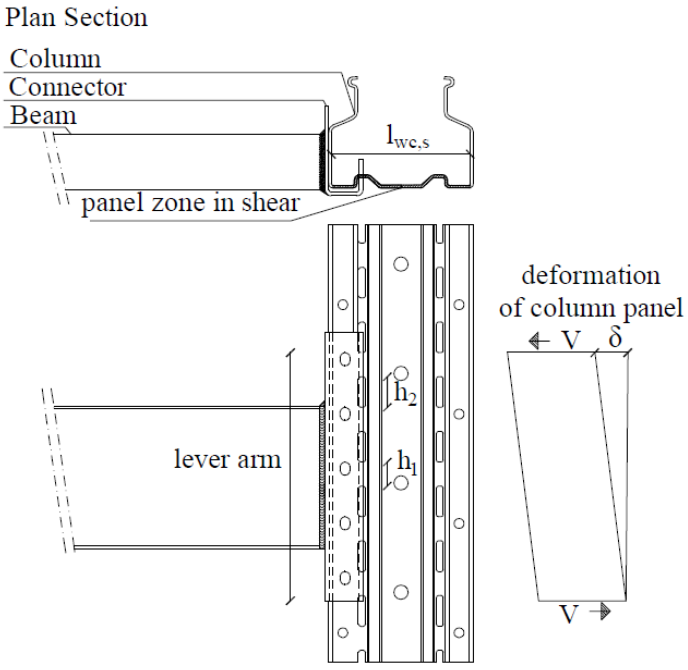

Figure 39. *Model of the panel zone in shear component.*

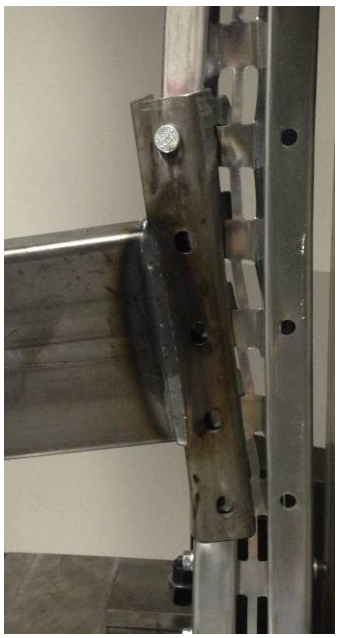

Figure 40. *Deformation of the column web in shear observed in the experimental test 70/150-1242A.*

The relationships for the initial stiffness and an ultimate strength implemented in the CM are reported in Table 10.

Table 10. Ultimate flexural strength and initial stiffness of contributing rack connection components.

Member		*Component*	*Model*	*Ultimate Strength*	*Initial Stiffness*
Weld	*a*	*Weld*	*rigid-plastic*	$F_{wel}\frac{J_w f_{y,w}}{h_b y_w}$	∞
Beam	*b*	*Beam flange tension zone*	*rigid-plastic*	$F_{bf,t}=b_{eff,b}t_b f_{y,b}$	∞
	b	*Beam flange compression zone*	*rigid-plastic*	$F_{bf,c}=b_{eff,b}t_b f_{y,b}$	∞
	c	*Connector web tension zone*	*elasto-plastic*	$F_{cow,t}=\omega_{co}b_{eff,co}t_{co}f_{y,co}$	$k_{cow,t}=\frac{Eb'_{eff,co}t_{co}}{d_{wco}}$
	c	*Connector web compression zone*	*elasto-plastic*	$F_{cow,c}=\omega_{co}b_{eff,co}t_{co}f_{y,co}$	$k_{cow,c}=\frac{Eb'_{eff,co}t_{co}}{d_{wco}}$
Connector	*d*	*Connector in bending tension zone*	*elasto-plastic*	$M_{co,b}=W_{pl,co}f_{y,co}$	$k=\frac{1}{\frac{l_1^3}{3EJ_{co}}+\frac{1}{EJ_{co}}(\frac{l_2^2 l_1}{2}-\frac{l_2^3}{2}+\frac{l_2^3}{3})+\frac{1,2l_1}{GA_{co}}+\frac{1,2l_2}{GA_{co}}}$
	d	*Connector in bending compression zone*	*elasto-plastic*	$M_{co,b}=W_{pl,co}f_{y,co}$	$k=\frac{1}{\frac{(2z_c)^3}{8EJ_{co}}+\frac{1.2(z_c)}{GA_{co}}}$
	e	*Tabs in bending and in shear*	*elasto-plastic*	$F_{t,s}=\frac{f_{u,co}A_{v,tab}}{\sqrt{3}}$	$k_{t,s}=\frac{1}{\left(\frac{l_F^3}{3EI}+\frac{1.2l_F}{GA_v}\right)}$
	f	*Column web in punching*	*elasto-plastic*	$F_{cw,p}=0.6d_m t_{cw}f_{u,cw}$	$k_{cw,p}=\frac{1}{\left(\frac{\chi l_{cw,p}}{4GA_{cw,p}}+\frac{l_{cw,p}^3}{192EJ_{cw,p}}\right)}$
	g	*Column web bearing*	*elasto-plastic*	$F_{cw,b}=2.5\alpha f_{u,cw}h_{tab}t_{cw}$	$k_{cw,b}=12k_b k_t h_{tab}f_{u,cw}$
	h	*Column web in tension*	*elasto-plastic*	$F_{cw,t}=\omega b_{eff,t}t_{cw}f_{y,cw}$	$k_{cw,t}=\frac{Eb'_{eff,t}t_{cw}}{d_{wc,t}}$
	h	*Column web in compression*	*elasto-plastic*	*min:* $F_{cw,b}=F_{cw,cr}\left[\frac{1}{\lambda}\left(1-\frac{0.22}{\lambda}\right)\right]$ $F_{cw,cr}=\omega b_{eff,c}t_{cw}f_{y,cw}$	$k_{cw,c}=\frac{Eb'_{eff,c}t_{cw}}{d_{wc,c}}$
Column	*i*	*Column web in shear*	*elasto-plastic*	$F_{cw,s}=\frac{f_{y,cw}A_{vc,net}}{\sqrt{3}}$	$k_{cw,s}=\frac{0,38E}{\left(\frac{\sum h_1}{A_{vc}}+\frac{\sum h_2}{A_{vc,net}}\right)}$

3.4 Evaluation of rack connection mechanical features

3.4.1 Ultimate moment

A sketch of the mechanical model to predict the flexural resistance of a rack connection with a *M5* connector (five tabs, as shown in Figure 3) is shown in Figure 41 a) as an example.

Springs representing the behavior of the components of the weld (weld type *a*, as shown in Table 10) and of the beam (*b*, *c*) are located at the level of the beam flanges. The springs representing the connector components (*d*, *e*, *f*, *g*, *h*) are located at the level of tabs in tension zone, and at the centre of compression in compression (denoted CC in Figure 41 a)) zone. The lever arm of the spring representing the column web in shear (*i*) is equal to the distance from the centre of compression and the point of the application of the reaction force in tension zone. The centre of rotation (denoted CR in Figure 41 a)) is assumed at the level of beam bottom flange.

The weakest component governs the resistance of each row, so that the model can be modified into the model of Figure 41b), where:

$F_{weakest} = \min(F_{cw,p}; F_{cw,b}; F_{cw,t}; F_{t,s})$ and $F_{weakest,beam} = \min(F_{cow,i}; F_{bf,i})$.

The ultimate behavior of connection is described assuming the plastic distribution of internal forces. From condition of equilibrium, the reaction in compression zone $Z \le F_{cw,c}$ is equal to the sum of plastic forces $F_{weakest}$ acting in each tension row. The flexural resistance of connector protruding over the flange surface of the beam $M_{co,b}$ cannot be exceeded; and so the distance of the centre of compression from the centre of rotation z_c, can be determined from equation (30):

$$z_c = \frac{M_{co,b}}{Z} \tag{30}$$

where:

Z is the reaction force in compression zone;

$M_{co,b}$ is the flexural resistance of connector;

Founded the centre of compression, the plastic flexural resistance of the connection $M_{u,num}$ can be predicted by using equation (31):

$$M_{u,num} = \min\left(F_{wel} h_b = M_{u,weld}; F_{weakest,beam} h_b = M_{u,beam}; F_{weakest} \sum_i^r h_i + M_{co,b} = M_{u,connector}; F_{cw,s} z_{eq} = M_{u,panel} \right) \tag{31}$$

where:

$M_{u,weld}$ is the ultimate bending moment of the weld;

$M_{u,beam}$ is the ultimate bending moment of the beam;

$M_{u,connector}$ is the ultimate bending moment of the connector;

$M_{u,panel}$ is the ultimate bending moment of the column panel;

h_i is the distance of *i* tension component (*i=1:4*) from the centre of rotation at the bottom flange of beam-end section;

z_{eq} is the equivalent lever arm.

The flexural resistance of upper part of connector should be checked; when the bending moment generated by forces acting in upper rows is greater than the value of the flexural resistance of connector $M_{co,b}$, these forces have to be reduced to a value of $\psi F_{weakest}$ in order to satisfy moment equilibrium.

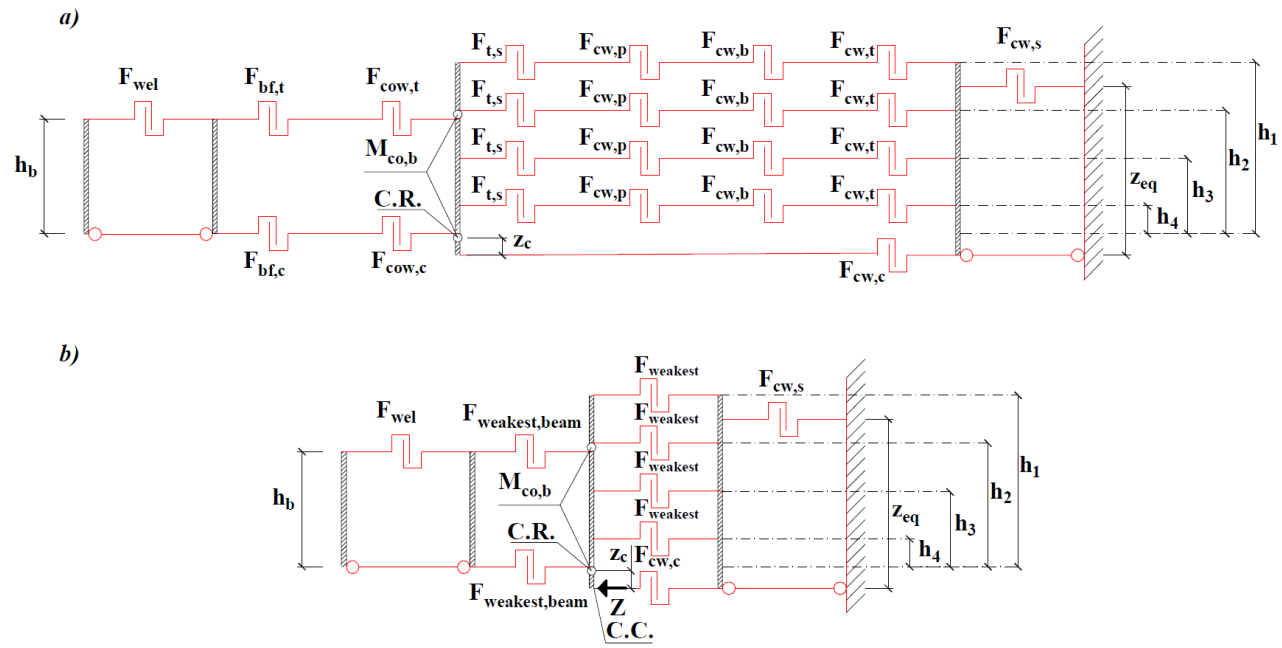

Figure 41. *Mechanical model to predict the flexural resistance.*

The proposed model can predict the connection ultimate moment with accuracy when the failure is produced by one of the joint member in series (beam, weld or column), even if they were not infinite ductile. While, if the connection failure is related to the connector member, the assumption of a plastic distribution of forces requires that all connector components are ductile, because they work in parallel; nevertheless, experimental tests showed that this hypothesis for the connector components is acceptable.

3.4.2 Initial elastic rotational stiffness

The mechanical model used to predict the initial rotational stiffness of the same connection type is shown in Figure 42.

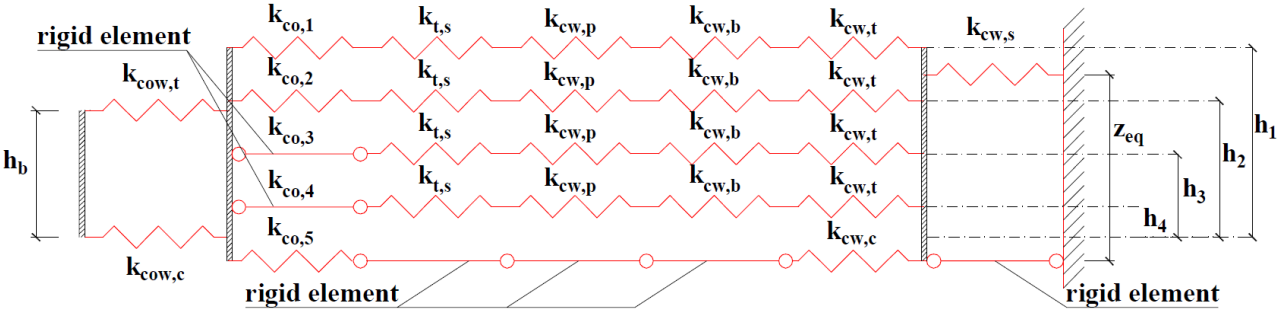

Figure 42. *Mechanical model to predict the rotational stiffness.*

The procedure to evaluate the rotational stiffness is depicted in Figure 43 a). The first step is the computation of effective stiffness $k_{eff,r}$ (32) of each row ($r=1:5$) from the stiffness of each component ($j=1:5$) Figure 43 b).

$$K_{eff,r} = \frac{1}{\sum_{j=1}^{5} \frac{1}{k_{j,r}}} \tag{32}$$

By means of the equation of equilibrium to the translation (33), the prediction of the equivalent overall stiffness k_{eq} (34) in tension ($r=1:4$) (Figure 43 c) can be obtained:

$$\sum_{r=1}^{4} k_{eff,r} s_r = \sum_{r=1}^{4} k_{eff,r} h_r \varphi = k_{eq} h_{eq} \varphi \tag{33}$$

$$k_{eq} = \frac{\sum_{r=1}^{4} k_{eff,r} h_r}{h_{eq}} \tag{34}$$

where:
s_r is the displacement in correspondence of the equivalent overall stiffness point;
φ is the angle of rotation of the connector assumed like a rigid element;
h_r is the distance between row r and the centre of rotation;
$k_{eff,r}$ is the effective stiffness coefficient for row r taking into account the stiffness coefficients $k_{j,r}$ for the basic components;
h_{eq} is the equivalent distance from the centre of rotation: $h_{eq} = z_{eq} - z_c$;
where z_{eq} is the equivalent lever arm, that, by means of the equation of equilibrium to the rotation (35) can be obtained by the equation (36):

$$\sum_{r=1}^{4} k_{eff,r} s_r z_r = \sum_{r=1}^{4} k_{eff,r} h_r \varphi z_r = k_{eq} h_{eq} \varphi z_{eq} \tag{35}$$

$$z_{eq} = \frac{\sum_{r=1}^{4} k_{eff,r} h_r z_r}{k_{eq} h_{eq}} = \frac{\sum_{r=1}^{4} k_{eff,r} h_r z_r}{\sum_{r=1}^{4} k_{eff,r} h_r} \tag{36}$$

where:
z_r is the lever arm of the component on r row: $z_r = h_r + z_c$;
The last phase is to change the springs with axial stiffness into one spring with rotational stiffness S_n (Figure 43 d) e), equation (37).

$$S_n = \left(\frac{Z_n^2}{\sum_{i=1}^{2} \frac{1}{\bar{k}_{n,i}}} \right) (with \quad n = 1:3) \tag{37}$$

The prediction of the initial stiffness $S_{ini,num}$ of the whole model (Figure 43 f) can be obtained by the relationship (38):

$$S_{ini,num} = \frac{1}{\sum_{n=1}^{3} \frac{1}{S_n}} \tag{38}$$

It is interesting to notice how, assuming the centre of rotation coincident with the centre of compression (C.R. ≡ C.C.), the equations become those reported in [EN 1993-1-8, 2005].

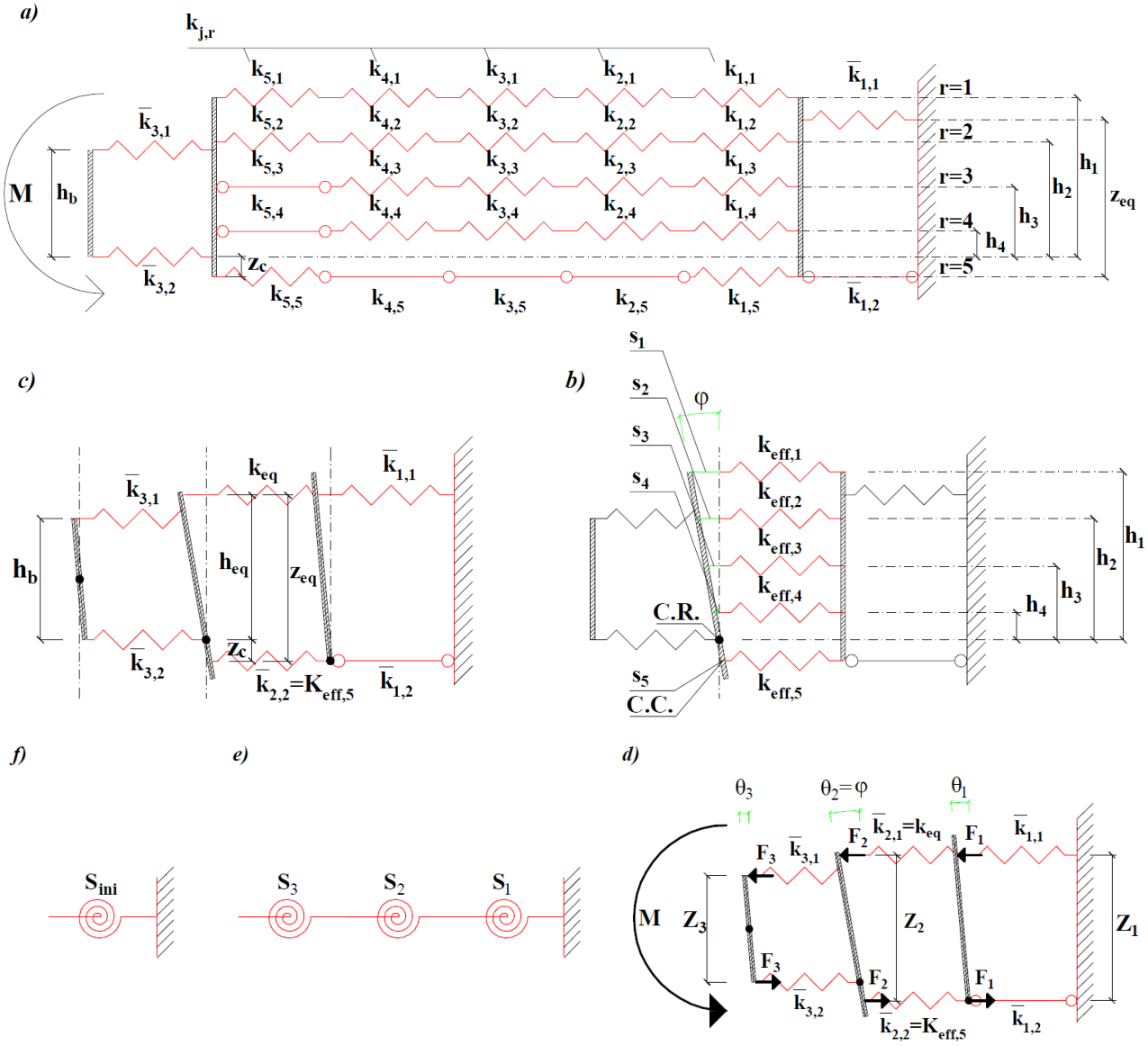

Figure 43. *Procedure to evaluate the initial elastic rotational stiffness of the connections.*

3.4.3 Comparison of results

The experimental and numerical initial rotational stiffnesses, $S_{ini,exp}$ and $S_{ini,num}$, respectively, are shown in Figure 44 while the experimental and numerical ultimate flexural strengths, $M_{u,exp}$ and $M_{u,num}$, respectively, are shown in Figure 45.

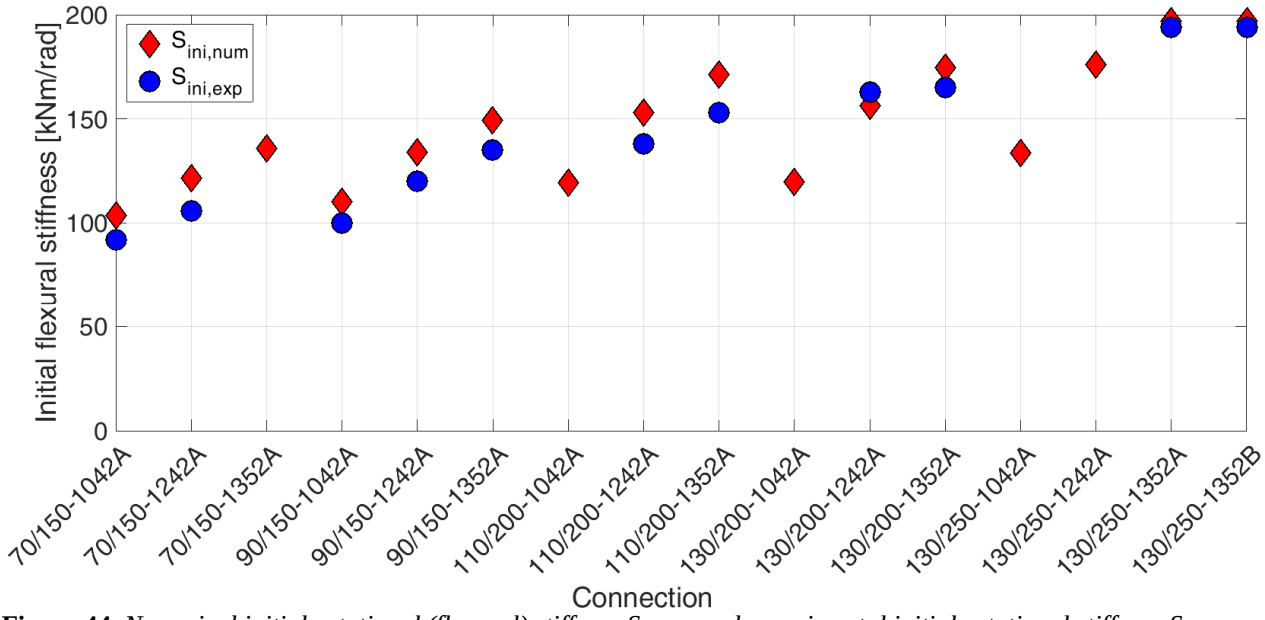

Figure 44. *Numerical initial rotational (flexural) stiffness $S_{ini,num}$ and experimental initial rotational stiffness $S_{ini,exp}$.*

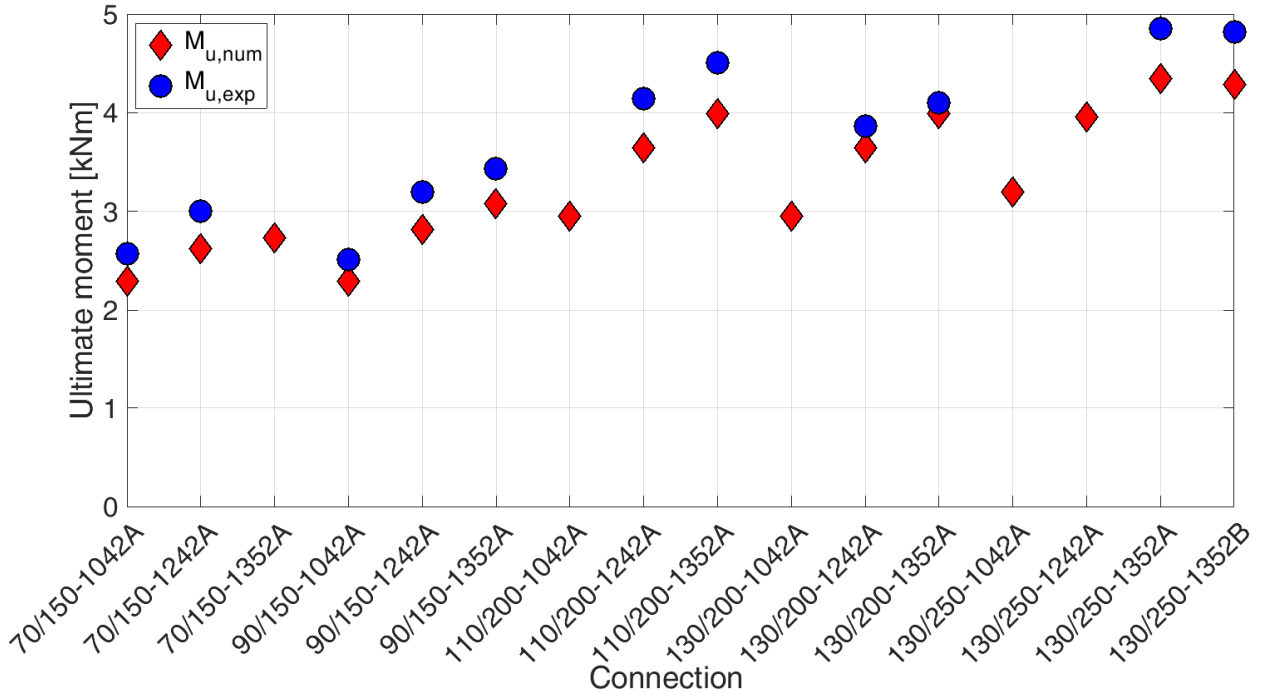

Figure 45. *Numerical ultimate flexural strength (moment) $M_{u,num}$ and experimental ultimate moment $M_{u,exp}$.*

The differences between the numerical and experimental results for initial rotational stiffness ($(S_{ini,num}-S_{ini,exp})/S_{ini,exp}$ *[%]*) and flexural resistance ($(M_{u,num}- M_{u,exp})/ M_{u,exp}$ *[%]*) are reported in Table 11, with observed failure modes from the experimental tests (Figure 46).

Table 11. Difference between experimental and numerical initial rotational stiffness and ultimate flexural strength of tested rack connections ($S_{ini,num}$-$S_{ini,exp}$)/$S_{ini,exp}$ *[%]* and ($M_{u,num}$- $M_{u,exp}$)/ $M_{u,exp}$ *[%]*) and observed experimental failure mode

Connection	Stiffness $\frac{(S_{ini,num} - S_{ini,exp})}{S_{ini,exp}}$ [%]	Moment $\frac{(M_{u,num} - M_{u,exp})}{M_{u,exp}}$ [%]	Failure Mode	
			Member	Component
70/150-1042A	13	-11	Connector	Column web in compression buckling
70/150-1242A	15	-13	Column	Column web in shear
90/150-1042A	10	-8	Connector	Column web in compression buckling
90/150-1242A	12	-12	Connector	Column web in punching
90/150-1352A	10	-10	Connector	Column web in punching
110/200-1242A	11	-12	Connector	Column web in punching
110/200-1352A	12	-11	Connector	Column web in punching
130/200-1242A	-4	-6	Connector	Column web in punching
130/200-1352A	5	-3	Connector	Column web in punching
130/250-1352A	2	-10	Connector	Tabs in shear
130/250-1352B	2	-9	Weld	Collapse of weld

i) Component: Column web in shear
Test 70/150-1242A
Deformation of column in shear

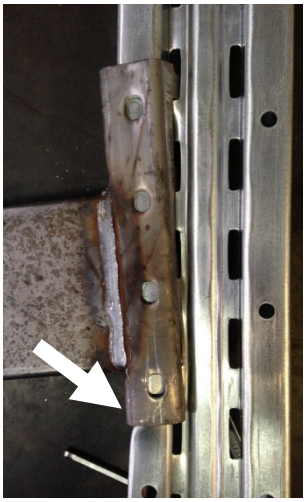

h) Component: Column web in compression
Test 90/150-1042A
Buckling of column web

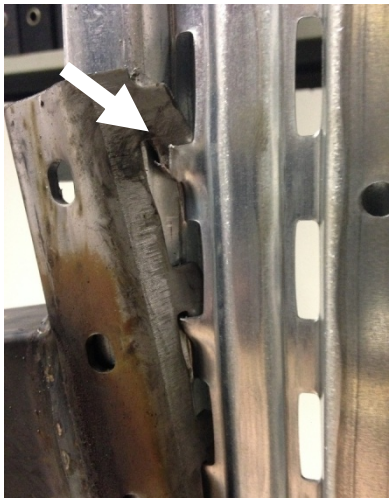

f) Component: Column web in punching
Test 90/150-1352A
Punching of column web

e) Component: Tabs in shear
Test 130/250-1352A
Failure of the tabs

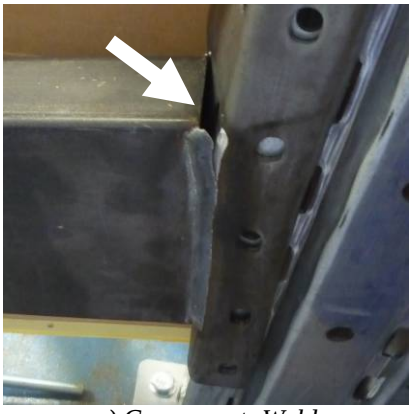

a) Component: Weld
Test: 130/250-1352B
Failure of Weld

Figure 46. *Failure modes observed in experimental tests.*

Generally, the mechanical model slightly overestimates stiffness (Figure 44) and underestimates moment (Figure 45) but results agree. Examining connections with identical columns, increasing the beam cross-section and the number of tabs in the connector generally increase stiffness and moment (Figure 44 and Figure 45). In connections with the same beam and connector, increasing the column cross-section the stiffness increases (Figure 44), while moment is dependent on failure mode (Figure 45).
As the welded connection does not influence deformation at the joint, it has no impact on initial rotational stiffness. Two-sided welds (as in test 130/250-1352B) do indeed reduce connection flexural capacity compared to three sided welds (test 130/250-1352A). The obtained results confirm the good agreement among the experimental data and theoretical approach
In order to classify all rack connections according to Eurocode 1993-1-8, the following ratios have been considered:

$$RS_{num} = \frac{S_{ini,num}}{S_b} \qquad RS_{\exp} = \frac{S_{ini,\exp}}{S_b}$$

$$RM_{num} = \frac{M_{u,num}}{M_b} \qquad RM_{\exp} = \frac{M_{u,\exp}}{M_b}$$

where:
$S_{ini,num}$ and $S_{ini,exp}$ are the numerical and experimental initial elastic stiffness of the connection respectively;
$M_{u,num}$ and $M_{u,exp}$ are the numerical and experimental ultimate moment of the connection respectively;
M_b is the ultimate plastic moment and S_b (39) the stiffness of the beam:

$$S_b = \frac{EJ_b}{L_b} \tag{39}$$

with E the elastic modulus of steel, J_b the inertia moment of the beam and L_b the length of the beam used in the rack system (2700 mm, as indicated by the manufacturer).
These ratios, for all tests, are reported in Figure 47.

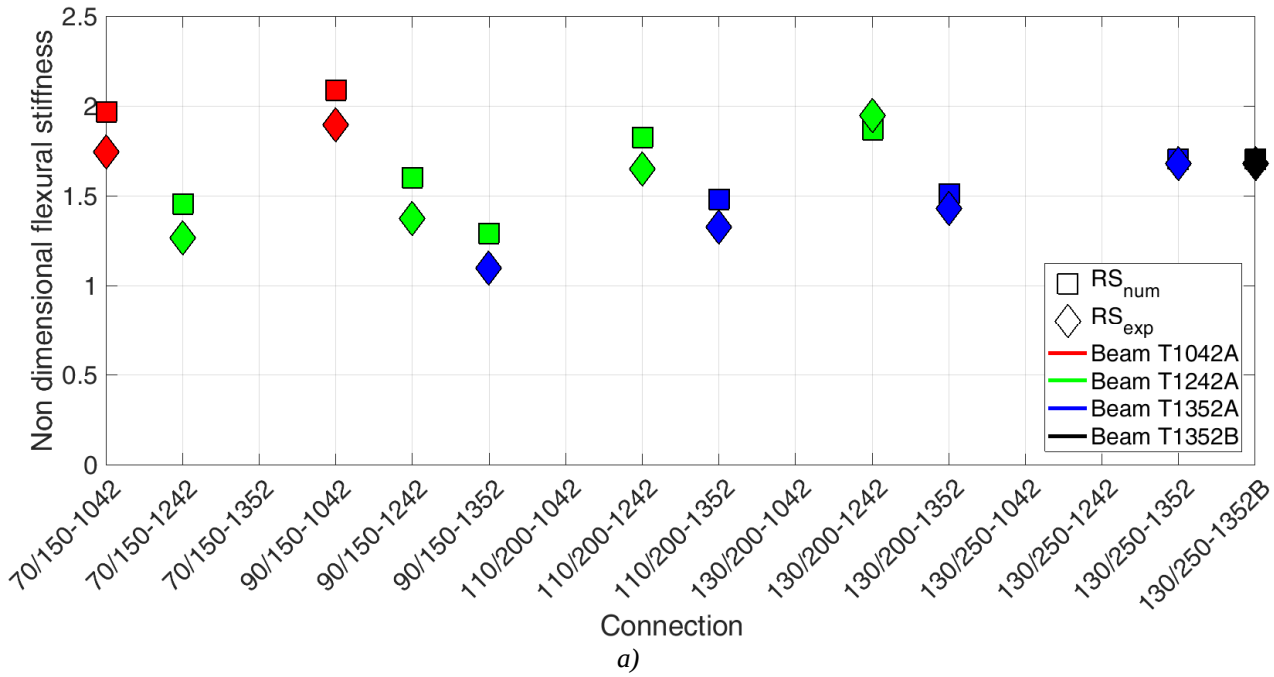

a)

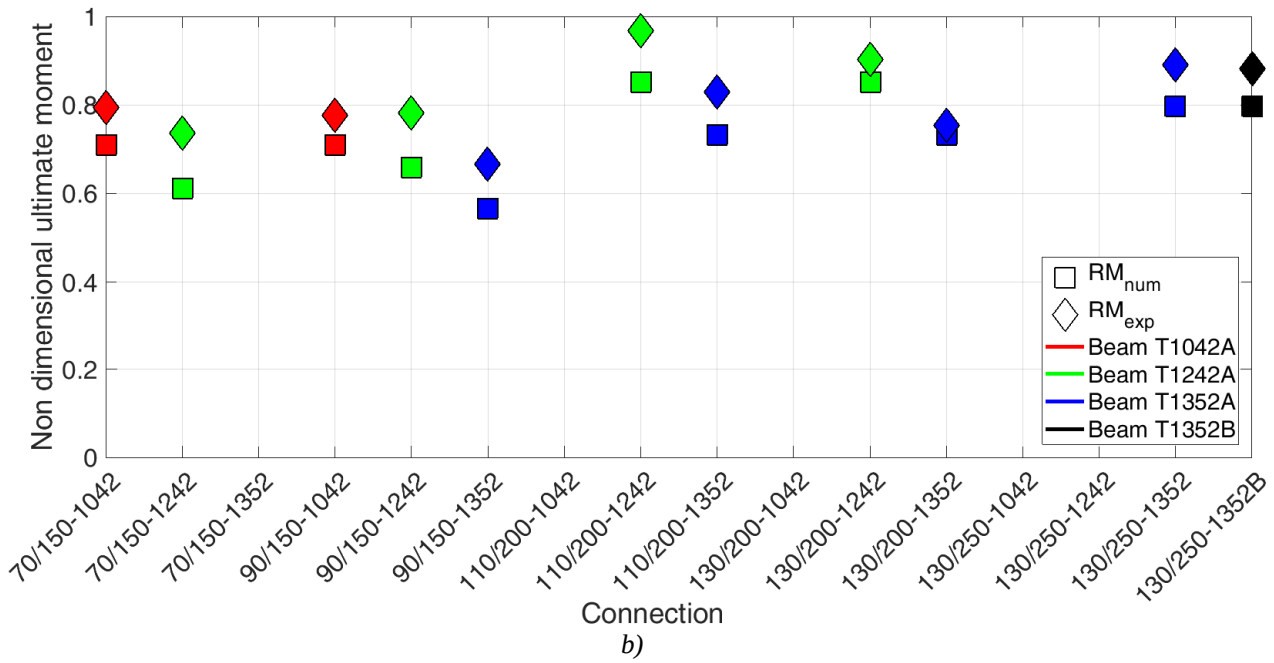

b)

Figure 47. *a) Non dimensional values of experimental and numerical stiffness. b) Non dimensional values of experimental and numerical ultimate moment.*

Obtained ratios (Figure 47) allow the connection as semi-rigid for stiffness and partial-strength joint to respect the bending moment in according to [EN 1993-1-8, 2005] to be classified.

The proposed model checks the experimental tests regarding their failure mode and allows the influence of the geometrical and mechanical features of each component on connection collapse to be evaluated.

In order to support the previous observation, the ratios between the resistance values of the connector components in tension ($F_{t,s}$, $F_{cw,p}$, $F_{cw,b}$ and $F_{cw,t}$) and their maximum value ($F_{cw,t,max}$ founded in test 130/250-1352A) are reported in Figure 48.

It is observed that the weakest component in tension zone is the column web in punching $F_{cw,p}$, when the thickness of column is 1.5 mm (70/150 and 90/150 column type, see Figure 34). Increasing the column thickness to 2 mm the weakest component continues to be the column web in punching but its resistance is closed to the one of tabs $F_{t,s}$ (test with 110/200 and 130/200 column type). $F_{t,s}$ is the weakest component when the thickness of column is 2.5 mm (test with 130/250 column type, see Figure 48).

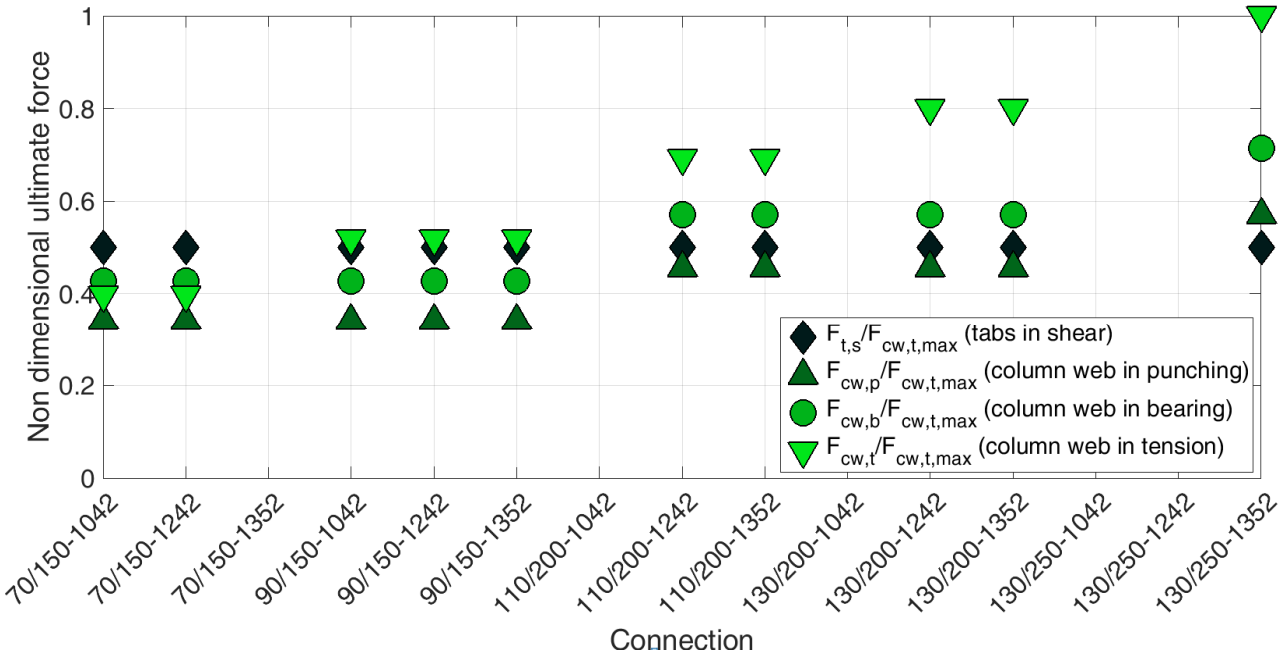

Figure 48. *Non dimensional resistance of connector components in tension zone.*

The flexural resistance of the connection $M_{u,num}$, is the minimum value among the values of bending moment related to each member: beam ($M_{u,beam}$), welding ($M_{u,weld}$), connector ($M_{u,conector}$) or column panel ($M_{u,panel}$) (31).
The ratios between ultimate moment of each components respect to their maximum value ($M_{u,panel,max}$ for tests with 130/250 column type) are reported in Figure 49.
The CM approach allows a value of the ultimate moment similar to experimental one, which depends on the component which fails during the test, to be obtained.
$M_{u,beam}$ and $M_{u,weld}$ are related to the type of beam and welding respectively; $M_{u,panel}$ is related to the equivalent lever arm z_{eq} and the resistance of panel zone in shear, and the value of $M_{u,conector}$ is related to the weakest components of the connector member.
The flexural resistance of the connection is often the connector one $M_{u,connector}$ (Figure 49), increasing the width of the column the probable collapse associated to the panel $M_{u,panel}$ is avoided, the column panel collapse was obtained for the test 70/150-T1242 (Figure 40). In each case the ultimate flexural resistance of beam $M_{u,beam}$ and welding $M_{u,weld}$ is greater than connector one $M_{u,connector}$, except for 130/250-T1352B test (two-sided welding, Figure 26), where the collapse is associated to the failure of welding $M_{u,weld}$. These results were confirmed in the experimental test.

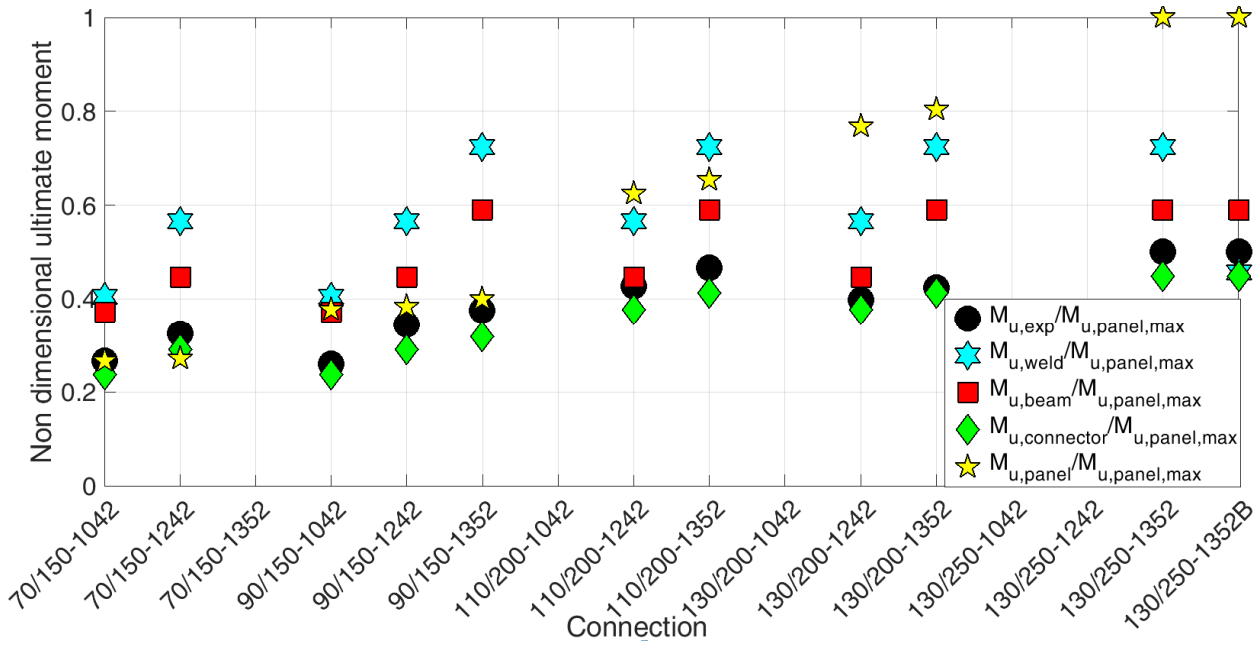

Figure 49. *Non dimensional value of the ultimate flexural resistance for each component of tested connections.*

The ratios between stiffness of each component (for all test with the 1352A beam) and their maximum value ($K_{cow,c}$=$k_{cow,t}$) are shown in Figure 50. The biggest reduction on the joint global stiffness is due to the bearing of the column web $k_{cw,b}$, the tabs in bending $k_{t,s}$ and the connector in bending $k_{co,1}$. Findings are confirmed by the member deformations obtained in the experimental tests.

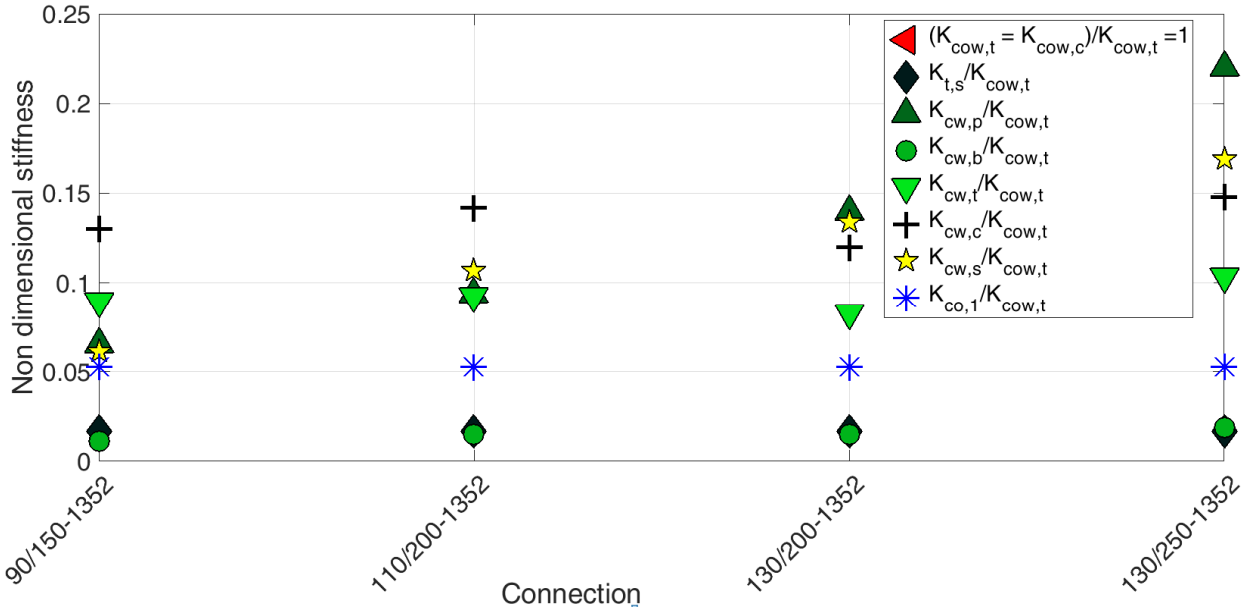

Figure 50. *Non dimensional values of the stiffness associated to each component (test with 1352A beam).*

3.5 Connection non-linear moment-rotation curve

The proposed mechanical model allows the failure mode of rack connection and its weakest component to be predicted; in addition the initial elastic rotational stiffness ($S_{ini,num}$) and ultimate moment ($M_{u,num}$) are evaluated with a good agreement. Nevertheless, it was noting that only these

two parameters are not sufficient for an analytical representation of the non-linear moment-rotation curve of rack connections, whose knowledge is fundamental for a reliable analysis of MRFs under seismic force. On the basis of this consideration, an analytical procedure has been proposed with the goal to obtain an adequate approximation of the elasto-plastic moment-rotation curve of rack joints.
The non-linear moment-rotation curve is identified by three ranges:
The first one corresponds to a linear behavior:

$$M = S_{ini,num}\theta$$

It is valid provided that the bending moment M is less than the connection elastic moment $M_{e,num}$.
The elastic moment $M_{e,num}$ is evaluated by the mechanical model, evaluating the yield strength of connection components, replacing the ultimate stress with the yield stress.
The obtained equations are: $F_{t,s,y} = \frac{f_{y,co} A_{v,tab}}{\sqrt{3}}$ for tabs in bending and in shear; $F_{cw,p,y} = 0.6 d_m t_{cw} f_{y,cw}$ for the column web in punching and $F_{cw,b,y} = 2.5\alpha f_{y,cw} h_{tab} t_{cw}$ for the column web in bearing.
Following the previously described steps, the value of the smaller yielding strength at the connector member is evaluated by $F_{weakest,y} = \min(F_{cw,p,y}; F_{cw,b,y}; F_{cw,t,y}; F_{t,s,y})$.
The connection elastic moment $M_{e,num}$ is then obtained assuming a linear elastic distribution of internal forces, with the value of $F_{weakest,y}$ in the component longer from the centre of rotation C.R.
Taking into account the model with five tabs, $F_{weakest,y}=F_{1,y}$ is the force in the component with a distance h_1 from the C.R.; the elastic strength on the other components $F_{r,y}$, with: r = 2:4, can be obtained by using the equation: $\frac{F_{1,y}}{h_1} = \frac{F_{r,y}}{h_r}$.
From condition of equilibrium the elastic reaction in compression zone Z_e is evaluated, and it is equal to the sum of each elastic forces acting in each tension row.
The distance of the elastic centre of compression z_e is obtained by using: $z_e = \frac{M_{co,b,e}}{Z_e}$, where: $M_{co,b,e} = W_{el,co} f_{y,co}$ is the elastic flexural resistance of connector protruding over the flange surface of the beam, with: $W_{el,co}$ the elastic section modulus of the connector.
Founded the elastic centre of compression, the elastic flexural resistance of the connection $M_{e,num}$ can be predicted by using equation: $M_{e,num} = \left(\sum_i^r F_{r,y} h_i + M_{co,b,e} \right)$ with r = *1:4*
where:
h_i is the distance of i tension component (i=*1:4*) from the C.R.

The second range is non-linear as suggested by Eurocode 3 in its Annex J (CEN 1997):

$$M = \frac{S_{ini,num}}{\left(\frac{M}{M_{e,num}} \right)^{\xi}} \theta \quad \text{for } M_{e,num} < M \le M_{u,num}$$

where the coefficient ξ=2 is proposed for this connection typology.
Finally, the third behavioral range is assumed to be perfectly plastic i.e. $M=M_{u,num}$.
In Figure 51 the experimental (exp) and numerical (num) curves for all tested connections are shown. The values of elastic rotation $\theta_{e,num}$, elastic numerical moment $M_{e,num}$, ultimate rotation $\theta_{u,num}$ and ultimate numerical moment $M_{u,num}$ are identified too.

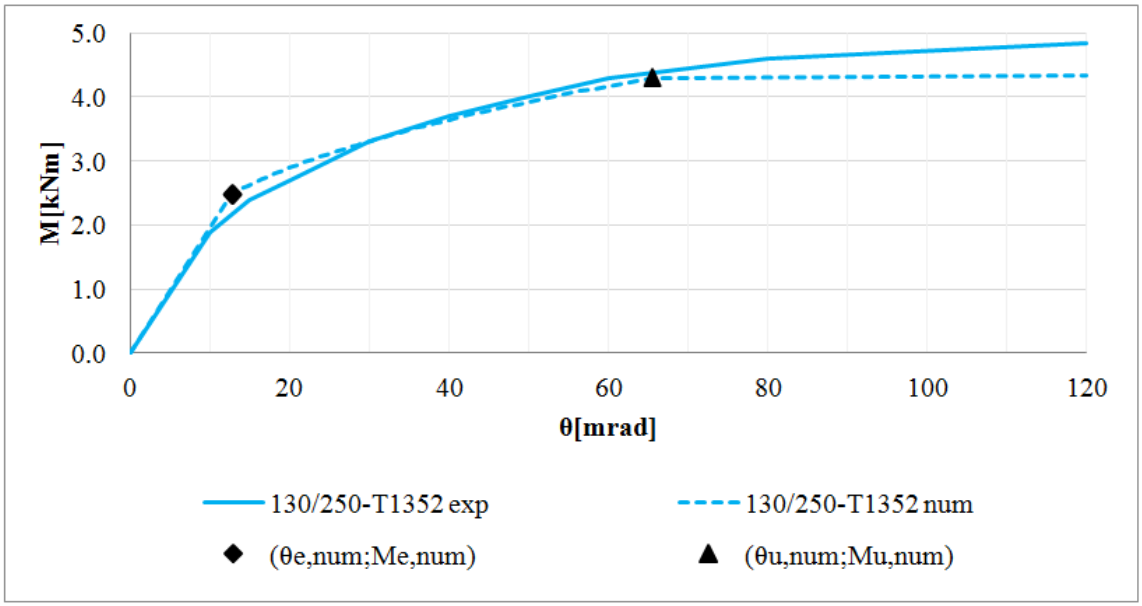
5.0
4.0
3.0
2.0
1.0
0.0
M[kNm]
0
20
40
60
80
100
120
θ[mrad]
130/250-T1352 exp
130/250-T1352 num
(θe,num;Me,num)
(θu,num;Mu,num)

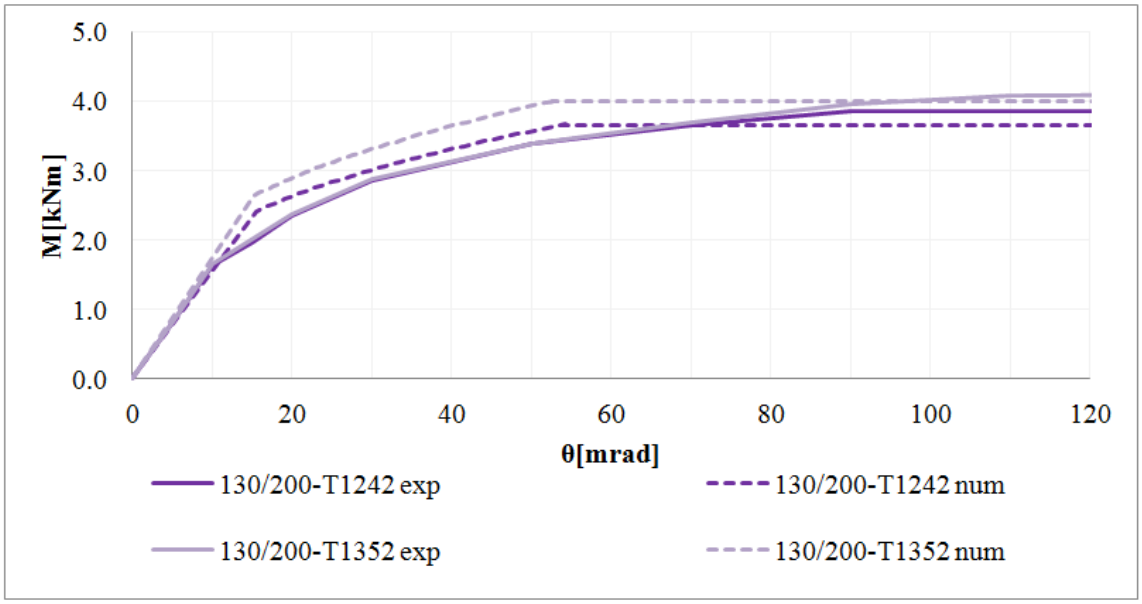
5.0
4.0
3.0
2.0
1.0
0.0
M[kNm]
0
20
40
60
80
100
120
θ[mrad]
130/200-T1242 exp
130/200-T1242 num
130/200-T1352 exp
130/200-T1352 num

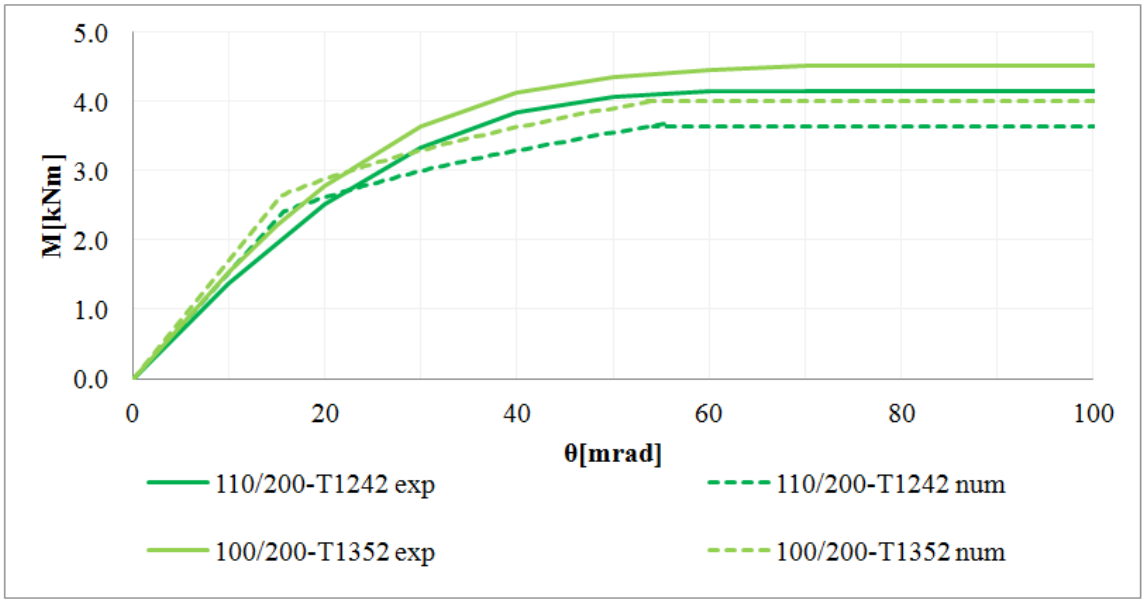
5.0
4.0
3.0
2.0
1.0
0.0
M[kNm]
0
20
40
60
80
100
θ[mrad]
110/200-T1242 exp
110/200-T1242 num
100/200-T1352 exp
100/200-T1352 num

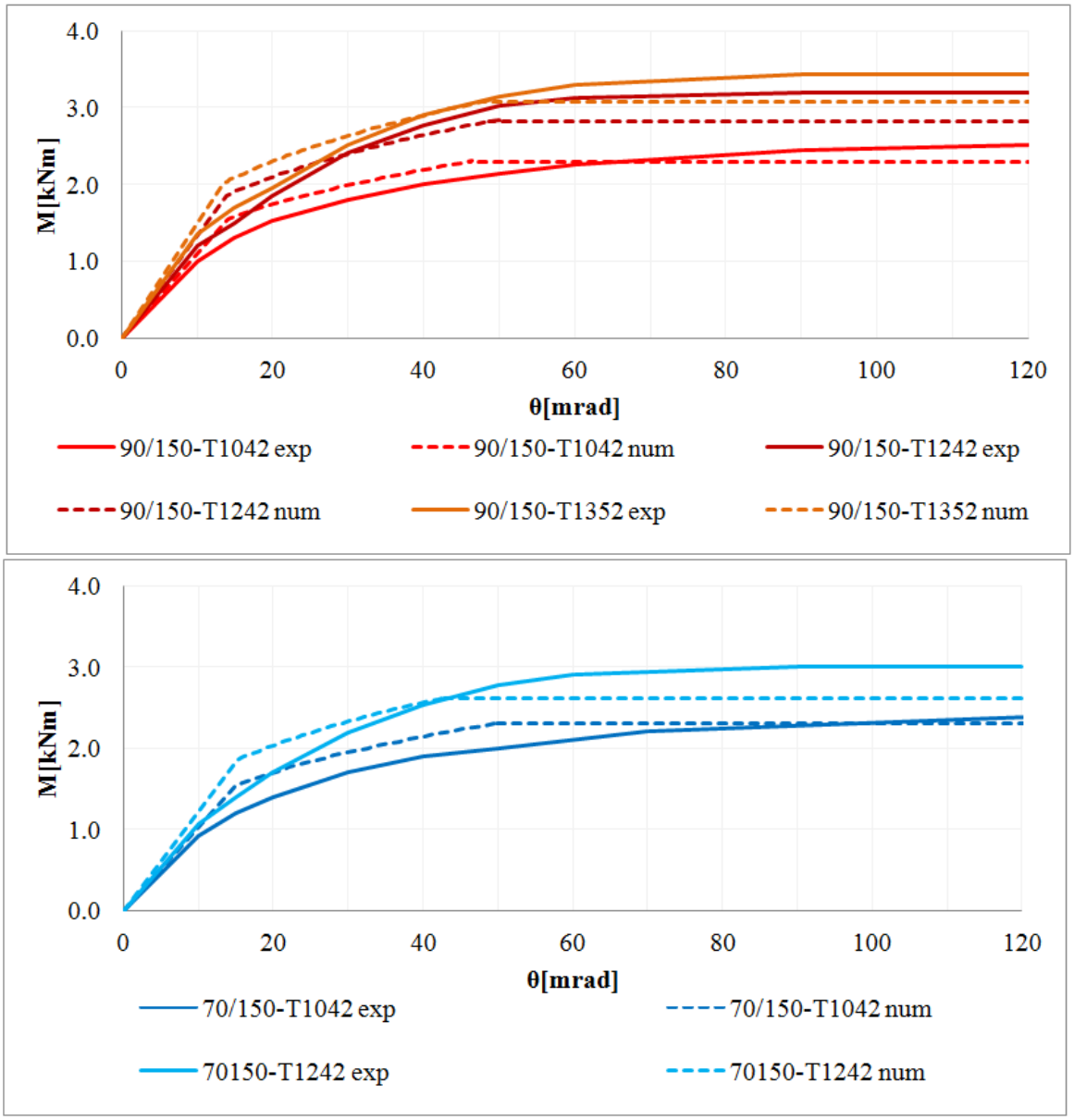

Figure 51. *Theoretical and experimental rack connection moment-rotation curves.*

Results show as theoretical curves well fit the experimental ones, confirming the accuracy of the proposed non-linear equation to approximate the elasto-plastic behavior of rack connections.

3.5.1 Summary of main results

The Component Method has been applied to evaluate the mechanical properties of steel rack connections, in particular their initial flexural elastic stiffness and ultimate moment. The method can be applied to any kind of connection, provided that the basic sources of strength and deformation are properly identified and modeled. Evaluating the influence of each component on the structural response of rack joints, the proposed approach allows the prediction of the beam-column joint failure mode. With the goal to perform reliable seismic analyses of whole moment resisting frame structures, an analytical non-linear equation has been proposed to approximate the effective elasto-plastic behavior of rack beam-to-column joints. The accuracy of the proposed mechanical model has been checked by comparison with experimental results. In conclusion, it appears as a complementary method to expensive experimental testing required by standard codes

and moreover it can be used to improve the structural behavior of rack connections which are produced in long series. Finally, depending on limited geometrical data and mechanical features, the designer can use it for a preliminary assessment of any type of rack joints.

3.6 Influence of mechanical and geometric uncertainty on rack connection structural response

Analytical analyses have showed how the moment-rotation curve of rack connections is influenced by several design parameters: structural properties of connection members (beam, connector, weld and column), steel material (mechanical) properties, and geometric manufacturing details. The propagation of uncertainty in component geometry and mechanical properties to the response of the complete connection in terms of initial elastic flexural stiffness and ultimate moment is herein evaluated. The proposed mechanical model based on the application of the CM is adopted to conduct a Monte Carlo simulation of rack connections. These Monte Carlo simulations are then used to explore the variability of connection response to more accurately assess the structural performance of these joints. The numerical modeling is performed for all configurations Table 12.
In additional to the uncertainty quantification, a sensitivity analysis is performed to identify the quantities influencing joint structural response. With these findings, quality control efforts could be focused on promoting stability in statistical parameters to ensure reliability of rack joints [Melcher and Kala, 2003 and Gervasio et al., 2004]. Monte Carlo simulation of several models of steel rack connections is used to assess component vs. system sensitivity [Bian et al., 2017 and Smith et al., 2016] and to evaluate the resultant variability in the value of initial rotational stiffness and ultimate flexural capacity from uncertainty in steel material properties and geometric manufacturing tolerances.

Table 12. Rack connections tested and members used to assemble them (● Experimental Test, ■ Numerical Test).

Beam	**Weld**	**Connector**	**Column**				
			70/150	90/150	110/200	130/200	130/250
1042	A	M4	● - ■	● - ■	■	■	■
1242	A	M5	● - ■	● - ■	● - ■	● - ■	■
1352	A	M5	■	● - ■	● - ■	● - ■	● - ■
1042	B	M4	■	■	■	■	■
1242	B	M5	■	■	■	■	■
1352	B	M5	■	■	■	■	● - ■

3.7 Probabilistic model

The current design specifications which define the allowable tolerances on geometric properties and material properties for rack connection members are shown in Table 13. Mechanical and geometric requirements for each rack connection member are summarized in Table 14 and Table 15 respectively.

Table 13. Design specifications.

Member	**Material**	**Material Properties - Code**
Beam	S275JRH	EN 10219-1 Cold formed welded structural hollow sections of non-alloy and fine grain steels. Part 1: Technical delivery conditions
Connector	S235JR	EN 10025-2 Hot rolled products of structural steels Part 2: Technical delivery conditions for non-alloy structural steels
Column	S350GD	EN 10346 Continuously hot-dip coated steel flat products Technical delivery conditions
Member	**Material**	**Geometric Features - Code**

Beam	S275JRH	EN 10219-2 Cold formed welded structural hollow sections of non-alloy and fine grain steels Part 2: Tolerances, dimensions and sectional properties
Connector	S235JR	EN 10051 Continuously hot-rolled strip and plate/sheet cut from wide strip of non-alloy and alloy steels – Tolerances on dimensions and shape
Column	S350GD	EN 10143 Continuously hot-dip coated steel sheet and strip – Tolerances on dimension and shape

Table 14. Mechanical requirements.

Designation	Nominal steel grade	Yield strength f_y [Mpa]	Tensile strength f_u [Mpa]
Beam 1042 – 1242 – 1352	S275JRH	$275 \leq f_y$	$430 \leq f_u \leq 580$
Connector M4 – M5	S235JR	$235 \leq f_y$	$360 \leq f_u \leq 510$
Column 70/150 – 90/150]	S350GD	$350 \leq f_y$	$420 \leq f_u$
Column 110/200 – 130/200]	S350GD	$350 \leq f_y$	$420 \leq f_u$
Column 130/250	S350GD	$350 \leq f_y$	$420 \leq f_u$

Table 15. Geometric tolerances.

Designation	Tolerance Cross-section [%]	Nominal thickness [mm]	Tolerance thickness [mm]
Beam 1042 (100x40x2)	±0.8%	2	±0.2
Beam 1242 (120x40x2)	±0.8%	2	±0.2
Beam 1352 (130x50x2)	±0.8%	2	±0.2
Connector M4 – M5	**Deterministic**	3.5	±0.26
Column 70/150 – 90/150		1.5	±0.08
Column 110/200 – 130/200	**Deterministic**	2	±0.09
Column 130/250		2.5	±0.12

For beams, which are roll-formed tubular cross-sections, geometric tolerances exist for their shape and thickness. For columns and connectors, which are stamped and folded, tolerances exist only for thickness; due to their irregular and unusual shape, shape tolerances are assumed to be deterministic. Table 14 and Table 15 serve as initial assumptions for the Monte Carlo simulations performed herein.

3.7.1 Characterization of random variables

The mean (μ_{MC}), coefficient of variation (V_{MC}) and probability distribution adopted in Monte Carlo simulations for material properties (yielding stress f_{yi} and ultimate stress f_{ui}) of each connection member (beam (subscript b), connector (subscript co), and column (subscript cw)) are reported in Table 16. Properties of material random variables were determined through six available coupon tests performed in accordance with [ISO 6892-1, 2009] on different steel coils used for each member. The experimental mean stress (μ_{exp}) and the corresponding experimental coefficient of variation (V_{exp}) are reported in Table 16. This coefficient of variation was less than 0.05 for several test sets (f_{yb}, f_{ub}, f_{ycw} f_{ucw}). In the judgment of the author, these coefficients of variation are not representative of typical variability and it would have been imprudent to adopt such low values in a study of connection uncertainty. Therefore, for those material parameters the coefficient of variation has been set to a minimum value of 0.05.
The deterministic values for material properties (f_{Det}), used to obtain the numerical results previously shown, can be found in Table 16. Deterministic values f_{Det} were obtained by coupon tests on the coil steel of rack connection members. These deterministic values, corresponding to the experimental connection tests, differ only slightly from the mean values of the properties used in the probabilistic analysis.

Table 16. Values of yielding and ultimate stress [N/mm^2] of rack connection member steel.

Values	Beam		Connector		Column					
Nominal Thickness [mm]	t_b=2		t_{co}=3.5		t_{cw}=1.5		t_{cw} =2		t_{cw} =2.5	
Mechanical Properties [N/mm^2]	f_{yb}	f_{ub}	f_{yco}	f_{uco}	f_{ycw}	f_{ucw}	f_{ycw}	f_{ucw}	f_{ycw}	f_{ucw}
Probabilistic Values										
μ_{MC}	451	471	278	374	406	454	419	480	425	469
V_{MC}	0.10	0.05	0.05	0.05	0.05	0.05	0.05	0.05	0.11	0.08
Probability Distribution	Normal	Normal	Normal	Normal	Normal	Normal	Normal	Normal	Normal	Normal
Experimental Values										
μ_{exp} [N/mm^2]	451	471	278	374	406	454	419	480	425	469
V_{exp}	0.10	0.01	0.05	0.05	0.03	0.03	0.04	0.05	0.11	0.08
Deterministic Values										
f_{Det} [N/mm^2]	451	474	282	366	416	461	416	460	416	461

For Monte Carlo simulations, the Young's modulus E, was assumed normal, with V_{MC}=0.1, the steel shear modulus G=E/[2(1+ν)], was chosen as a dependent random variable, with ν=0.3 the Poisson's ratio. Uniformly distributed pseudorandom values, in the ranges defined by design code tolerances, are adopted for the member geometric parameters (Table 17).

Table 17. Ranges of geometric parameters.

Designation	Range cross-section H=height - B=base [mm]	Nominal thickness t [mm]	Range thickness [mm]
Beam 1042 (100x40x2)	H [99.2 - 100.8] – B [39.68 - 40.32]	2	[1.9 – 2.1]
Beam 1242 (120x40x2)	H [119.04 - 120.96] – B [39.68 - 40.32]	2	[1.9 – 2.1]
Beam 1352 (130x50x2)	H [128.96 - 131.04] – B [49.6 - 50.4]	2	[1.9 – 2.1]
Connector M4 – M5	**Deterministic**	3.5	[3.24 - 3.76]
Column 70/150 – 90/150	**Deterministic**	1.5	[1.42 - 1.58]
Column 110/200 – 130/200		2	[1.91 - 2.09]
Column 130/250		2.5	[2.38 - 2.62]

3.8 Probabilistic results

3.8.1 Rack connection flexural capacity

To characterize the stochastic response of rack connections, 10,000 samples are conducted on each rack connection assembly in the Monte Carlo simulation (Table 12), with component material property and geometric uncertainty as described. The difference $(M_{MC}-M_{Det})/M_{Det}$ between the mean from the simulations (M_{MC}) and the deterministic value (M_{Det}), for the ultimate moment of connection with a weld type A, are reported in Table 18.

The ratio $(M_{MC}-M_{Det})/M_{Det} \leq 0$ indicates detrimental system effects: the mean of the ultimate moment is lower than the deterministic mean and therefore system effects are not beneficial. Thus, a design that uses mean member properties to predict the flexural capacity of the rack joint will over-estimate the mean connection ultimate moment. In connections where $(M_{MC}-M_{Det})/M_{Det} \geq 0$, a design using mean member properties will under-estimate the ultimate moment of the rack joint. In these connections, system effects increase flexural capacity. However, it should be noted that in both cases the mean of the ultimate moment obtained by Monte Carlo simulation is very close to deterministic one.

Table 18. Differences $(M_{MC}-M_{Det})/M_{Det}$ [%] in the evaluation of the ultimate moment. (MC) Monte Carlo simulations, (Det) Deterministic values.

Beam	Weld	Connector	Column				
			70/150	90/150	110/200	130/200	130/250
1042	A	M4	-1.75%	-1.49%	2.16%	2.16%	-0.21%
1242	A	M5	-2.80%	-1.49%	1.99%	1.99%	-0.82%
1352	A	M5	-2.43%	-1.50%	2.72%	2.72%	1.22%

The mechanical model can also provide insight into connection failure mode. Flexural capacity $M_{u,num}$ is the minimum of the ultimate bending moment of each member (31): the weld ($M_{u,weld,A}$ for connection with a weld type A, three sided welding, or $M_{u,weld,B}$ for connection with a weld type B, double sided welding), the beam $M_{u,beam}$, the connector $M_{u,connector}$ and the column $M_{u,panel}$. The mean of ultimate bending moment of each member as determined from the Monte Carlo simulation is shown in Figure 52 for all connections along with the experimental ultimate moment $M_{u,exp}$.

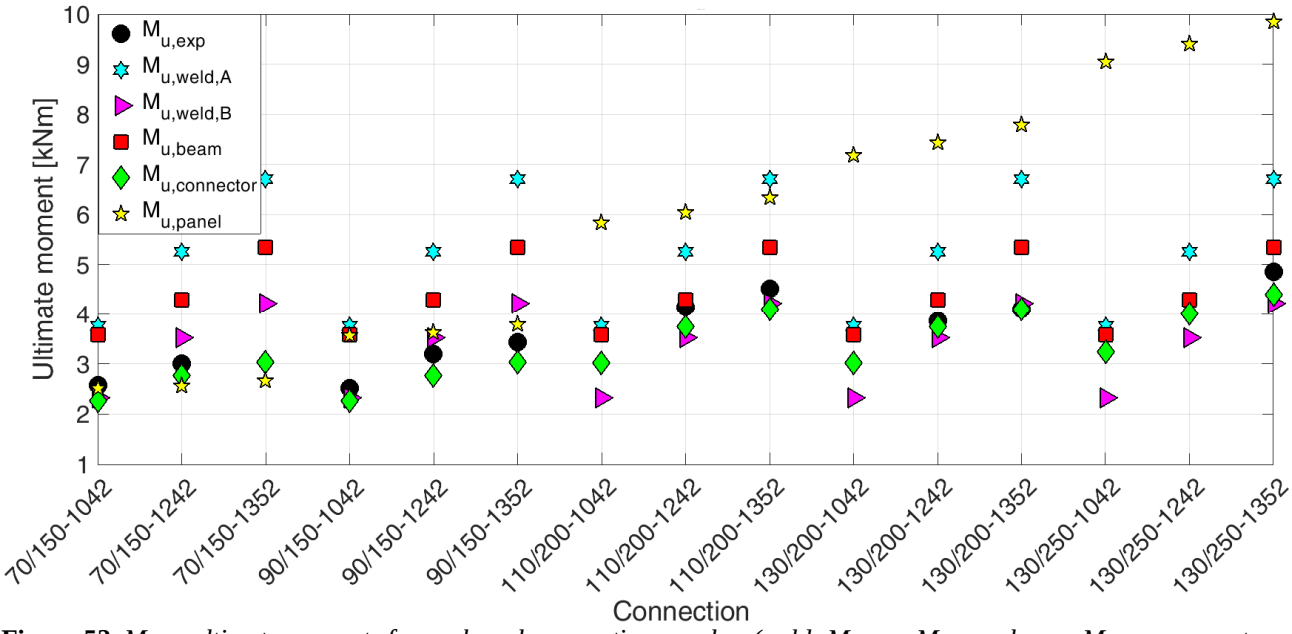

Figure 52. *Mean ultimate moments for each rack connection member (weld: $M_{u,weld,A}$ $M_{u,weld,B;}$ beam: $M_{u,beam;}$ connector: $M_{u,connector;}$ column: $M_{u,panel}$) obtained from Monte Carlo simulation and experimental ultimate moment ($M_{u,exp}$).*

It can be observed that adopting a weld type B on two sides of the beam-end section, the weld ($M_{u,weld,B}$) is the weakest member and collapses (test: 110/200-1042B, 110/200-1242B, 130/200-1042B, 130/200-1242B, 130/250-1042B, 130/250-1242B and 130/250-1352B). Otherwise (weld type A) the failure mode is related to the weakest component of the connector ($M_{u,connector}$). Regardless of weld type, in tests 70/150-1042, 90/150-1042, 90/150-1242 and 90/150-1352 failure is due to the connector member ($M_{u,connector}$), while in tests 70/150-1242 and 70/150-1352 the failure is due to the collapse of the column panel ($M_{u,panel}$). As expected, in tests with the same column, increasing the geometrical dimensions of the beam (1042 → 1352), $M_{u,weld,A}$, $M_{u,weld,B}$ and $M_{u,beam}$ result in an increase. In increasing the number of tabs in the connector (1042 → 1352), $M_{u,connector}$ increases. Increasing the geometrical dimensions of the column (70/150 → 130/250), the mean ultimate moment of the column panel ($M_{u,panel}$) increases. Weld ultimate moment ($M_{u,weld,B}$ and $M_{u,weld,A}$) and beam ultimate moment ($M_{u,beam}$) depend only on the type of beam. The most probable weakest member and corresponding failure mode, which yield the ultimate moment of the connection assembly, are reported in Table 19. These results are in agreement with the experimental results (Table 11).

Table 19. Connection members and their component with highest collapse probability.

Connection	Failure Mode	
	Member	Component
70/150-1042A	Connector	Column web in compression Buckling
70/150-1242A	Column	Column web in shear
70/150-1352A	Column	Column web in shear
90/150-1042A	Connector	Column web in compression Buckling
90/150-1242A	Connector	Column web in punching
90/150-1352A	Connector	Column web in punching
110/200-1042A	Connector	Column web in punching
110/200-1242A	Connector	Column web in punching
110/200-1352A	Connector	Column web in punching
130/200-1042A	Connector	Column web in punching
130/200-1242A	Connector	Column web in punching
130/200-1352A	Connector	Column web in punching
130/250-1042A	Connector	Tabs in shear
130/250-1242A	Connector	Tabs in shear
130/250-1352A	Connector	Tabs in shear
70/150-1042B	Connector	Column web in compression Buckling
70/150-1242B	Column	Column web in shear
70/150-1352B	Column	Column web in shear
90/150-1042B	Connector	Column web in compression Buckling
90/150-1242B	Connector	Column web in punching
90/150-1352B	Connector	Column web in punching
110/200-1042B	Weld	Collapse of weld
110/200-1242B	Weld	Collapse of weld
110/200-1352B	Connector	Column web in punching
130/200-1042B	Weld	Collapse of weld
130/200-1242B	Weld	Collapse of weld
130/200-1352B	Connector	Column web in punching
130/250-1042B	Weld	Collapse of weld
130/250-1242B	Weld	Collapse of weld
130/250-1352B	Weld	Collapse of weld

The discussion above is based on comparing the mean flexural capacities of the members. In any individual MC simulation, however, the failure mode may differ from that predicted by the mean. In order to illustrate the change in failure mode that occurs from the combination of the random variables, the percentage of failure mode for all rack connections is shown in Figure 53 and Figure 54, connections with weld type A and type B respectively.

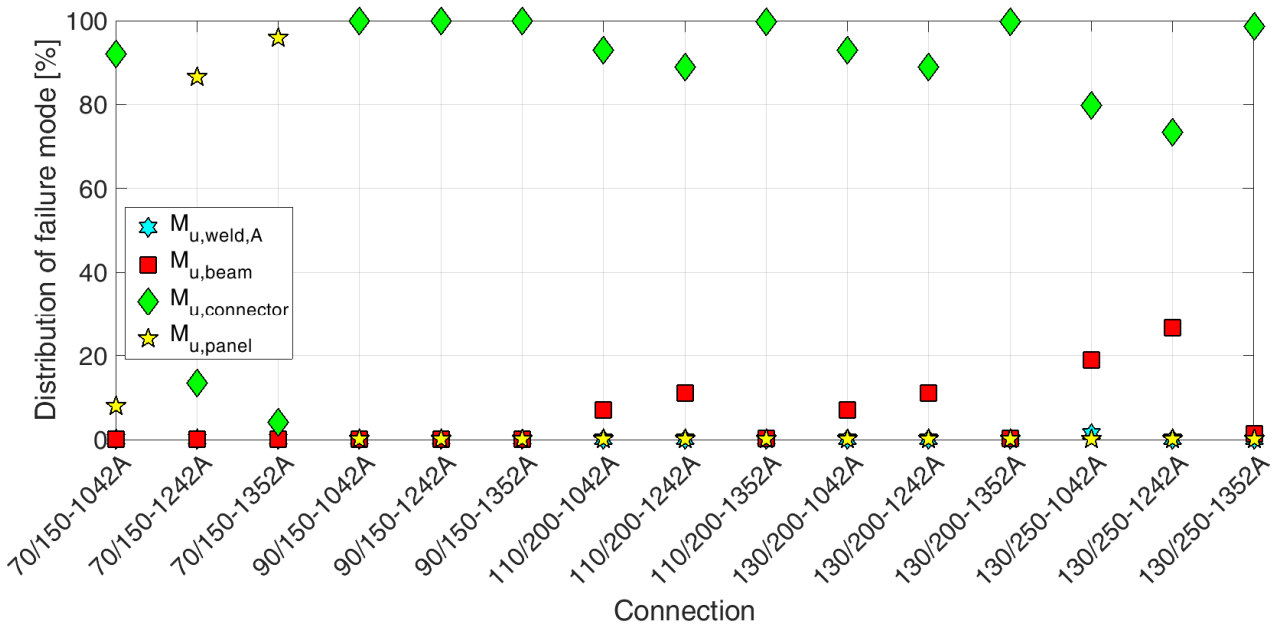

Figure 53. *Distribution of failure modes (configurations with weld type A).*

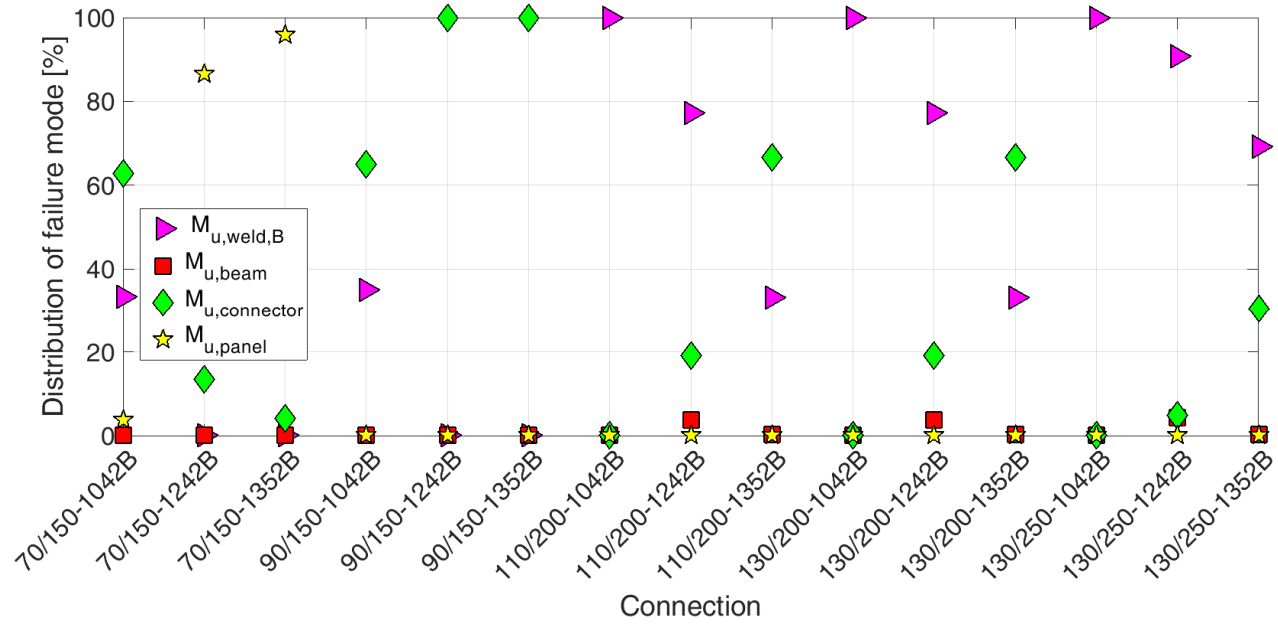

Figure 54. *Distribution of failure modes (configurations with weld type B).*

The difference between the mean ultimate moment of connections with weld type B ($M_{u,num,B}$) and the mean ultimate moment of connections with weld type A ($M_{u,num,A}$), is shown in Table 20.

Table 20. Difference ($(M_{u,numB}-M_{u,num,A})/M_{u,num.A}$) [%] in the mean ultimate moment.

Column	***70 150***	***70 150***	***70 150***	***90 150***	***90 150***	***90 150***	***110 200***	***110 200***	***110 200***	***130 200***	***130 200***	***130 200***	***130 250***	***130 250***	***130 250***
Beam	***1042***	***1242***	***1352***	***1042***	***1242***	***1352***	***1042***	***1242***	***1352***	***1042***	***1242***	***1352***	***1042***	***1242***	***1352***
Difference	-2%	0%	0%	-2%	0%	0%	-23%	-6%	-2%	-23%	-6%	-2%	-27%	-11%	-5%

In all cases shown in Figure 53, weld ultimate moment ($M_{u,weld,A}$) does not contribute to the governing failure mode. Tests with a weak column (70/150-1242A and 70/150-1352A, see Figure 53) are more likely to fail due to the collapse of the column panel ($M_{u,panel}$). At the same time, test 70/150-1042A is more likely to fail because of the collapse of the connector member, particularly via column buckling (Table 19). In fact, because of a shorter bottom flange of the connector (connector M4), the compression force in test 70/150-1042 is more concentred compared to test

70/150-1242 and 70/150-1352, leading to the buckling of the column web. In the other connections, with an adequate weld on three sides of the beam-end section (connection type A), the connector member ($M_{u,connector}$) dictates failure.

For connections with weld type B (Figure 54), $M_{u,weld,B}$ is the limiting factor (excepting test 70/150-1242B, 70/150-1352B, 90/150-1242B, 90/150-1352B, 110/200-1352B and 130/200-1352B) and reduces the ultimate moment of joints (Table 20). Another observation is that for weld type B connections, there is substantial uncertainty in which component causes failure of the connection. In practice, this weld type would generally be avoided. In accordance with [EN 1993-1-8, 2005] the fillet welds should be continuous around the corner for a distance of at least twice the leg length of the weld.

The coefficient of variations (CoV) for the ultimate moment of connection members ($M_{u,weld,A}$ $M_{u,weld,B}$ for weld, $M_{u,beam}$ for beam, $M_{u,connector}$ for connector and $M_{u,panel}$ for column) and connections ($M_{u,num,A}$ for connection type A and $M_{u,num,B}$ for connection type B) are shown in Table 21.

Table 21. Coefficient of variation for the ultimate moment of members and for the moment capacity of rack joints.

Column	***70 150***	***70 150***	***70 150***	***90 150***	***90 150***	***90 150***	***110 200***	***110 200***	***110 200***	***130 200***	***130 200***	***130 200***	***130 250***	***130 250***	***130 250***
Beam	***1042***	***1242***	***1352***	***1042***	***1242***	***1352***	***1042***	***1242***	***1352***	***1042***	***1242***	***1352***	***1042***	***1242***	***1352***
$\mathbf{M_{u,weld,A}}$	0.05	0.05	0.05	0.05	0.05	0.05	0.05	0.05	0.05	0.05	0.05	0.05	0.05	0.05	0.05
$\mathbf{M_{u,weld,B}}$	0.05	0.05	0.05	0.05	0.05	0.05	0.05	0.05	0.05	0.05	0.05	0.05	0.05	0.05	0.05
$\mathbf{M_{u,beam}}$	0.10	0.10	0.07	0.10	0.10	0.07	0.10	0.10	0.07	0.10	0.10	0.07	0.10	0.10	0.07
$\mathbf{M_{u,connector}}$	0.05	0.05	0.05	0.05	0.05	0.06	0.05	0.05	0.05	0.05	0.05	0.05	0.06	0.06	0.06
$\mathbf{M_{u,panel}}$	0.06	0.06	0.06	0.06	0.06	0.06	0.06	0.06	0.06	0.06	0.06	0.06	0.12	0.11	0.11
$\mathbf{M_{u,num,A}}$	0.05	0.05	0.06	0.05	0.05	0.05	0.05	0.05	0.05	0.05	0.05	0.05	0.06	0.06	0.06
$\mathbf{M_{u,num,B}}$	0.05	0.05	0.06	0.05	0.05	0.05	0.05	0.05	0.04	0.05	0.05	0.04	0.05	0.05	0.05

It is worth noting a general reduction in the value of the connection ultimate moment CoV; the mean of the member CoVs is greater than that of the joint (≈ 0.05) (Table 21). This reduction in variability is beneficial and is a consequence of the plastic redistribution of forces in rack joint. To illustrate this uncertainty propagation from the members to the connection, histograms of member and connection ultimate moment are shown in Figure 55 for test 130/250-1352.

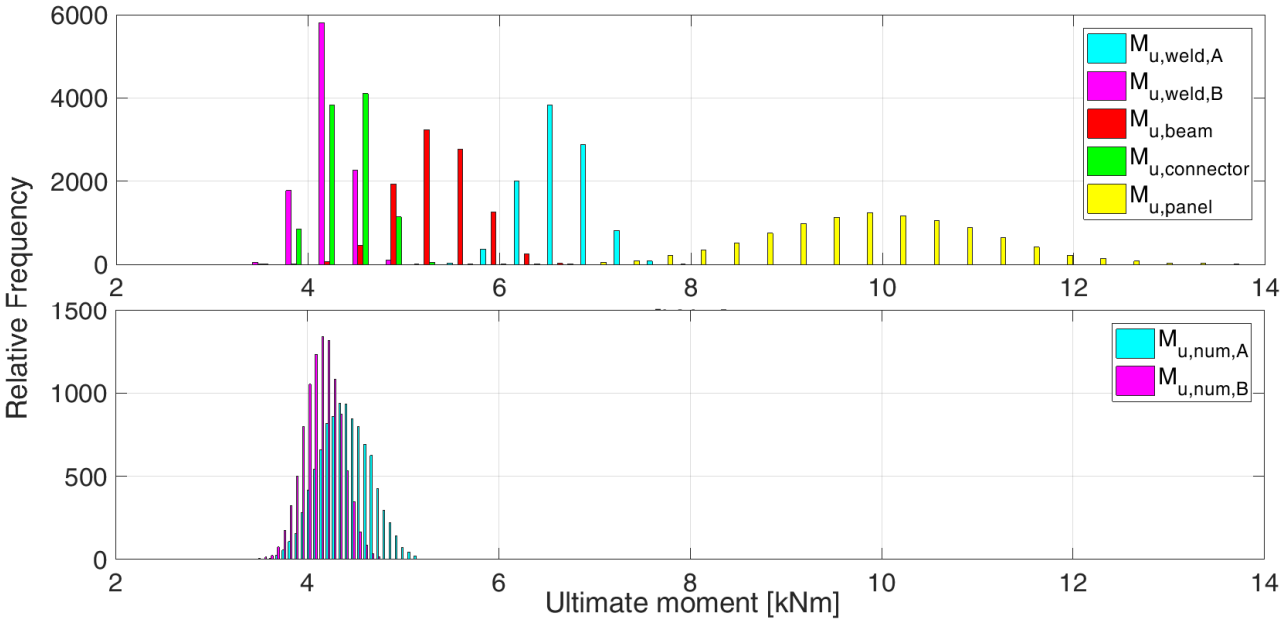

Figure 55. *Histograms of member ultimate moment and Histograms of rack connection ultimate moment (weld type A – $M_{u,num,A}$ and weld type B – $M_{u,num,B}$). (Test 130/250-1352).*

For connection type A, the failure mode is the minimum of $M_{u,connector}$ and $M_{u,beam}$ and the connector ultimately dictates failure. The same connection with the weaker weld (type B) has a higher probability of failure due to the collapse of the weld ($M_{u,weld,B}$) (Figure 55). The ultimate moment of the connection also decreases ($M_{u,num.B}<M_{u,num,A}$) as well as the CoV of rack joint (see Table 21). To further characterize these rack connections, kurtosis and skewness for the distributions of ultimate moment are shown in Table 22.

Table 22. Kurtosis (K.($M_{u,num,i}$)) and Skewness (S.($M_{u,num,i}$)) of the ultimate moment distribution for all rack connections (Connection type A, i=A; Connection type B, i=B).

Column	***70 150***	***70 150***	***70 150***	***90 150***	***90 150***	***90 150***	***110 200***	***110 200***	***110 200***	***130 200***	***130 200***	***130 200***	***130 250***	***130 250***	***130 250***
Beam	***1042***	***1242***	***1352***	***1042***	***1242***	***1352***	***1042***	***1242***	***1352***	***1042***	***1242***	***1352***	***1042***	***1242***	***1352***
K.($M_{u,num,A}$)	2.85	2.93	2.93	2.92	2.92	2.92	3.35	3.55	3.04	3.35	3.55	3.04	3.16	3.36	2.73
K.($M_{u,num,B}$)	2.97	2.93	2.93	2.95	2.92	2.92	2.96	3.27	3.04	2.96	3.27	3.04	2.96	3.16	3.01
S.($M_{u,num,A}$)	0.01	-0.08	-0.03	0.09	0.09	0.08	-0.07	-0.15	0.07	-0.07	-0.15	0.07	-0.16	-0.21	0.03
S.($M_{u,num,B}$)	-0.07	-0.08	-0.03	-0.05	0.09	0.08	0.00	-0.19	-0.09	0.00	-0.19	-0.09	0.00	-0.12	-0.04

A normal distribution with skewness (≈ 0) and kurtosis (≈ 3) is a good approximation of the connection ultimate moment histogram.

3.8.2 Rack connection rotational stiffness

The dimensionless differences (S_{MC}-S_{Det})/S_{Det} between the mean (from the simulations - S_{MC}) and the deterministic value (based on average properties - S_{Det}) of the initial elastic rotational stiffness are reported in Table 23.

Table 23. Differences (S_{MC}-S_{Det})/S_{Det} [%] in the evaluation of the initial elastic rotational (flexural) stiffness. (MC) Monte Carlo simulations, (Det) Deterministic values.

Beam	**Weld**	**Connector**	**Column**				
			70/150	90/150	110/200	130/200	130/250
1042	A	M4	-0.57%	-0.64%	-0.46%	-0.46%	-0.69%
1242	A	M5	-0.61%	-0.70%	-0.06%	-0.04%	-0.46%
1352	A	M5	-0.60%	-0.69%	-0.04%	-0.01%	-0.44%

(S_{MC}-S_{Det})/S_{Det} ≤ 0 for all connections, indicating that the mean stiffness is slightly lower than the deterministic stiffness (minimum value -0.7%) and therefore not all system effects are beneficial. Thus, a design that uses mean member properties to predict the initial rotational stiffness of the rack joint will modestly over-estimate the mean flexural stiffness.

The prediction of the initial rotational stiffness $S_{ini,num}$ of the entire connection is obtained from $S_{ini,num} = \frac{1}{\sum_{n=1}^{3} \frac{1}{S_n}}$ (38) where: S_1 is the rotational stiffness for the column panel, S_2 the rotational stiffness for the connector and S_3 the rotational stiffness for the beam. Assuming a rigid plastic behavior for the weld component, it does not influence flexural stiffness of the connection.

The values of the initial rotational stiffness of connection members (column *S1*, connector *S2* and beam *S3*) and rack connection ($S_{ini,num}$) are reported in Figure 56.

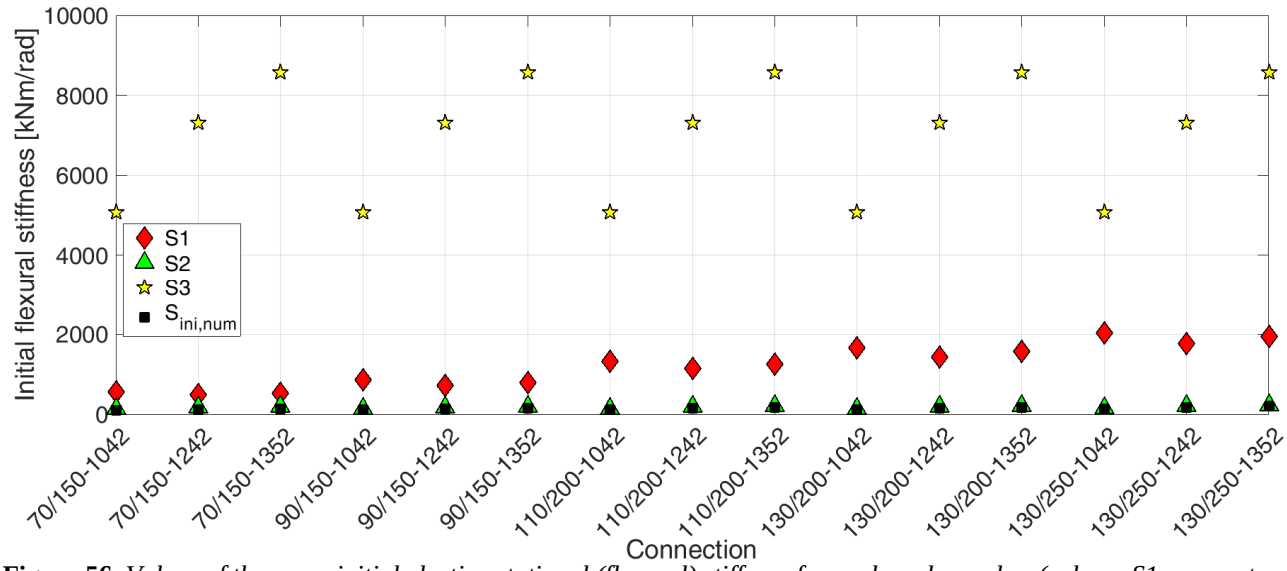

Figure 56. *Values of the mean initial elastic rotational (flexural) stiffness for each rack member (column S1, connector S2 and beam S3) and connection ($S_{ini,num}$) obtained in Monte Carlo simulation.*

Recall that *S1*, *S2* and *S3* can be considered as three springs in series. The most deformable element is connector (*S2*) whose stiffness is similar to that of the entire connection ($S_{ini,num}$). The effect of the stiffness of the beam (*S3*) on the connection can be neglected (as neglecting the contribution of beam deformation does not meaningfully change the connection stiffness). As expected, in reducing the cross-section of the column (130/250 → 70/150), the flexural stiffness of the column (*S1*) decreases. Within the connector components, the deformation of the tabs (Figure 57 a)), connector flange (Figure 57 b)) and column web in bearing (Figure 57 c)) have the greatest influence on joint deformation and will govern.

a) Component: Tab in bending and shear ($K_{t,s}$)
Test 130/250-1352A
Deformation of tab

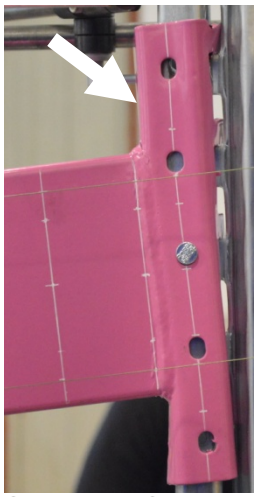

b) Component: Connector in bending($K_{co,1}$)
Test 130/250-1352A
Deformation of connector flange

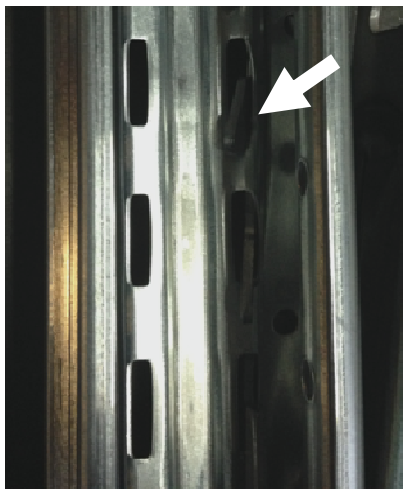

c) Component: Column web in bearing($K_{cw,b}$)
Test 90/150-T 1242A
Deformation of column web at holes

Figure 57. *Connector component deformation observed in experimental tests.*

The coefficient of variation (CoV) for the flexural stiffness of connection members (*S1* for column, *S2* for connector and *S3* for beam) and connections ($S_{ini,num}$) are shown in Table 24.

Table 24. Coefficient of variation for the flexural stiffness of members and the flexural resistance of rack joints.

Column	***70 150***	***70 150***	***70 150***	***90 150***	***90 150***	***90 150***	***110 200***	***110 200***	***110 200***	***130 200***	***130 200***	***130 200***	***130 250***	***130 250***	***130 250***
Beam	***1042***	***1242***	***1352***	***1042***	***1242***	***1352***	***1042***	***1242***	***1352***	***1042***	***1242***	***1352***	***1042***	***1242***	***1352***
S1	0.11	0.11	0.11	0.11	0.11	0.11	0.11	0.11	0.11	0.11	0.11	0.11	0.11	0.11	0.11
S2	0.09	0.08	0.08	0.09	0.08	0.08	0.09	0.09	0.09	0.09	0.09	0.09	0.09	0.09	0.09
S3	0.12	0.12	0.12	0.12	0.12	0.12	0.12	0.12	0.12	0.12	0.12	0.12	0.12	0.12	0.12
$S_{ini,num}$	0.09	0.09	0.09	0.09	0.08	0.08	0.09	0.09	0.09	0.09	0.09	0.09	0.09	0.09	0.09

As opposed to the reduction in CoV observed in the ultimate moments of the rack joints, joint flexural stiffness CoV has greater dispersion (≈ 0.09). This effect is a consequence of the connection members acting in series. In determining the ultimate moment of the joint, the weakest component is critical while for stiffness, each component contributes to the overall connection flexural stiffness. The CoV of the overall connection ($S_{ini,num}$) is similar to that of the connector (*S2*) thus confirming the reduced influence of column (*S1*) and beam (*S3*). These results are highlighted by the histograms of the flexural stiffness of members and connection (Figure 58, for test 130/250-1352).

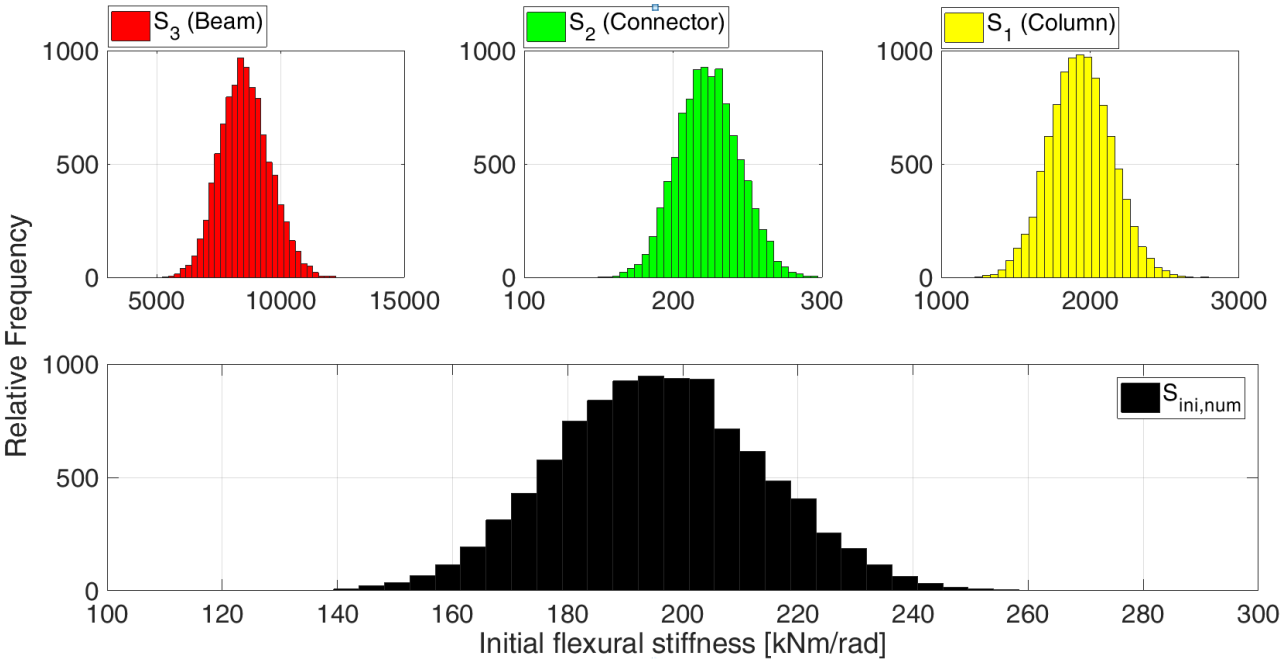

Figure 58. *Histograms of flexural stiffness for members and connection (Test 130/250-1352).*

In Table 25 the values of kurtosis and skewness of the flexural stiffness distributions for all rack connections are reported.

Table 25. Kurtosis (K.($S_{ini,num}$)) and skewness (S.($S_{ini,num}$)) of flexural stiffness for all rack connections.

Column	***70 150***	***70 150***	***70 150***	***90 150***	***90 150***	***90 150***	***110 200***	***110 200***	***110 200***	***130 200***	***130 200***	***130 200***	***130 250***	***130 250***	***130 250***
Beam	***1042***	***1242***	***1352***	***1042***	***1242***	***1352***	***1042***	***1242***	***1352***	***1042***	***1242***	***1352***	***1042***	***1242***	***1352***
K.($S_{ini,num}$)	2.83	2.85	2.85	2.81	2.83	2.84	2.84	2.85	2.87	2.84	2.84	2.86	2.90	2.90	2.90
S.($S_{ini,num}$)	0.03	0.00	0.00	0.03	0.00	0.00	0.03	0.01	0.01	0.02	0.01	0.01	0.08	0.08	0.08

The symmetry of the connection flexural stiffness histograms is highlighted by a skewness ≈ 0 for all connections. A kurtosis mildly less than 3 allows to assume the normal distribution as a good approximation to fit the connection flexural stiffness histogram.

3.9 Summary of main results

The flexural resistance and initial elastic flexural stiffness of CFS rack connection are affected by the local response of connection component. This response derives from the component structural details and it is influenced by the uncertainty in steel mechanical properties and geometrical features. In order to explore the impact of these parameters, Monte Carlo simulation of several rack connection assemblies is developed adopting random values to simulate the effect of the variability in the steel yielding stress, steel ultimate stress and geometrical features of the beam, connector and column. For development of simulations, statistical properties of material random variables were assumed on results of experimental tests, the variability in geometric tolerances was assumed in accordance with current standard code requirements and the structural response of rack joints was modeled by a mechanical model based on the Component Method. Monte Carlo simulations indicate that the variability of geometric and mechanical properties mitigates in the evaluation of the connection ultimate moment (CoV≈0.05). This redistribution occurs due to plasticity in the rack joint and the weakest link fails first. The variability in the flexural stiffness is greater (CoV≈0.09) due to components in series compounding to contribute to total connection stiffness. Finally, a normal probability distribution function well fits for both the connection ultimate moment and initial flexural stiffness histograms.
Results further highlight the effect on failure mode and ultimate moment due to varying connection configurations. A two-sided weld is insufficient. With an adequate weld, connection failure mode mainly depends to the collapse of the weakest component in the connector member. The flexural stiffness of the rack joint is limited by the connector stiffness, and is thus the most critical feature which should be controlled with greater accuracy in the manufacturing process.

4 FE NUMERICAL MODEL

4.1 Pinching in steel rack joints: numerical modeling and effects on structural response

Experimental tests on rack connections have highlighted a pinching in hysteresis loops, with the consequence of a reduced dissipated hysteretic energy and load carrying capacity. In this chapter, a simplified FE numerical "Pinching Model", capable to simulate the cyclic mechanical response of beam-to-column joints is developed. The numerical model is checked by the comparison with both literature data and experimental results of laboratory tests.
The proposed model is characterised by three links placed in parallel: two "composed links" describe the non-linear bending moment-rotation curve of the joint, and a linear elastic link transfers the axial and shear force from the beam to the column. The model is appropriate to investigate the down-aisle seismic response of rack systems and it can be easily implemented in commercial software packages, commonly used for non-linear seismic vulnerability analyses. Features of the model can be estimated from few structural data, through the mechanical model previously developed, and it does not require expensive cyclic experimental tests.
For a deeper understanding of the effects of pinching in the seismic response and to highlight the potentiality of the proposed model a case-study example is also considered. The case-study concerns a rack system, whose beam-to-column joints are modeled using two numerical approaches which differ in the deterioration of the rotational stiffness of joints. Non-linear dynamic analyses, with simulated ground acceleration time-histories, are carried out.

4.1.1 Design of earthquake resistant steel racks

Steel storage pallet racks may be designed in accordance with a non-dissipative structural behavior, assuming a linear material constitutive law, or with a dissipative structural behavior. In this last case, the dissipative capacity may be taken into account explicitly through a non-linear analysis or implicitly through a linear elastic analysis, under a reduced elastic response spectrum scaled by the seismic behavior factor q >1 [EN 1998-1-1, 2004]. It is worth noting that in rack systems, only beam-to-column joints and base-plate joints are able to provide a post-elastic behavior. In fact, all the other members (beams, diagonals and uprights) are usually formed by thin-walled CFS, so they belong to 3rd or 4th class according to [EN 1993-1-1, 2005] and their response is limited to the elastic field without providing a stable post-elastic behavior. The assessment of q-factor is a fundamental task, which requires to accurately investigate the peculiar features of these systems.
Numerical studies [Baldassino and Bernuzzi, 2000] on the influence of beam-to-column joint behavior, on the down-aisle response of storage racks, suggest implementing frame model with semi-rigid joints. In [Bernuzzi et al., 2004] the increment of the seismic capacity of rack structures through bracing systems has been investigated. European standard provisions [EN 16681, 2013 and FEM 10.2.08, 2011] require a q-factor not greater than 2 for non-dissipative structural behavior, but they do not give rules to assess its effective value. For this purpose, several non-linear pushover analyses on full-scale steel rack systems and numerical models have been carried out in the last decade [Brambilla et al., 2015, Rosin et al., 2009 and Castiglioni et al., 2014, Yin et al., 2018 (b)], showing q-factors greater than 1.5, even if tested rack systems were not designed according to the capacity design approach.
It should be noted that in the pushover method, lateral forces are applied to the structure and increased monotonically [EN 1998-1-1, 2004], so that only the knowledge of the monotonic moment-rotation curve of joints is required. The negative issue affecting this approach is that the effective hysteretic response of beam-to-column joints is neglected, even if cyclic experimental test on rack joints have shown the unstable behavior of their hysteresis loop [Bernuzzi and Castiglioni, 2001, Aguirre, 2005 and Yin et al., 2016].

This structural behavior is expected to reflect on the seismic response of an overall rack system, with the direct consequence that the load carrying capacity of a whole rack structure will be reduced. This aspect is investigated through a simplified numerical Pinching Model (PM) for beam-to-upright joints herein developed and implemented in a software package; which allows a preliminary assessment of the effective reliability of quasi-static pushover analyses.

4.1.2 Rack connection hysteresis loop

The shape of the experimental hysteresis loop is similar to literature ones: the envelope of the cyclic joint response is comparable with the monotonic curve, as observed in [Yin et al., 2016], and the stiffness of reloading branches decreases progressively with the evolution of the test, hence resulting in a non-negligible pinching. The pinching is due to tabs of the connector, which lose partial contact with the surrounding column web at column slots because of the permanent deformation produced by previous cyclic loading (Figure 59). The pinching phenomenon results in the accelerated reloading stiffness degradation with increasing displacement loading [Bernuzzi and Castiglioni, 2001]. Moreover, the slope of the unloading path is equal to the initial elastic one, so that the pinching increases with progressive cycles, as observed in [Aguirre, 2005].
The pinching phenomenon can be high pronounced, as cycles subsequent to the first can have an initial reloading branch with a zero stiffness (slippage phenomenon).

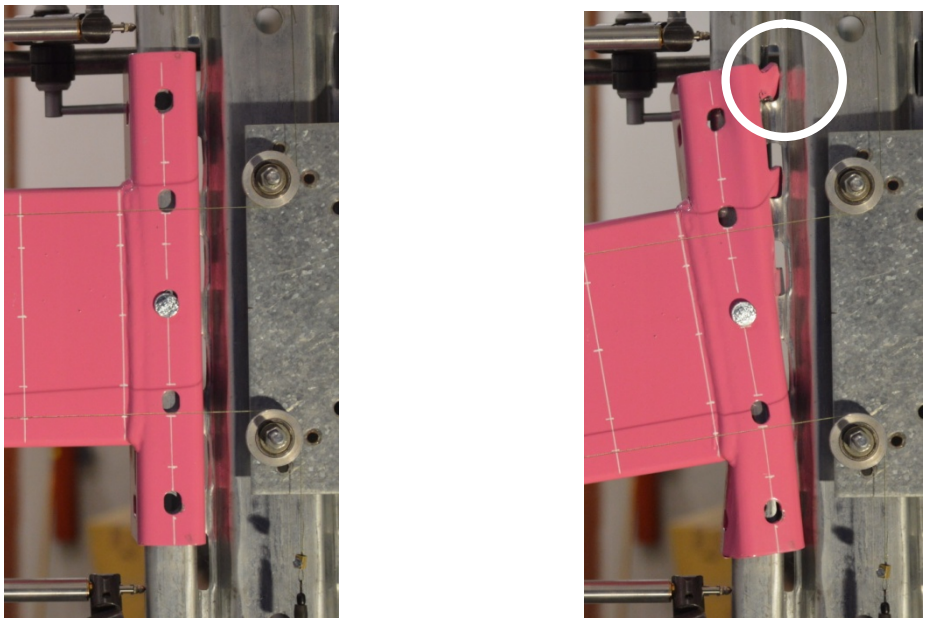

a) *b)*

Figure 59. *a) Undeformed configuration of the connector; b) Deformed configuration of the connector with tabs in plastic range.*

4.2 The proposed Pinching Model

The proposed Pinching Model (PM) is an implicit numerical model whose main requirements are:
- to be formed by a combination of link elements available in commercial software with the purpose to be easily implemented in FE non-linear analysis packages currently available in engineering offices;
- to give an evaluation, on the safe side, of effects of rack joint behavior on the seismic response of rack systems;
- to be described through a few parameters without the need to perform specific cyclic experimental tests.

Following approaches proposed in [Baldassino and Bernuzzi, 2000 and Abdel-Jaber et al., 2005], the behavior of the connector is modeled in terms of the monotonic bending moment-rotation law, with a multi-linear relationship capable to simulate accurately the joint response. Differently from models developed in [Baldassino and Bernuzzi, 2000 and Abdel-Jaber et al., 2005], which describe only the monotonic behavior of joints, the PM is capable to describe the hysteresis loop of joints, showing the pinching phenomenon exhibited in experimental tests.
In literature, the Pivot model [Dowel et al., 1998, see Figure 60] has been recently used to evaluate the influence of the joints on the rack systems response [Bernuzzi and Simoncelli, 2016]. In this implicit model, in addition to the knowledge of the monotonic M-θ joint curve, the values of pointer points (P^+ and P^-) are required, to define the slope of the unloading branches. After the first half-cycle, the unloading phase is represented by the BC line, defined by points B and P^- until the bending moment reduces to zero (point C) and then is followed by a slippage branch to the origin (CD). Reloading branch is along the line from origin to the last point reached in the previous half-cycle.

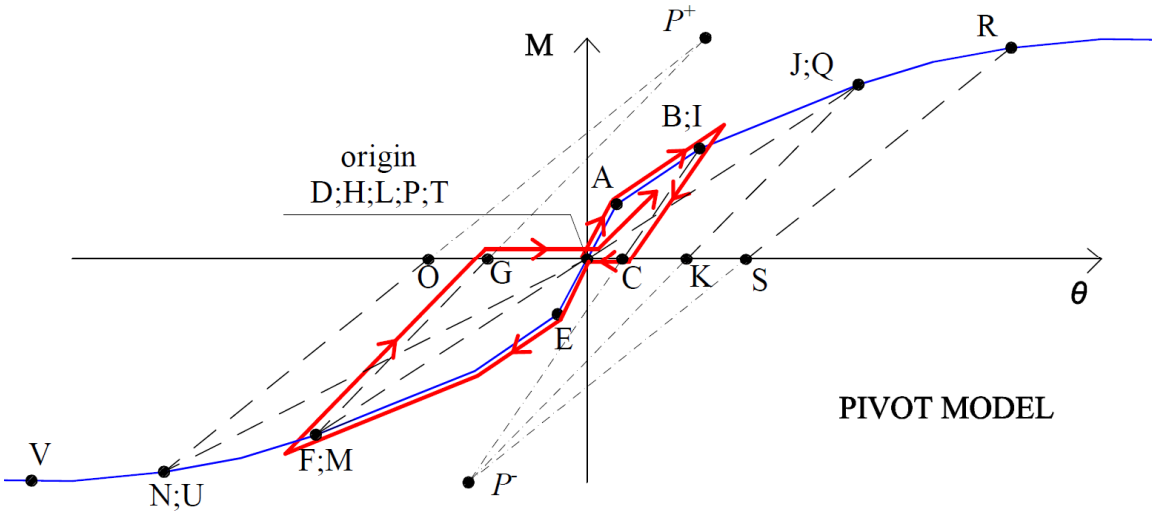

Figure 60. *Cyclic response according to the Pivot model (Dowel et al., 1998).*

The disadvantage of the Pivot model is that the unloading phase, until the bending moment reduces to zero, is followed by a slippage branch until the origin. As a consequence, the model cannot be considered on the safe side in the modeling of joints with high pronounced pinching (slippage phenomenon).
The proposed PM (Figure 61 a) is formed by three elements placed in parallel: a first "composed link" constituted by a rotational link with a multi-linear moment-rotation constitutive law in series with a gap link; a second "composed link" constituted by another rotational link in series with a hook link, and as third element, a link with a linear elastic force-displacement relationship to carry the shear and axial forces (Figure 61a).

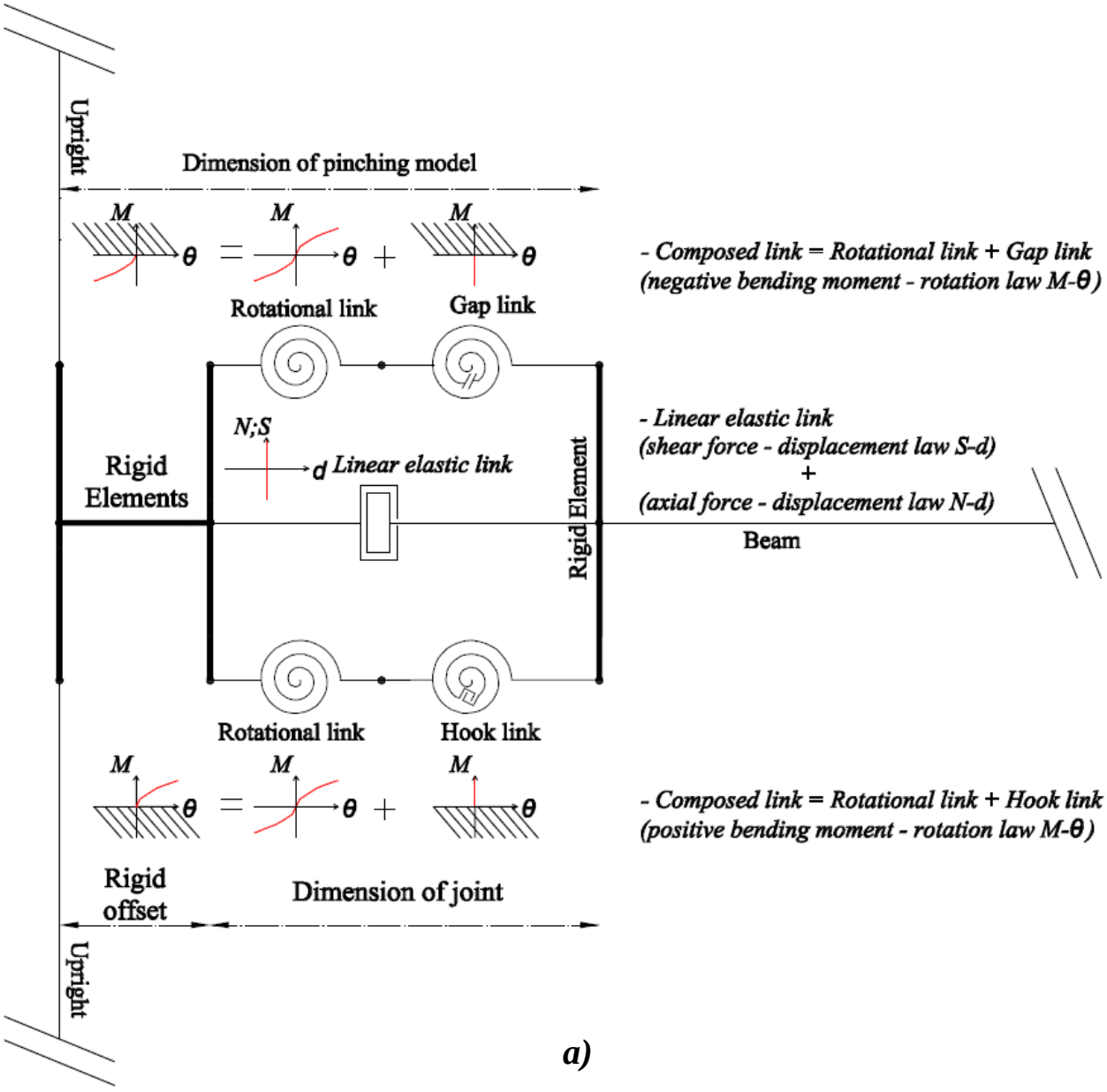

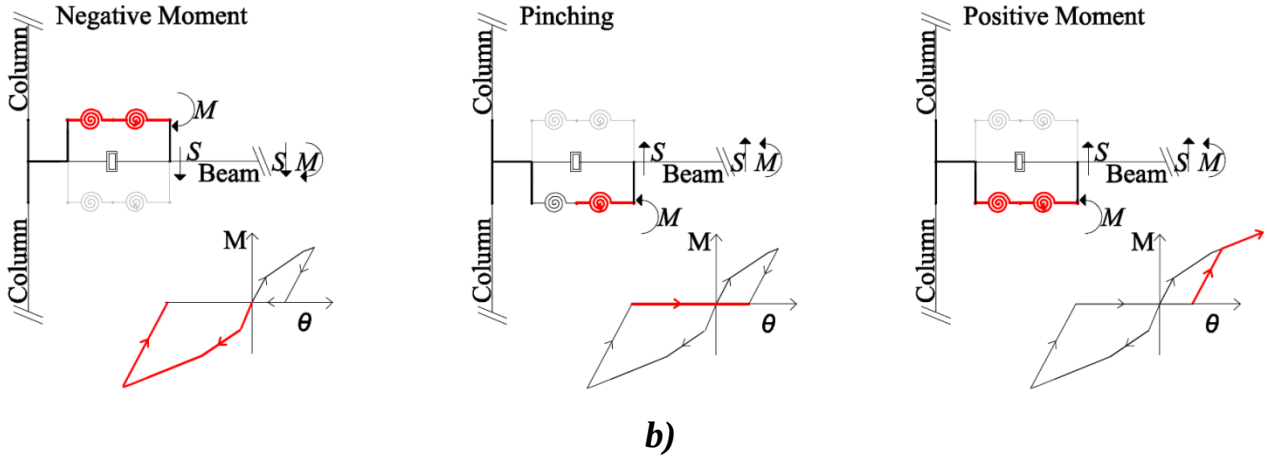

Figure 61. *a) The Pinching Model (PM). b) Effect of the "composed link" on the pinching behavior.*

Rotational links describe the moment-rotation law of the joint approximating the experimental monotonic curve with a numerical multi-linear curve, which passes through an adequate number of experimental points (M-Θ).
The pinching phenomenon is described by means of two links that transfer only negative and positive bending moment, the "gap link" and the "hook link" respectively. These links are placed in series with rotational links, forming two "composed links" which work alternately, depending on the bending moment sign transferred by the beam. Gap and hook links are assumed to be infinitely rigid, with a stiffness much higher than the bending initial stiffness of the rotational links [SAP 2000, 2016]. The contribution of the "composed link" to the pinching response is shown in Figure 61 b).
The third linear elastic link (Figure 61 a) is placed in parallel with the two composed links to restrain the other degrees of freedom of the joint. The linear elastic link is modeled by two force-displacement (d) infinitely rigid curves; it transfers the axial (N) and shear (S) force from the beam to the column.
The PM has a finite length equal to the distance between the upright axis and the beam-end section (Figure 62). Rigid elements connect the beam to links and links to the upright, defining the joint physical size (Figure 61 a).

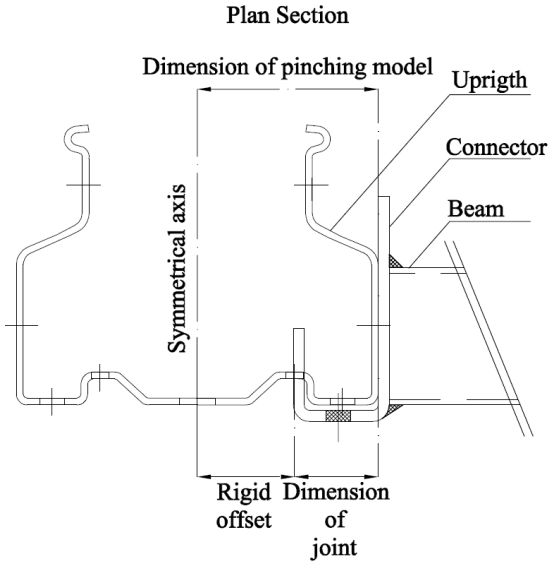

Figure 62. *Plan of the upright-beam joint and size of the Pinching Model.*

The proposed PM describes the slippage phenomenon, differently from the commonly used Pivot model [Dowel et al., 1998], reloading curve has essentially zero stiffness, the target point for this curve is at the deformation reached under the previous unloading cycle (follow points in the alphabetical order starting from the origin in Figure 63. Finally, the slope of unloading branches is equal to the initial elastic one.

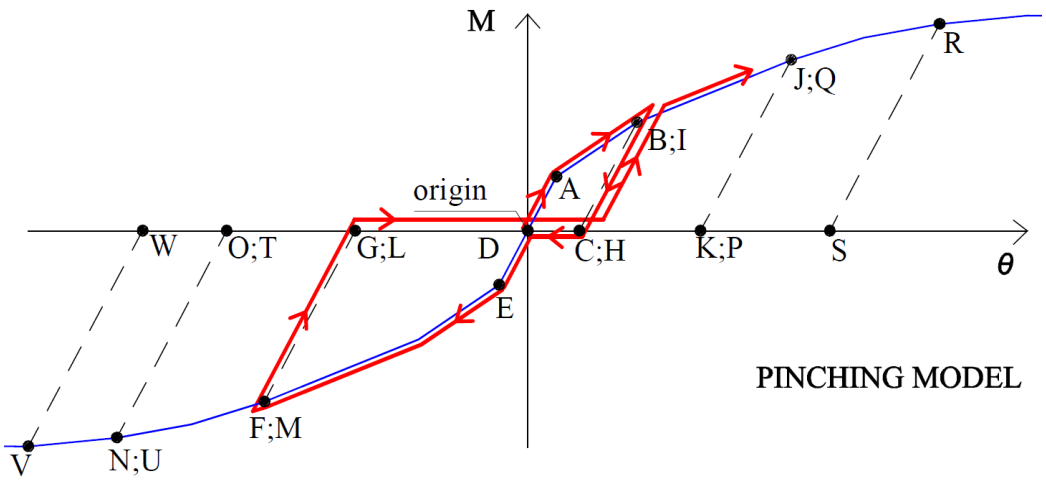

Figure 63. *Cyclic response according to Pinching model (PM).*

4.2.1 Check of the Pinching Model

In order to validate the PM, data acquired during the research campaign have been used; the comparison with the *C* joint (Figure 3) is reported in the following. The experimental setup has been modeled by means of a commercial non-linear FE analysis package [SAP 2000, 2016]; the members (upright and beam) have been modeled by one-dimensional frame elements assuming to have a linear elastic response, the PM has been introduced to describe the beam-to-column joint behavior.

A rotational multi-linear link fitting the experimental backbone moment-rotation curve, has been chosen to describe the joint flexural behavior. The slope of the unloading branch of the rotational link is constant and equal to the initial elastic one.

The comparison between numerical and experimental moment-rotation curves, for type *C* joint, is shown in (Figure 64).

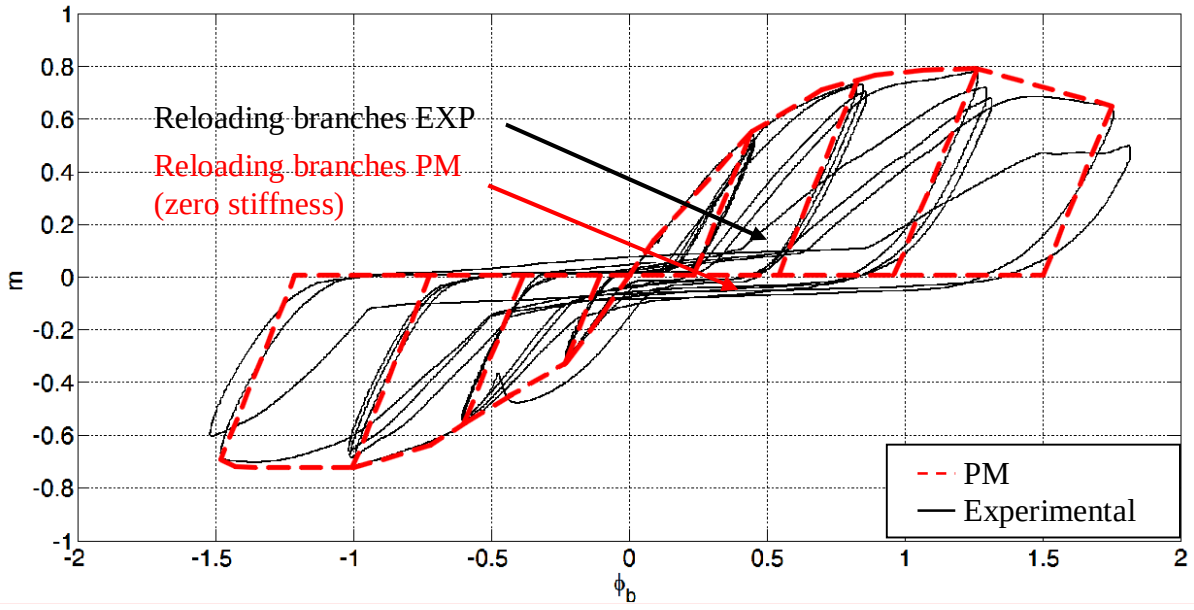

Figure 64. *Non-dimensional moment-rotation curves of specimen C-c1 (Table 1).*

It can be noted that the PM well fits the envelope curve and the slope of the unloading branch.

The pinched part of the response in the PM is simplified, but this approximation is on the safe side. The PM reloading branches have zero stiffness (Figure 64) so that the PM is not able to consider the increase of the reloading stiffness (observed in the experimental curve) until the maximum rotation reached in the previously cycle. In fact, the PM is able to describe pronounced non-linear slippage (reloading braches with zero stiffness). This corresponds to a reduction of the energy dissipated in the hysteric loop: the energy is not dissipated for repeated hysteretic loops with the same amplitude; an increasing of the dissipated energy is only obtained for moments increasing on the monotonic curve.
In addition, the proposed PM was also checked by comparison with the cyclic response of rack joints tested by Aguirre (2005), who tested connectors under a loading history that included series of three cycles of equal amplitudes (±30, ±60, and ±90 mm); the maximum displacement of the series was increased until the joint failed.
The comparison among numerical and literature results are plotted in Figure 65. The numerical curve fits the experimental one highlighting the accuracy of the proposed model. The good agreement among experimental and numerical results confirms that the proposed PM is suitable to describe the rack joint behavior with high pronounced pinched hysteresis loops.

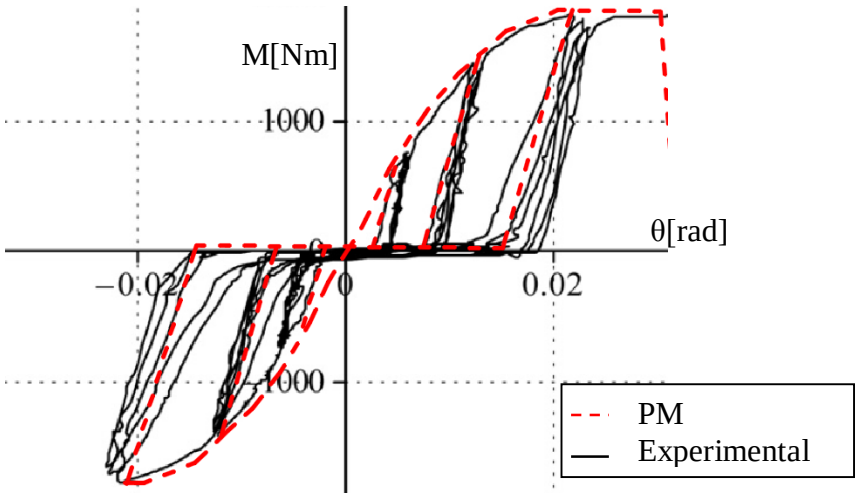

Figure 65. *Bending moment-rotation law (M-θ), comparison between literature (Aguirre, 2005) and numerical results.*

4.3 Pinching effects

4.3.1 Analysis of a SDOF

To give a preliminary evaluation of effects of pinching on the structural response of a SDOF, a non-linear time-history (NLTH) analysis is carried out on a T-shaped joint using two FE numerical models, which differ in the response of the hysteresis loop. Energy time-histories and structural responses are compared in the following.
The case-study is a T-shaped specimen representing an exterior rack beam-column joint.
The specimen is formed by a 550 mm long column and a 400 mm long beam (from the external-face of the upright). Main details of the rack joint are sketched in Figure 66.

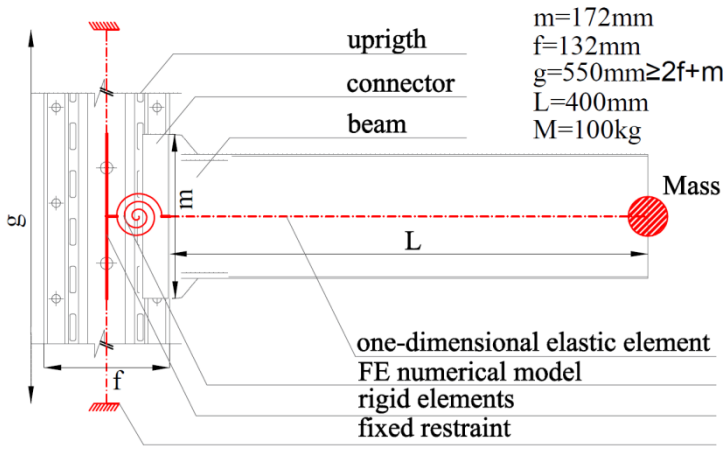

Figure 66. *Case-study: T-shaped joint.*

The numerical model of the case-study is developed by means of SAP 2000. The column is fixed at both ends and members are modeled by one-dimensional frames with a linear elastic response.
The connection is modeled using two different rotational numerical models, differing in terms of the deterioration of the rotational stiffness: the classical Takeda Model [Takeda et al., 1970] (TM) and the Pinching Model (PM).
In both models the same response is considered for sagging (positive) and hogging (negative) bending moment.
The TM is chosen because it is widely used to model the non-linear response of beam-to-column joints with a stable behavior not affected by a pronounced pinching. It is worth pointing out that in the TM, the form of the cycle is stable with larger energy absorption capability respect to the PM. In the TM, the unloading is along a line with the same slope of the initial elastic one (Figure 67). When reloading, the curve follows a line to the backbone curve for loading in the opposite direction. The target point for this line is at the maximum deformation that occurred in that direction under previous load cycles (follow points in the alphabetical order starting from the origin in Figure 67).

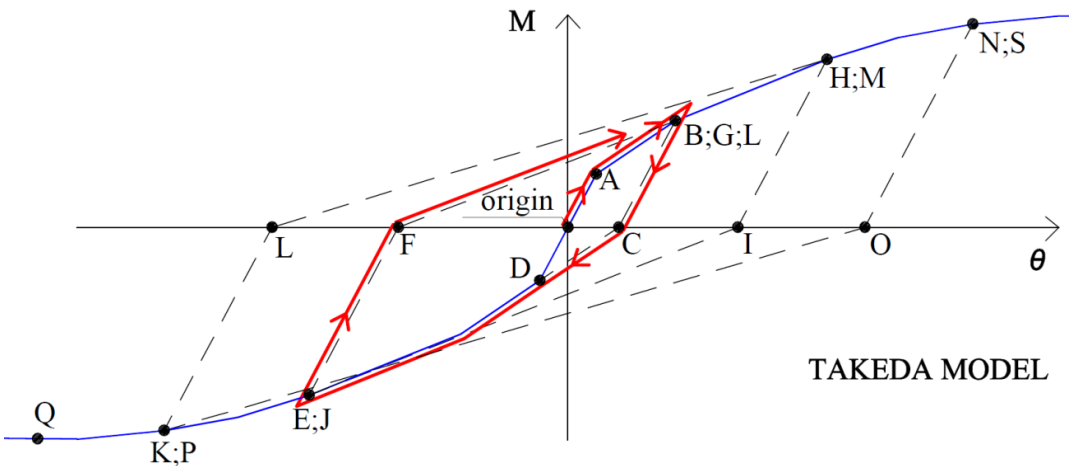

Figure 67. *Cyclic response according to Takeda model (TM) [Takeda et al., 1970].*

In conclusion, the two models have the same backbone curve, but they differ in the energy dissipation via hysteresis under dynamic loading.

4.3.2 Non-linear time-history

In order to identify effects of pinching, a non-linear time-history (NLTH-A) analysis is carried out and results obtained using the two different models (TM - PM) are compared.

The dynamic analysis is performed considering a concentrated mass at the beam-end section (Figure 66) submitted to the vertical acceleration history shown in Figure 68.
In particular, the NLTH-A is characterised by a time variation which rises linearly from a value of 0 m/s^2 at the time zero to a maximum value of 3 m/s^2 at the time 0.125 s, and then it drops down to 0 m/s^2.

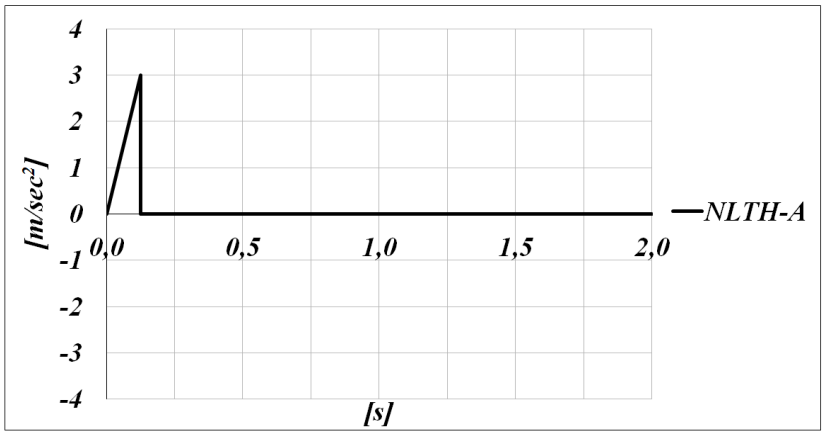

Figure 68. *Acceleration of NLTH-A.*

4.3.3 Energy equation for a SDOF system

It is worth noting that when a viscous damped single mass elastic oscillatory system, SDOF, vibrates subjected to an unidirectional horizontal ground motion, its equilibrium equation can be expressed by:

$$m\ddot{u} + c\dot{u} + f_s = -m\ddot{u}_g \tag{40}$$

where:
m = mass;
c = viscous damping;
f_s = restoring force;
u = relative displacement of the mass with respect to the "ground";
and u_g = "ground displacement" ($u_t = u + u_g$ is the total displacement of the mass).
Considering the instantaneous displacement $du = \dot{u}dt$, the energy balance equation (41) is derived from the integration over time of (40):

$$\underbrace{\int m\ddot{u}\dot{u}dt}_{Ek} + \underbrace{\int c\dot{u}\dot{u}dt}_{Ec} + \underbrace{\int f_s\dot{u}dt}_{Ea=Ee+Eh} = -\underbrace{\int m\ddot{u}_g\dot{u}dt}_{Ei} \tag{41}$$

The first term depicts the “relative” kinetic energy of the system (*Ek*), as measured with respect to the ground, representing energy temporarily stored in the kinematics of the system. The second term is the damping energy dissipated by viscous damping (*Ec*), and the third is termed the absorbed energy (*Ea* = *Ee* + *Eh*), which is composed of recoverable elastic strain energy (*Ee*) and irrecoverable hysteretic energy (*Eh*). The right-hand-side term is conventionally defined as the “relative input energy” (*Ei*) that, if it is evaluated at the end of ground motion duration, it differs from absolute input energy in the very short and very long period ranges only [Erol et al. 2008, Uang et al. 1990].
By virtue of removing any influence of damping, in the case-study model, c is considered equal to zero; this also ensures that all the energy is dissipated via hysteresis only.

4.3.4 Comparison of results

Displacements of the control point (that is the beam-end section) for both hysteretic models (TM and PM) are reported in Figure 69. Displacements are equal until the first sign change; then, in TM it decreases while in PM it oscillates with constant amplitude. The same behavior characterises the value of the connection bending moment (Figure 70). In TM the value of the moment tends to zero, in PM it is stable.

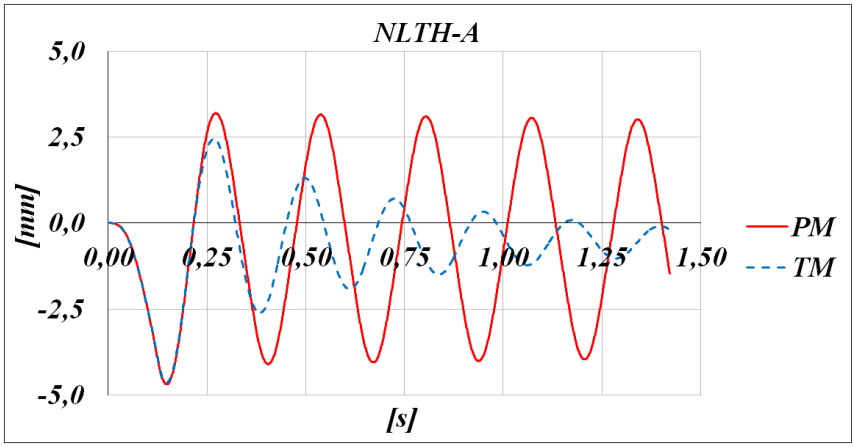

Figure 69. *Displacement of control point. NLTH-A.*

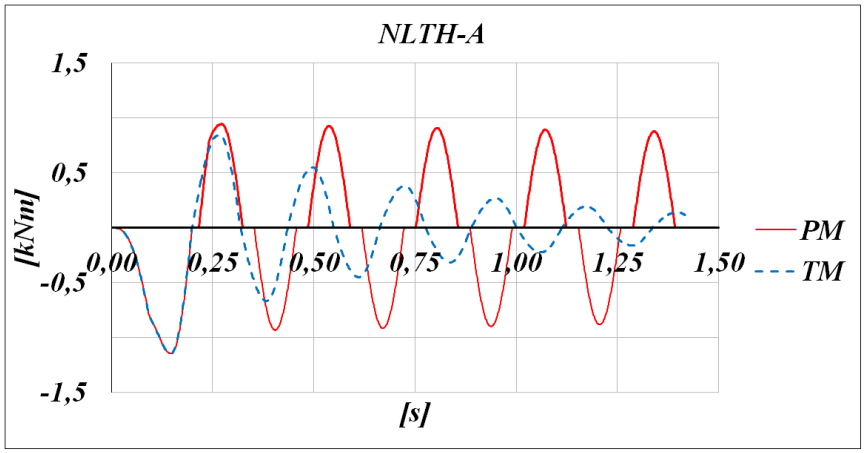

Figure 70. *Value of bending moment. NLTH-A.*

The energy time-history is shown in Figure 71. Hysteresis loops of PM and TM are shown in Figure 72, Figure 73 and Figure 74.

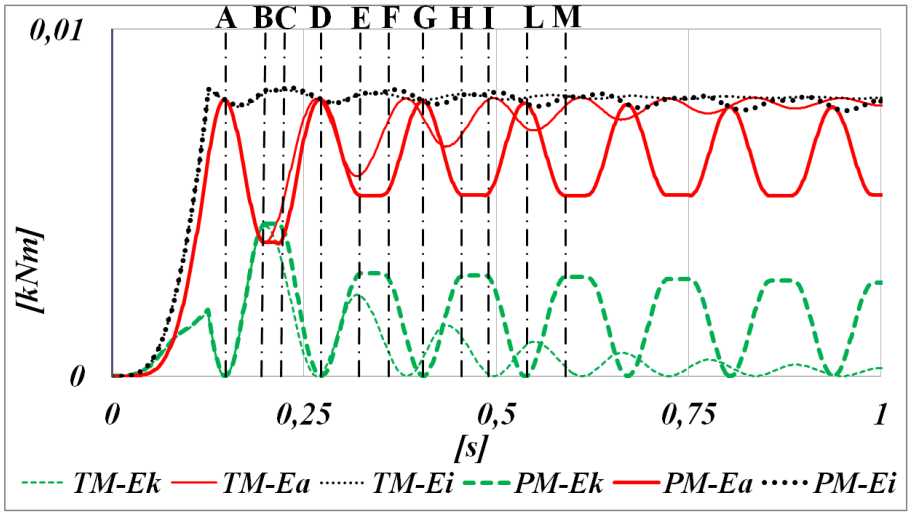

Figure 71. *Values of energies. NLTH-A.*

PM and TM have a similar behavior until the time t=A (letters A,B, ...M are reported in Figure 71 and Figure 72) at the maximum value of the control point displacement.
For t =A, Ea reaches its maximum value (*Ea=Ei*) and *Ek=0* (Figure 71).
Then, *Ei* remains constant and the control point starts moving in the opposite direction with a reduction of *Ea*; this happens because the elastic energy (*Ee*) is recovered in the unloading branch A-B, see Figure 72 (note that the first cycle starts with negative moment).
The *Ee* recovered is transformed in *Ek* to satisfy energy balance (41).
This behavior can be observed in the increment of *Ek* for both models (from t=A to t=B, Figure 71).
After t=B, the two models show a different behavior: TM is characterised by an increment of *Ea* and a reduction of *Ek* (from t=B to t=D, see Figure 71); vice versa, PM, characterised by the slippage phenomenon (B-C branch, Figure 72), can only dissipate energy in C-D branch, see Figure 72. This behavior causes the increment of *Ea* and the reduction of *Ek* (from t=C to t=D, see Figure 71).
Both models recover *Ee* in the unloading branch (D-E branch, Figure 72). This energy will be dissipated in the subsequent hysteresis loop: in TM, blue dashed line of Figure 73; in PM in F-G branch, after slippage (E-F branch), see Figure 73.
It is interesting to highlight how in TM, the dissipated energy in the reloading cycle is greater than recovered elastic energy in the unloading cycle: *Ea* (reloading cycle) ≥ *Ee* (unloading cycle). This behavior causes the reduction of the control point displacement, until the condition *Ea=Ei* and *Ek=0*.
Vice versa, PM reaches a dynamic equilibrium condition with a pseudo-linear-elastic behavior that is PM works in a pseudo elastic field (identified by the two red circles in Figure 74).
In each reloading branch the dissipated energy is the elastic strain energy (*Ea=Ee*) and the same is recovered in the subsequent unloading cycle.
This behavior can be observed in the transformation between *Ek* and *Ea* (Figure 71).
The consequence of this behavior is the oscillation with constant amplitude of the control point, see Figure 69.

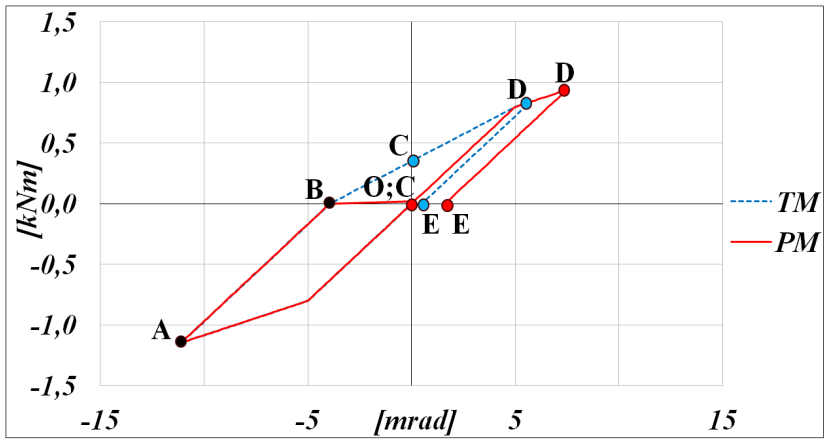

Figure 72. *Moment-rotation curves. First cycle. NLTH-A.*

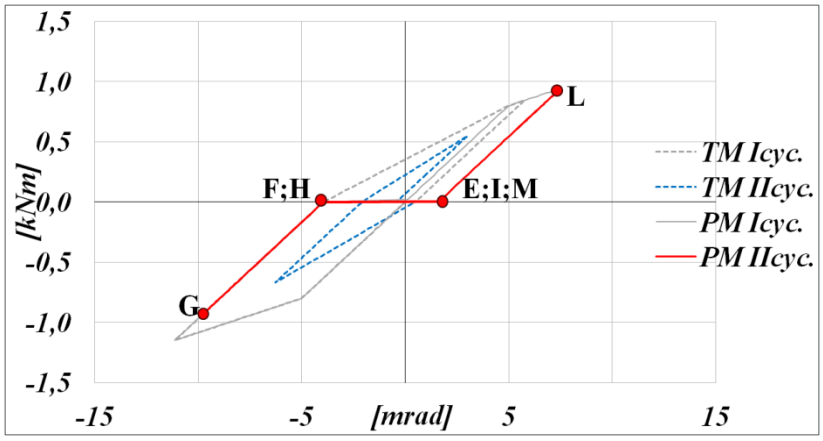

Figure 73. *Moment-rotation curves. First (I) and (II) second cycle. NLTH-A.*

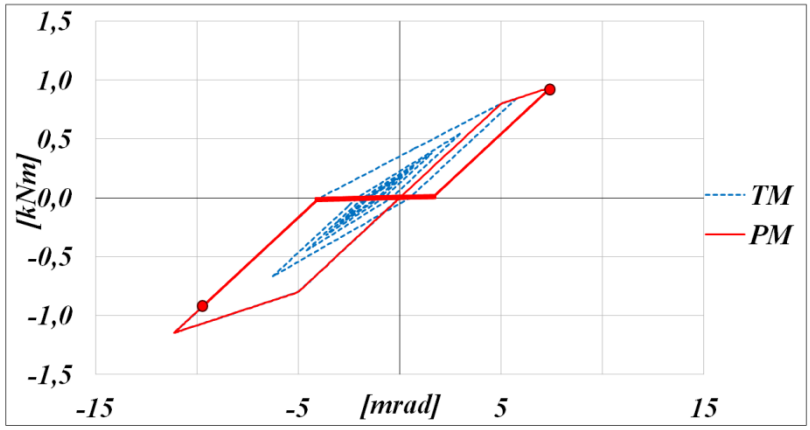

Figure 74. *Moment-rotation curves. NLTH-A.*

The study reveals that, monotonic behavior is not well correlated to dynamic performance of structures. Numerical comparisons have shown that a pinched behavior in hysteresis loops, with a reduced dissipated energy, changes the structural response of structures. Hence, some care should be exercised whenever discussing the energy-dissipation characteristics of different systems, since the reliable evaluation of the dissipated energy influences the dynamic performance of structures.

4.4 Effects of the pinching on the seismic response of steel pallet racks

4.4.1 The case study

For a deeper understanding of effects of the non-linear behavior of rack joints on the seismic response of steel pallet rack systems, a case-study is discussed.
The case study is a two-bay four-story medium-rise double-entry pallet rack. The width of the upright frame is 1200 mm. Storage levels have a constant inter-story height of 2000 mm and a bay length of 2800 mm. No bracing system is present in the down-aisle direction, whereas in the cross-aisle direction uprights are braced with a system of diagonals and horizontal struts (Figure 75). Reference is herein made to rack constructed with the same uprights, beams and connectors used for the type *C* joint (1352 for beams, 130/250 for uprights). Geometrical features of specimens are listed in Table 26. Types of steel used for CFS members are: S350GD, with a yielding strength f_{yk}=350 N/mm^2, for uprights, and S250GD, with a yielding strength f_{yk}=250 N/mm^2, for beams.
Regarding to vertical loads, two pallets, with 800 kg mass each, are placed on each bay at all levels, for a total number of 16 pallets, corresponding to the nominal service load.

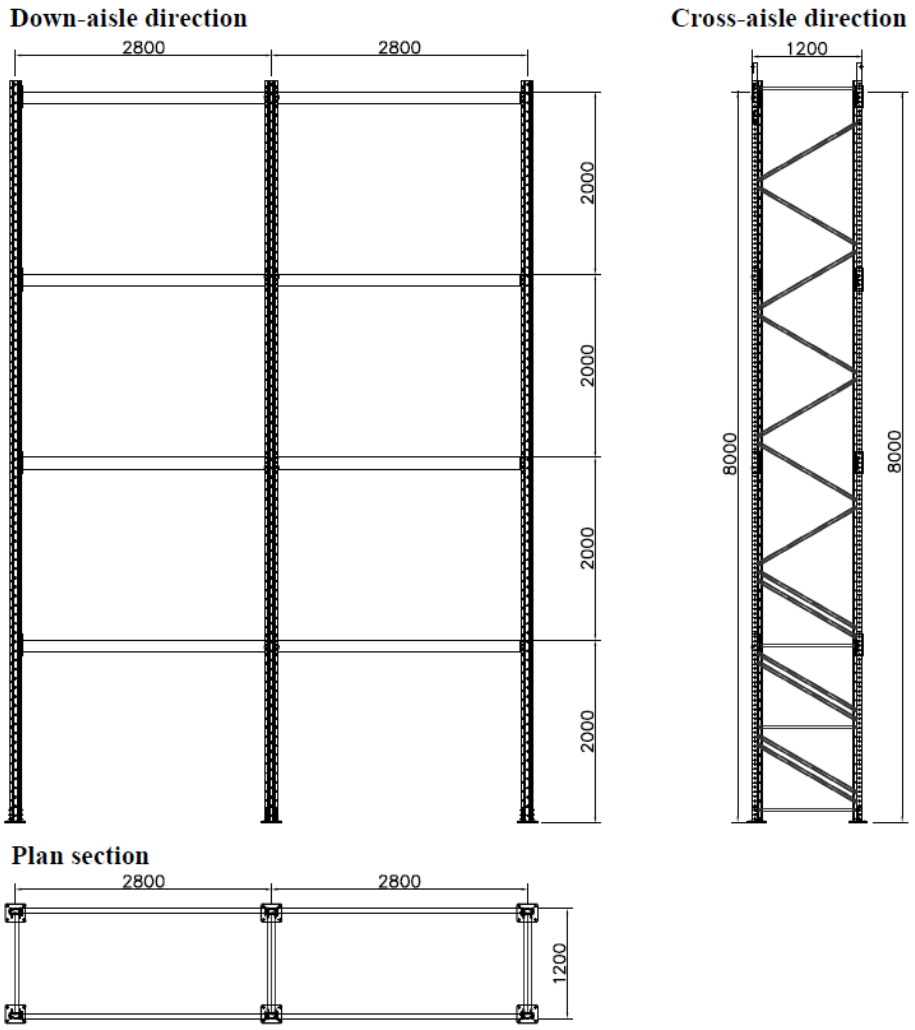

Figure 75. *Structural scheme of the rack system [mm].*

Table 26. Features of rack system.

Number of levels	*Number of bays*	*Inter-story beams [mm]*	*Length of beams [mm]*	*Type of upright*	*Type of beam*	*Type of connector*	*Load on couple of beams [kg]*
4	*2*	*2000*	*2800*	*130/250*	*1352*	*M5*	*1600*

The FE model of the rack structure model is developed adopting the code SAP 2000, considering linear elastic elements for columns and beams, while hinges with rotational linear elastic spring are used for base-plate joints. With the aim to evaluate the effects of pinching in the cyclic behavior of rack joints, beam-to-column joints are modeled by means of two cyclic joint models: the classical Takeda model (TM) and the PM.

4.4.2 Time domain non-linear dynamic analysis

To assess the seismic vulnerability of the rack structure chosen as case-study, a time domain non-linear dynamic analysis is performed. The seismic elastic spectra are defined in accordance with the Italian code [NTC, 2008] for type A ground and three different sites (Scarperia, Florence and Milan) with different design peak ground acceleration (PGA) (Table 27).

For each site, seven synthetic ground motion spectrum-compatible earthquakes fitting the site target spectrum are generated through the code SIMQKE [Gelfi, 2012] and used as input for the non-linear time-history analysis. Each earthquake lasts 20 s.

Table 27. Values of the elastic response spectra.

Seismic Parameters		Sites		
		Scarperia	Firenze	Milano
T_{NCR} [years]	reference return period	475	475	475
P_{NCR}	reference probability of exceedance	10%	10%	10%
a_g [g]	design peak ground acceleration (PGA)	0.20	0.13	0.05
S	soil factor	1.41	1.50	1.50
η	damping correction factor	1.00	1.00	1.00
T_B [s]	lower limit of the period of the constant spectral acceleration branch	0.152	0.157	0.149
T_C [s]	upper limit of the period of the constant spectral acceleration branch	0.456	0.471	0.447
T_D [s]	value defining the beginning of the constant displacement response range of the spectrum	2.405	2.125	1.798
W [kN]	weight on rack	128	128	128

4.4.3 Numerical results

Results of non-linear dynamic analyses, in terms of the maximum displacement of the control point (the centre of mass at the upper load level) and the base shear, are shown in Figure 76.

The green colour refers to the TM, while the red colour refers to the PM; the symbol shape refers to different values of the PGA: rhombus - a_g = 0.05 g; triangle - a_g = 0.13 g; circle - a_g = 0.2 g; Table 27; the average of results for each value of a_g is shown by the same larger symbol.

As a general remark the pinching influences the seismic response of the whole structure. Figure 76 shows how the values of displacements (d_{PM}) and base shears (F_{PM}) obtained with the PM are greater than those obtained with the TM (d_{TM} and F_{TM} respectively). Increasing the value of the PGA a_g, these differences increase. Average values of maximum displacements and base shears for the two models (TM and PM) and their differences ($E_{r,d}$ and $E_{r,F}$ respectively) are listed in Table 28.

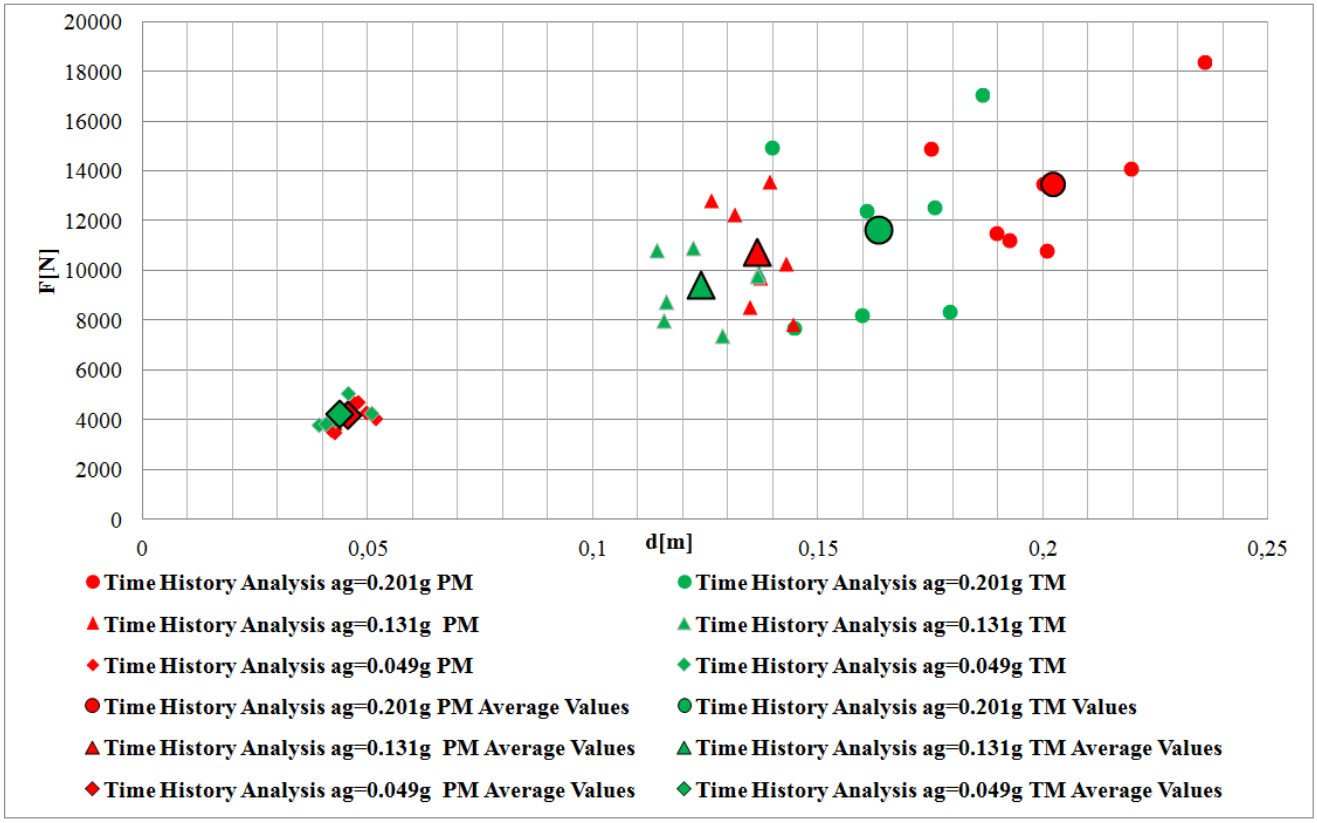

Figure 76. *Base shear-control point displacement. Numerical results obtained by the proposed PM and by TM for different values of PGA [g].*

Table 28. Numerical results obtained with PM and with TM for different accelerograms.

Type of Model	Average value of maximum displacement [m]	$E_{r,d}$ $\frac{(d_{PM}-d_{TM})}{d_{TM}}$	Average value of base shear [N]	$E_{r,F}$ $\frac{(F_{PM}-F_{TM})}{F_{TM}}$
Time History Analysis ag=0.201g PM Average Values	0.2022	23.5%	13467	15.8%
Time History Analysis ag=0.201g TM Average Values	0.1637		11629	
Time History Analysis ag=0.131g PM Average Values	0.1365	9.9%	10713	14.0%
Time History Analysis ag=0.131g TM Average Values	0.1241		9396	
Time History Analysis ag=0.049g PM Average Values	0.0457	4.5%	4202	-1.0%
Time History Analysis ag=0.049g TM Average Values	0.0437		4242	

It can be noted that for the maximum selected PGA (a_g =0.2g - Scarperia), differences in the evaluation of the maximum displacement and related base shear cannot be neglected (*23.5%* and *15.8%* respectively).

These differences are due to the greatest plastic excursions undergone by joints in the PM. The greatest pronounced non-linear behavior can be explained considering the lesser energy dissipation in the PM with respect to the TM. As an example, observing the cyclic response of an external joint at the first storage level (Figure 77), it can be concluded that greater values of the rotation in the moment-rotation curve are obtained in the PM respect to the TM to dissipate the same energy. As a

consequence, the greater displacement and base shear can lead to a probable premature collapse of the structure in the PM. Although limited to a single case, results show that if the pinching is neglected, like it occurs in the TM, the seismic assessment is not reliable.

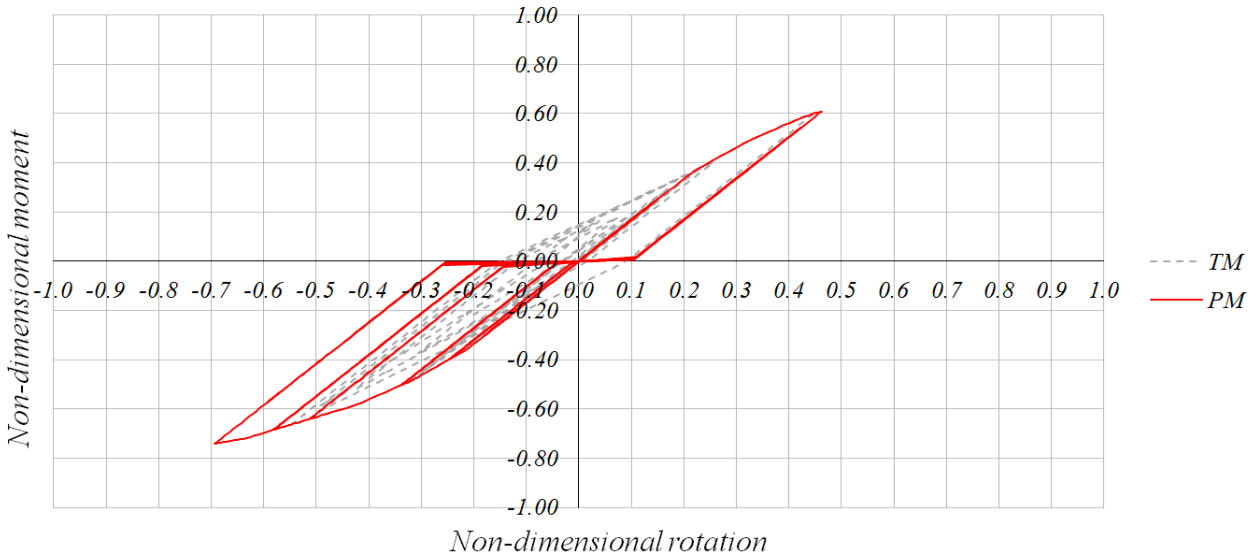

Figure 77. *Cyclic response of a joint by considering the TM or the PM.*

In earthquake engineering, strength and deformation capacities depend on cumulative damage.
Each component has a permanent memory of past damaging events and at any time it will remember all past excursions (cycles) [Krawinkler, 2009]. Another feature of the proposed PM, though approximate but just for this easy to be used, is that it remembers the history load which has contributed to the deterioration of the joint state of health and so it can be used to evaluate on the safe side the structural damage of a rack and its components after an earthquake.
Finally, it is worth noting that pushover analysis (static non-linear analysis with monotonic increasing horizontal loads), adequate in the evaluation of the seismic response of structures whose joints have a stable cyclic behavior, could give unreliable results if used to estimate the response of structures whose joints are characterized by a pronounced pinching phenomenon, like steel racks. In this case following the approach proposed in [Yin et al., 2018 (a)] non-linear time-history analyses, using models capable to describe the effective non-linear behavior of joints, are recommended to obtain a reliable evaluation of racking system seismic response.

4.5 Summary of main results

In the context of the seismic vulnerability analysis of steel storage pallet racks, seismic design approach currently performed in daily practice is based on the reduction of the elastic spectrum to the design spectrum via the use of the seismic behavior factor *q*. In the down-aisle direction, steel storage pallet racks behave like moment-resisting frames and their non-linear behavior is associated with joints. Experimental tests on rack joints have shown a non-negligible pinching and slippage in their cyclic response with a reduction of energy dissipation. Then rack joint behavior is expected to influence the seismic response of rack systems.
A numerical pinching model is proposed for the analysis of steel storage pallet racks under cyclic loads, taking into account the degradation of the rotational stiffness of joint hysteresis loops. The effectiveness of the proposed model is its fast tuning and easily implementation in commercially available non-linear finite element analysis software packages. The model is formed by common links placed in series and in parallel and it describes the high pronounced pinching phenomenon with the aim to perform reliable seismic analyses of rack structures. Moreover, it needs only the

knowledge of the monotonic moment-rotation law of rack joint, which can be analytically obtained by the proposed mechanical model, avoiding expensive cyclic experimental tests.

To check the proposed numerical model, several comparisons have been performed with both experimental results of laboratory tests and literature data. Comparisons gave very satisfactory results.

For a deeper understanding of the pinching effect, a case-study has been discussed, comparing two models of joints differing in the modeling of the deterioration of the rotational stiffness of joints.

An increment of displacement and base shear with a consequent reduction of load carrying capacity has permitted to conclude that the pinching phenomenon cannot be neglected in the design of rack structures. This highlight that the pushover analysis can be inadequate, vice versa non-liner dynamic analysis, with the proposed pinching model, is suggested to obtain a reliable seismic vulnerability assessment of rack systems.

5 CONCLUSIONS

Steel storage pallet racks are used worldwide for storage of palletized goods and are popular for their ease of construction, customization, and economy. Failure of racks can result in significant property loss and economic disruption.
Steel pallet racks are designed to be readily demountable and capable of re-assembly depending upon the volume of storage goods. Therefore, semi-rigid boltless beam-to-column connections are adopted. These joints govern the stability and earthquake resistance of rack systems in the unbraced down-aisle direction.
Rack connections are typically formed by beams welded to connectors equipped with tabs and columns with perforated cross-sections to accept these tabs joining beams and columns. The ingenious configuration of rack connections, which differ among different manufacturers, prevents the development of a common analytical model to predict the behavior of all types of rack joints.
The main goals of this research are to clarify the mechanical behavior of rack boltless connections and to develop a theoretical model capable to analytically describe the non-linear moment-rotation curve of these joints. The knowledge of the connection non-linear structural response is then used to develop a FE model, which is used to evaluate the influence of rack joints on the global seismic response of industrial storage systems. Developed models represent reliable tools to perform a structural design of rack system and its connections.
In the first phase of this research, the monotonic moment-rotation curve of joints is identified through experimental tests on several rack connections using the single cantilever test setup according to EN 15512. Collected observations include the major failure modes and the effects of various parameters. Then, following conclusions can be drawn.
Tested joints can be considered semi-rigid joints with reference to the stiffness, and partial-strength joints with reference to the resistance, according to EN 1993-1-8.
The collapse of a connection depends on the failure of the weakest component. As a general remark, connection collapse mainly depends on the failure of the connector. Tabs try to tear the column web slot (punching of column web). A complete rupture of tabs happens in the case of specimens with thick column (failure of tabs). In the case of thin column with shallow beam the connection failure is due to the local buckling of column web.
In all specimens, a high ductility, depending on the large plastic deformation of tabs and connector flange, is observed.
Regarding the layout of welding of beam to the connector, the findings reveal that a double-sided welding can cause a premature failure of the connection. Thus, this welding configuration is detrimental and reduces the performance of the connection. An adequate welding, all around the beam-end section, results in a better performance of the connection in terms of flexural capacity.
The same connections are analysed under cyclic load. Cyclic tests show a pronounced pinching, which affects these types of dry joints. An increase in the number of tabs minimizes the pinching and increases both the ultimate moment and initial elastic rotational stiffness.
For each connection, the backbone curve fits the monotonic one, but ultimate rotations assume lower values than in monotonic tests. The failure mode of the connections with a double-sided welding was governed by the premature failure of the weld. Collapse of the other specimens was due to the premature unlocking of the connector from the column. To avoid the disconnection between connector and column, tested joints are equipped with additional bolts. Bolted rack connections are characterized by a greater dissipated energy, representing a cost-effective alternative to “tab connectors".
The findings show that the connection performance significantly relies on the geometrical and mechanical features of connection members (beam, beam-end weld, connector and column). In the second phase of the research project, a mechanical model, based on the Component Method, is developed to theoretically evaluate the structural response of rack connections. The mechanical model appears a reliable method to calculate the connection moment capacity, flexural stiffness and

failure mode. Moreover, a non-linear equation is proposed to approximate the elasto-plastic response of tested joints.
The proposed approach can be considered as a complementary method to expensive experimental testing required by standard codes to evaluate the rack connection structural behavior. It can be used to improve the performance of rack joints, which are produced in long series, and the designer can use it for a preliminary assessment of all type of rack joints.
In the third phase of the study, the propagation of uncertainties in the component geometry and mechanical properties to the response of the connection in terms of initial elastic flexural stiffness and ultimate moment is evaluated. A Monte Carlo simulation is conducted. Results indicate that the variability of geometric and mechanical properties mitigates in the connection ultimate moment. This redistribution occurs due to plasticity in the rack joint and the weakest link fails first. The variability in the flexural stiffness is greater due to components in series compounding to contribute to total connection stiffness. A normal probability distribution function well fits both the connection ultimate moment and initial flexural stiffness histograms.
Results further highlight the effect on connection behavior due to varying connection configurations. With a welding all around the beam-end section, connection failure mode mainly depends to the collapse of the weakest component in the connector member. Moreover, connector stiffness limits the connection flexural stiffness. These results highlight the connector to be the most critical member whose features should be controlled with greater accuracy in the manufacturing process.
Finally, a non-linear finite element (FE) model that simulates the structural response of rack joints is developed. Its accuracy is validated against both experimental and literature results. To evaluate the influence of rack joints on the seismic non-linear dynamic response of steel storage pallet racks, numerical analyses of these structures are performed. Results show an increment of the maximum displacement and base shear with a consequent reduction of load carrying capacity in those systems whose joints have a pronounced pinching, which cannot be neglected in the design of rack structures.

5.1 Design recommendations

Probabilistic results, supported by experimental tests, confirm that an adequate welding, all around the beam-end section, is recommended to avoid a reduction in the flexural capacity of rack connections. In accordance with EN 1993-1-8, the requirement that the fillet weld should be continuous around the corner for a distance of at least twice the leg length of the weld, should be introduced in the rack current design codes.
MC simulation provided useful information about the parameters influencing joint structural response. It has been highlighted that connector has the greater influence on the structural behavior of rack connections. Quality control efforts should be focused on promoting stability in statistical parameters of connector components to ensure reliability of rack joints.
The proposed mechanical model could be adopted as a complementary method to experimental tests required by standard codes to define the rack connection behavior.
Finally, it has been shown that the pinching phenomenon plays a key role in the design of rack structures, so a pushover analysis can be inadequate to perform a reliable seismic vulnerability assessment of racks. Therefore, a non-linear dynamic analysis, with an appropriate FE pinching model like that proposed in the present Thesis, is recommended.

5.2 Recommendations for future research

Nowadays, in the design of an earthquake resistant structure, with a dissipative structural behavior, the material nonlinearity may be taken into consideration explicitly through a non-linear analysis or

implicitly through a linear elastic analysis, reducing the seismic forces by the seismic behavior factor *q*. Non-linear static "pushover" analysis is usually performed to evaluate the *q*-factor. Nevertheless, it has been observed that this analysis does not consider the stiffness and strength degradation of the cyclic response of beam-to-column joints, which, in the case of steel storage pallet racks, is usually affected by pronounced pinching. Further researches are recommended to give estimations of the seismic behavior factor of racks, in down-aisle direction, through the incremental dynamic analysis (IDA), taking into account the effective cyclic elasto-plastic behavior of beam-to-column joints.

Moreover, experimental tests have shown that additional bolts in rack connections can increase the structural performance of beam-to-column rack joints in terms of ultimate moment, ductility and dissipated energy. Nevertheless, the use of bolts for all joints would be uneconomical and would nullify advantages of dry connections in rack structures, so further researches are needed to identify the minimum number of bolted joints and their distribution in the structure to satisfy an assigned seismic performance.

ACKNOWLEDGEMENTS

I sincerely extend my gratitude to my tutors Professor Maurizio Orlando, Professor Andrea Vignoli and Professor Klaus Thiele for their advices given through this project. I thank Professor Kara D. Peterman and Professor Sanjay R. Arwade for their suggestions. I gratefully acknowledge the Italian Rack Manufacturing Company ROSSS SpA, Scarperia and San Piero, Florence (IT), especially the President Stefano Bettini and the Engineer Giovanni Lavacchini, for supporting this research work and kindly supplying specimens and hosting the experimental setup. Moreover, I greatly appreciate the skillful work of Mr. S. Giordano, Mr. F. Bruni and Mr. E. Barlacchi of the SMTL of the Department of Civil and Environmental Engineering of Florence for their assistance in the experimental work.

REFERENCES

Abdel-Jaber, M., Beale, R.G., Godley, M.H.R. (2005). "Numerical study on semi-rigid racking frames under sway". *Computers and Structures*, 83, 2463–2475.

Aguirre, C. (2005). "Seismic behavior of rack structures". *Journal of Constructional Steel Research*, 61, 607–624.

AISC (2010). "Specification for Structural Steel Buildings", AISC, Chicago, IL.

André, F., Bachman, R. E., Mahoney, M. G. (2006). "Performance-Based Seismic Design of Pallet-Type Steel Storage Racks". *Earthquake Spectra*, Vol. 22, No. 1, pp. 47-64.

Aribert, J. M., Lachal, A., Moheissen M. (1990). "Interaction du voilement et de la resistance plastique de l'ame d'un profile lamine soumis a una double compression locale". *Construction Metallique, No. 2.*

AS/NZS 4084. Steel storage racking, Standards Australia/ Standards New Zealand. Sydney, Australia, 2012.

ATC-24 (1992). "Guidelines for Cyclic Seismic Testing of Components of Steel Structures for Buildings". Report No. ATC-24, Applied Technology Council, Redwood City, CA.

Bajoria, K.M., Talikoti, R.S. (2006). "Determination of flexibility of beam-to-column connectors used in thin walled cold-formed steel pallet racking systems". *Thin-Walled Structures*, 44 372–380.

Baldassino, N., Bernuzzi, C. (2000). "Analysis and behaviour of steel storage pallet racks". *Thin-Walled Structures*, 37, 277 – 304.

Baldassino, N., Zandonini, R. (2011). "Design by testing of industrial racks". *Adv. Steel Constr.* 7 (1), 27–47.

Ballio G., Mazzolani F. (1983). Theory and Design of Steel Structures. Spon Press Editor.

Bernuzzi, C., Castiglioni, C. A. (2001). "Experimental analysis on the cyclic behavior of beam-to-column joints in steel storage pallet racks". *Thin-Walled Structures*, 39, 841–859.

Bernuzzi, C., Chesi, C., Parisi, M. A. (2004). "Seismic behaviour and design of steel storage racks". *13th World Conference on Earthquake Engineering*. Vancouver, B.C., Canada 1-6, Paper No. 481.

Bernuzzi, C., Simoncelli, M. (2016). "An advanced design procedure for the safe use of steel storage pallet racks in seismic zones". *Thin-Walled Structures*, 109, 73–87.

Bertocci, L., Comparini, D., Lavacchini, G., Orlando, M., Salvatori, L., Spinelli. P. (2017). "Experimental, numerical, and regulatory P-Mx-My domains for cold-formed perforated steel uprights of pallet-racks". *Thin-Walled Structures*, vol. 119, pp. 151-165, ISSN:0263-8231.

Bertocci, L., Comparini, D., (2015). Assessment of the static and seismic behaviour of cold-formed steel structures trough experimental tests and nonlinear finite element analyses. Thesis, University of Florence, Italy.

Bian, G., Chatterjee, A., Buonopane, S.G., Arwade, S.R., Moen, C.D., Schafer, B.W., (2017), "Reliability of cold-formed steel framed shear walls as impacted by variability in fastener response". *Engineering Structures* 142 84–97.

Borghini, A., Gusella, F., Vignoli, A. (2017). "Seismic vulnerability of existing R.C. buildings: A simplified numerical model to analyse the influence of the beam-column joints collapse". *Engineering Structures*, 121, 19–29.

Brambilla, G., et all. (2015). "Seisracks2: Progetto di ricerca EU-RECCS Reasearch Project, Comportamento sismico di scaffalature metalliche porta pallet". *Costruzioni Metalliche*.

Cardoso, F.S., Rasmussen, K.J.R. (2016). "Finite element (FE) modelling of storage rack frames". *Journal of Constructional Steel Research, 126, 1–14.*

Castiglioni, C. A., Kanyilmaz, A., Angeretti, M., Brambilla, G., Chiarelli, G. P., Bernuzzi, C. (2014). "Experimental results of full scale pushover tests of project SEISRACK2 (seismic behaviour of steel storage pallet racking systems)" *Proc. 2nd European Conference on Earthquake Engineering*, Istanbul 25–29.

Chen, W.F., Newlin, D.E. (1973). "Column Web Strength of Beam-to-Column Connections". *Journal of the Structural Division, ASCE,* Vol. 99, No. ST9.

Dai L., Zhao X. Rasmussen K. J. R. (2018). "Flexural behaviour of steel storage rack beam-to-upright bolted connections". *Thin-Walled Structures,* 124, 202-217.

Díaz, C., Martí, P., Victoria, M., Querin, O. M. (2011). "Review on the modelling of joint behaviour in steel frames". *Journal of Constructional Steel Research,* 67, 741–758.

Dowell, R. K., Seible, F., Wlson, E. L. (1998). "Pivot hysteresis model for reinforced con-crete members". *ACI Struct. J.*, 607–617.

EN 15512 (2009) Steel static storage systems — adjustable pallet racking systems — principles for structural design. CEN European Committee for Standardization; 137.

EN 16681 (2013) Steel static storage systems – Adjustable pallet racking system – Principle for seismic design, CEN European Committee for Standardization.

EN 1993-1-1, Eurocode 3 (2005) Design of steel structures - Part 1-1: General rules and rules for buildings.

EN 1993-1-5, Eurocode 3 (2006) Design of steel structures - Part 1-5: Plated structural elements.

EN 1993-1-8, Eurocode 3 (2005) Design of steel structures- Part 1-8: Design of joints.

EN 1998-1-1, Eurocode 8 (2004) Design of structures for earthquake resistance - Part 1: General rules, seismic actions and rules for buildings.

EN 10219-1 Cold formed welded structural hollow sections of non-alloy and fine grain steels.

EN 10025-2 Hot rolled products of structural steels.

EN 10346 Continuously hot-dip coated steel flat products. Technical delivery conditions.

EN 10219-2 Cold formed welded structural hollow sections of non-alloy and fine grain steels.

EN 10051 Continuously hot-rolled strip and plate/sheet cut from wide strip of non-alloy and alloy steels – Tolerances on dimensions and shape.

EN 10143 Continuously hot-dip coated steel sheet and strip – Tolerances on dimension and shape.

Erol Kalkan, E., Kunnath, S. K. (2008). "Relevance of Absolute and Relative Energy Content in Seismic Evaluation of Structures". *Advances in Structural Engineering* Vol. 11 No. 1.

Faella, C., Piluso, V., Rizzano, G. (2000). "Structural Semi-Rigid connections – Theory, Design and Software". CRC Press, Boca Raton, Florida.

FEM 10.2.02 (2001), The Design of Static Steel Pallet Racks, Federation Européenne de la Manutention, Vers. 1.02.

FEM 10.2.08 (2011) Recommendations for the design of static steel storage pallet racks in seismic conditions, Federation Européenne de Manutention, Vers. 1.00

Gelfi, P. (2012). SIMQKE_GR developed by P. Gelfi. Version 2.7 – 9th.

Gervasio, H., Simoes da Silva, L., Borges, L., (2004). "Reliability assessment of the post-limit stiffness and ductility of steel joints". *Journal of Constructional Steel Research* 60, 635-648.

Gilbert, B.P., Rasmussen, K.J.R. (2010). "Bolted moment connections in drive-in and drive-through steel storage racks". *Journal of Constructional Steel Research*, 66, 755–766.

Giordano, S., Gusella, F., Lavacchini, G., Orlando, M., Spinelli, P. (2017). "Experimental tests on beam-end connectors of cold-formed steel storage pallet racks". *Proc. 8th European Conference on Steel and Composite Structures, Eurosteel 2017*, Copenhagen.

Godley, M. H. R.,(1997), "Plastic Design of Pallet Rack Beams". *Thin-Walled Structures* Vol. 29, Nos. 1-4, pp. 175-188.

Hancock G. J. (2003), "Cold-formed steel structures". *J. Constructional Steel Research*, 59 (4) 437-487.

Haque, A.B.M.R., Alam M.S. (2015). "Preliminary investigation on the over- strenght and force reduction factors for industrial racks clad buildings". *Proc. of the 11th Canadian Conference on Earthquake Engineering*.

International Standard ISO 6892-1:2009. Metallic materials – Tensile testing Part. 1: Method of test at room temperature.

Jaspart, J. P. (2000). "*General report: session on connections"*. Journal of Constructional Steel Research, 55, 69-89.

Krawinkler, H. (2009). "Loading Histories for Cyclic Tests in Support of Performance Assessment of Structural Components". *Proc. 3rd International Conference on Advances in Experimental Structural Engineering*, San Francisco.

Lima, L.R.O., Silva, LS., Vellasco, P.C.G., Andrade, S.A.L. (2004). "Experimental evaluation of extended endplate beam-to-column joints subjected to bending and axial force". *Engineering Structures* 26, Issue 10, 1333-1347.

Markazi, F. D., Beale, R. G., Godley, M. H. R. (1997). "Experimental analysis of semi-rigid boltless connectors". *Thin-Walled Structures*, 28, 57–87.

Markazi, F.D., Beale, R.G., Godley, M.H.R. (2001). "Numerical modelling of semi-rigid boltless connectors". *Computers and Structures*, 79, 2391-2402.

Melcher, J, Kala, Z., (2003), "The probabilistic verification of structural stability design procedures". In: Proceedings of the SSRC 2003 Annual Technical Session held in Baltimore, MD, SSRC, pp. 557-98.

Mitra N. (2012). An analytical study of reinforced concrete beam-t0-column joint behaviour under seismic loading. Thesis, University of Washington,

Mitra N. (2012). Pinching4 model. (OpenSees User Documetation); <http:// opensees.berkeley.edu/wiki/index.php/Pinching4_Material>.

Moen, C.D., Tao, F., Cole, R. (2016). "Monotonic and cyclic backbone response of single shear cold-formed steel screw-fastened connections". *Proceedings of the International Colloquium on Stability and Ductility of Steel Structures*, SDSS2016, Timisoara, Romania.

NTC 2008, Ministero delle Infrastrutture (2008). DM 14 gennaio 2008, Norme Tecniche per le Costruzioni.

Orlando, M., Lavacchini, G., Ortolani, B., Spinelli, P. (2017). "Experimental capacity of perforated cold-formed steel open sections under compression and bending". *Journal of Steel and Composite Structures*, vol.24, pp. 201-211, ISSN:1229-9367.

Peterman, K.D., Nakata, N., Schafer, B.W. (2014). "Hysteretic characterization of cold-formed steel stud-to-sheathing connections". *Journal of Constructional Steel Research*, 101, 254–264.

Peterman,K.D., Stehman, M. JJ, Madsen, R. L, Buonopane, S. G, Nakata N., Schafer, B. W. (2016). "Experimental seismic response of a full-scale cold-formed steel-framed building. I: System-level response". *Journal of Structural Engineering*, Volume 142, Issue 12 04016127.

Pozzati P. (1980). Teoria e Tecnica delle Strutture, Volume 3: Sistemi di travi, interpretazione del collasso, parte prima, travi metalliche. Editore Utet.

Prabha, P., Marimuthu, V., Saravanan, M., Arul Jayachandran, S. (2010). "Evaluation of connection flexibility in cold formed steel racks". *Journal of Constructional Steel Research*, 66, 863-872.

RMI. Specification for the Design, Testing and Utilization of Industrial Steel Storage Racks, ANSI MH16.1-2012, Rack Manufacturers Institute, Technical report.

Rodgers, J. E., Mahin, S. A. (2011). " Effects of Connection Deformation Softening on Behavior of Steel Moment Frames Subjected to Earthquakes". *International Journal of Steel Structures*, Vol 11, No 1, 29-37.

Rosin, I., Calado, L., Proença, J., Carydis, P., Mouzakis, H., Castiglioni, C., Brescianini, J. C., Plumier, A., Degee, H., Negro, P., Molina, F. (2009). "Storage racks in seismic areas, Final report". Research Fund for Coal and Steel, European Commission.

SAP 2000 (2016), Computers and Structures Inc., "CSI Analysis Reference Manual for SAP 2000", Berkeley CA.

Schafer, B.W., Ayhan, D., Leng, J,. Liu, P., Padilla-Llano, D., Peterman, K.D., Stehman, M., Buonopane, S.G., Eatherton, M., Madsen, R., Manley, B., Moen, C.D., Nakata, N., Rogers, C., Yu, C. (2016). "Seismic Response and Engineering of Cold-formed Steel Framed Buildings". *Structures*, 197-212.

Shah, S.N.R., Ramli Sulong, N.H., Khan, R., Jumaat, M. Z., Shariati, M. (2016)-(a). "Behavior of Industrial Steel Rack Connections". *Mechanical Systems and Signal Processing*, 70–71, 72 –740.

Shah, S.N.R., Ramli Sulong, N.H., Jumaat, M. Z., et al. (2016)-(b). "State-of-the-art review on the design and performance of steel pallet rack connections". *Eng. Fail. Anal.* 66, 240–258.

Shen, Y.L., Schneider, J., Tesfamariam, S., Stiemer, S.F., Mu, Z.G. (2013). "Hysteresis behavior of bracket connection in cross-laminated-timber shear walls". *Construction and Building Materials*, 48, 980–991.

Silva, LS., Santiago, A., Real, P. V. (2002). "Post-limit stiffness and ductility of end-plate beam-to-column steel joints". *Computers and Structures* 80, 515–531.

Silva, LS., Lima, L.R.O., Vellasco, P.C.G., Andrade, S.A.L. (2004). "Behaviour of flush end-plate beam-to-column joints under bending and axial force". *Steel and Composite Structures*, Volume 4, Issue 2, 77-94.

Ślęczka, L., Kozłowski, A. (2007). "Experimental and theoretical investigations of pallet racks connections". *Advanced Steel Construction*, Vol. 3, No. 2, pp. 607-627.

Smith, B.H., Arwade, S.R., Schafer, B.W., Moen. C.D. (2016). "Design component and system reliability in low-rise cold formed steel framed commercial building". *Engineering Structures*, 127, 434-446.

Takeda, T., Sozen, M. A., Nielsen, N. N. (1970). "Reinforced Concrete Response to Simulated Earthquakes". *Journal, Structural Division, ASCE*, Vol. 96, No. ST12, pp. 2557-2573.

Tilburgs, I.K. (2013). "Those peculiar structures in cold formed steel: "racking and shelving"". *Steel Construction* 6 (2) 95–106.

Tao, F., Cole, R., Moen, C.D. (2016). "Monotonic and cyclic backbone response of single shear sheathing-to-cold-formed steel screw-fastened connections". Wei-Wen Yu International Specialty Conference on Cold-Formed Steel Structures 2016 - Recent Research and Developments in Cold-Formed Steel Design and Construction, Baltimore, Maryland.

Tsai, K. C., Shiun Wu, Popov, E. P. (1995). "Cyclic performance of steel beam-column moment joints". *Engineering Structures*, 8, 596-602.

Uang, C.M. and Bertero, V.V. (1990). "Evaluation of seismic energy in structures". *Earthquake Engineering and Structural Dynamics*, 19, 77-90.

Winter, G. (1947). Strength of Thin Steel Compression Flanges, Transactions, American Society of Civil Engineers, 112, 527-554.

Yin, L., Tang, G., Li, Z., Zhang, M. (2018)-(a). “Responses of cold-formed steel storage racks with spine bracings using speed-lock connections with bolts II: Nonlinear dynamic response history analysis”. *Thin-Walled Structures* 125, pp. 89-99

Yin, L., Tang, G., Li, Z., Zhang, M., Feng, B. (2018)-(b). “Responses of cold-formed steel storage racks with spine bracings using speed-lock connections with bolts I: Static elastic-plastic pushover analysis”. *Thin-Walled Structures* 125, pp. 51-62

Yin, L., Tang, G., Zhang, M., Wang, B., Feng, B. (2016). “Monotonic and cyclic response of speed-lock connections with bolts in storage racks”. *Engineering Structures*, 116, 40–55.

Zaharia, R., Dubina, D. (1997). “Cold-formed steel trusses with semi-rigid joints”. *Thin-Walled Structures,* 29 (1-4), 273-87.

Zaharia, R., Dubina, D. (2006). “Stiffness of joints in bolted connected cold-formed steel trusses”. *Journal of Constructional Steel Research,* 62 (3), 240-9.

Zhao, X., Wang, T., Chen, Y., Sivakumaranc, K.S. (2014). “Flexural behavior of steel storage rack beam to-upright connections”. *Journal of Constructional Steel Research* 99, 161–175.

Zhao, X., Dai, L., Wang, T., Sivakumaranc, K.S., Chen, Y. (2017). “A theoretical model for the rotational stiffness of storage rack beam-to-upright connections”. *Journal of Constructional Steel Research* 133, 269–28.

PUBLICATIONS

The following journal and conference paper are based on the research contained in this Thesis.

Giordano, S., Gusella, F., Lavacchini, G., Orlando, M., Spinelli, P. (2017). "Experimental tests on beam-end connectors of cold-formed steel storage pallet racks". Proc. 8th European Conference on Steel and Composite Structures, Eurosteel 2017, Copenhagen.

Gusella, F., Orlando M., Vignoli A., Thiele, K., (2017). "Evaluation of rack connection flexural resistance by the component method" in: Proceedings of the XVI C.T.A. Conference, Venice 28-30 September.

Gusella, F., Orlando M., Vignoli A. (2017). "Effects of pinching in the hysteresis loop o rack connections" in: Proceedings of the XVII Convegno ANIDIS, Pistoia 17-21 September.

Gusella, F., Lavacchini, G., Orlando, M., (2018), "Monotonic and cyclic tests on beam-column joints of industrial pallet racks". *Journal of Constructional Steel Research*, 140, 92–107.

Gusella, F., Orlando M., Vignoli A., Thiele, K., (2018). "Flexural capacity of steel rack connections: via the component method". *The Open Construction and Building Technology Journal*, 12, 90-100.

Gusella, F., Orlando M., Thiele, K., (2018). "Evaluation of rack connection mechanical properties by means of the Component Method". *Journal of Constructional Steel Research* 149, 207–224.

Gusella, F., Orlando M., Spinelli P. (2019). "Pinching in Steel Rack Joints: Numerical Modelling and Effects on Structural Response". *International Journal of Steel Structures*, 19, 1, 131-146.

Gusella. F., Arwade, S.R., Orlando, M., Peterman, K.D (2019). "Influence of mechanical and geometric uncertainty on rack connection structural response". *Journal of Constructional Steel Research*, 153, 343-355.

Gusella. F., Orlando, M., Peterman, K.D (2019). "On the required ductility in beams and connections to allow a redistribution of moments in steel frame structures". *Engineering structures*, 179, 595-610.